Nonlinear Resonance in the Hydrogen Atom

by

Marshall Burns, B.S., Ph.D.

President, Ennex Technology Marketing, Inc., Austin, Texas
Graduate Research Assistant, Department of Physics, University of Texas at Austin

DISSERTATION

Presented to the Faculty of the Graduate School of
The University of Texas at Austin
in Partial Fulfillment
of the Requirements
for the Degree of

DOCTOR OF PHILOSOPHY

THE UNIVERSITY OF TEXAS AT AUSTIN

May, 1991

Set in BitStream Dutch using MicroSoft Word for Windows
(headings in BitStream Swiss, Symbols in MicroSoft Symbol)

Printed on Wednesday, May 1, 1991.

Our chief want in life
is somebody who shall make us
do what we can.

Ralph Waldo Emerson
The Conduct of Life, 1860, §VII ¶24

This work is dedicated to
the great teachers in my life:

(in order of appearance)

Mrs. Evelyn "*Mom*" Burns
Mr. Perry "*Dad*" Burns
Mr. Brown
Mr. Ron Mason
Dr. Henry Fenigstein
Mr. Chester Psica
Prof. Joseph Brown
Prof. Steven Weinberg
Prof. Linda E. Reichl

Abstract

Nonlinear Resonance in the Hydrogen Atom

Marshall Burns

Supervisor: Prof. Linda E. Reichl

A theoretical and computational analysis in both classical and quantum mechanics demonstrates the existence of nonlinear resonance zones in the 1-dimensional approximation for extreme Stark states of hydrogen perturbed by a microwave field. Comparison of simulations in the "physical" phase space with Koch's laboratory results provide the first explanation of the widths of his regions of suppressed ionization in terms of the expansion of nonlinear resonance zones. It is also confirmed that the locations of the said regions are predicted with great precision in terms of resonance zones.

Also included is the first demonstration of the existence of resonance zones in the quantum mechanical Hilbert space, and the overlap of the zones in a manner exactly analogous to the classical behavior.

Contents

1 Introduction

Motivation

Since the mid 1970's, two experimental teams have been studying the behavior of highly excited states of hydrogen perturbed by electromagnetic microwaves. Among their findings has been a series of stable regions in the space of energy levels of the atom. This is shown in Figure 1.1:

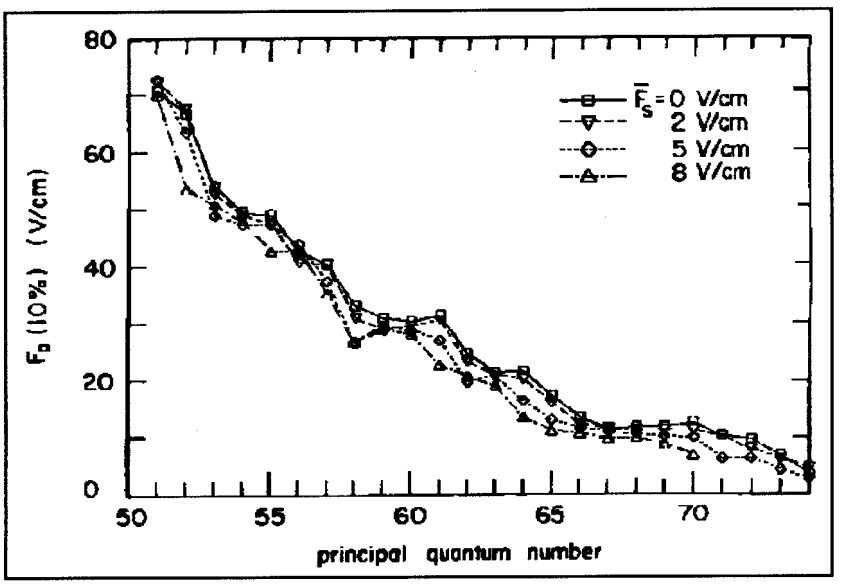

Figure 1.1. 10% ionization threshold of microwave-driven hydrogen versus initial energy level. This is the microwave peak field strength at which 10% of the atoms in the beam ionize. The microwave cavity has an electrostatic field applied; the data shown are for four different values of this field. The microwave frequency is $1.51 \cdot 10^{-6}$ (ν=9.92 GHz). [858KvL, Figure 2, reproduced with permission of the authors.]

This data show the perturbation strength at which the atoms start to ionize, as a function of initial energy level. The overall downward trend reflects the sensible fact that it takes less force to ionize a more highly excited atom. But there are regions where that trend is broken, where the ionization threshold remains roughly constant (or even increases slightly!) over a range of several energy levels. This intriguing feature of the data has been the subject of extended debate for many years. It has been widely agreed that the stable regions correspond to resonance zones (See Section 1.1.) in the phase space of the hydrogen atom, which is a nonlinear oscillator. But this has raised two questions that have gone unanswered until now:

- The excited states of hydrogen are in the quasi-classical regime; they are on the boundary of the correspondence principal and have behavior which may be described by either Hamilton's or Schrodinger's equations. The stability can be explained in classical mechanics in terms of resonance zones, but what is the corresponding explanation in quantum mechanics?
- The centers of the stable regions in the space of energy levels match very closely the predicted locations of particular resonance zones. (For more details, see Section 5.2.) But do the resonance zones also account for the *widths* of the stable regions?

The first question is answered here, in Chapter 4, by showing that the hydrogen atom Hilbert space in quantum mechanics has a resonance structure corresponding to that in the classical phase space.

The second question is also answered here, in the affirmative, by numerical simulations of the behavior of the atom at various levels of perturbation strength. These simulations, presented in Section 2.5 and discussed further in Section 5.2, show that the resonance zones corresponding to each stable region grow with the strength of the perturbation, reaching maximum widths before they break down and join the chaotic sea. These maximum widths are close to the widths of the stable regions observed in the laboratory.

While this work is motivated by the above experimental results, there are several other reasons that hydrogen is of interest. An isolated hydrogen atom is one of the simplest conceivable physical systems. Except under the conditions of high energy physics [§B.1], it is just a two-body system with a central, inverse-square-law force. The nonlinearity of that force, however, means that, when perturbed, the hydrogen atom is capable of extremely complicated behavior. The reasons for wanting to understand the behavior of hydrogen may be stated as:

- The simplicity of its structure makes it amenable to analysis.
- As a simple nonlinear system, its behavior when perturbed can be compared and contrasted to that of other simple systems demonstrating complex behavior, providing an important test for new theoretical ideas and possibly suggesting others.
- While definitely quantum mechanical in its ground state, its highly excited states are quasi-classical, thus offering an opportunity to study the issues of complexity at the threshold of the correspondence between classical and quantum mechanics.
- It is already exhaustively studied, both in classical and quantum mechanics, so that many tools for its analysis are already at hand.
- It is closely related to many other physical systems:
  - In classical mechanics, it is a prototype for a planetary system, or any 2-body gravitational system.
  - In quantum mechanics, it is the simplest atom, offering a gateway to the understanding of more complex atoms and of molecules.

Organization

This work is organized into five chapters and six appendices. The first (this) chapter gives the motivation of the research, explains the basic concepts, and sets up the model to be used. The next three chapters analyze the model from three different theoretical approaches: the classical "physical" phase space (Chapter 2), the classical action-angle coordinates (Chapter 3), and quantum mechanics (Chapter 4). The concluding Chapter 5 ties together the theoretical results with those from the laboratory.

In this introductory chapter, Section 1.1 defines *resonance* as it occurs in both linear and nonlinear systems. It also shows that, contrary to some opinion, nonlinear resonance occurs in quantum mechanics as well as classical. This is followed by a discussion of *integrability* in Section 1.2. The dynamics of the unperturbed hydrogen atom are laid out in Section 1.3. Then Section 1.4 brings the microwave perturbation into those dynamics and makes the restriction to extreme Stark states (the 1-dimensional approximation). This yields the model that is the focus of this work, the *harmonically driven Stark states of hydrogen*, or *HSH*, atom.

Chapter 2 studies the HSH atom in the ordinary, "physical" phase space of classical mechanics. This is the space spanned by the relative separation of the proton and electron and their relative momentum. Section 2.1 reviews the dynamics of the unperturbed atom in this perspective. The effect of the microwave perturbation on the phase paths is shown in Section 2.2. Section 2.3 goes to the *extended* physical phase space, and explains the nonlinear resonance zones in terms of infinite families of concentric dynamical tori in this space. The use of Poincare sections to study the families of tori is shown in Section 2.4. The important data on the effect of increasing the strength of the perturbation are in Section 2.5. It is these data that are used to show, later in Section 5.2, that the widths of the stable regions in the experimental ionization data are explained by the growth of resonance zones.

Chapter 3 again studies the classical behavior of the HSH atom, but this time in action-angle coordinates. In this perspective, the resonance structure of the phase space is directly manifested in the system energy. This structure takes the form of an infinite family of *primary resonances* which interact to cause further infinities of higher-order resonances. Since the action coordinate corresponds to the principal quantum number in quantum mechanics, this formulation of the problem provides a bridge between the theories in the physical phase space (Chapter 2) and in quantum mechanics (Chapter 4). Section 3.1 reviews the dynamics of the unperturbed atom in action-angle coordinates, and lays out the graphical techniques for visualizing the motion in them. Section 3.2 discusses the primary resonance structure arising under the perturbation. Advantage is taken of the direct manifestation of this structure in Section 3.3, where the dynamics of individual primary resonance zones are studied independent of the others. The *pendulum approximation*, an important method for calculating the shapes and radial widths of the primary resonance zones, is developed in Section 3.4. The interaction of two primaries, and the resulting secondary and higher-order resonances, are described in Section 3.5.

Chapter 4 gives the quantum mechanical view of the HSH dynamics. Section 4.1 reviews the dynamics of the unperturbed atom in this theory. The primary resonance structure arising under the perturbation is derived in Section 4.2. The special graphical techniques developed to visualize the quantum mechanical evolution are described in Section 4.3. In Section 4.4, the dynamics of individual primary resonance zones are studied using these techniques. A few data are presented on the overlap of neighboring resonances in Section 4.5.

Chapter 5 is a combined discussion of the theoretical and experimental findings. Section 5.1 reviews the results of the previous three chapters in a unified context. Then, in Section 5.2, these results are compared with specific laboratory data found in the literature. Finally, Section 5.3 offers suggestions for carrying on the work in this field.

The appendices provide reference information and detailed calculations. Appendix A is a handy table of data comparing the properties of the ground state and a highly excited state of hydrogen. Appendix B discusses the assumptions and approximation made in using the HSH model for hydrogen. Appendix C presents the results of the numerical procedure described in Section 3.5.1 for locating the secondary resonances. Various mathematical technicalities are handled in Appendices D. In particular, Appendix D.1 provides a useful table of conversion factors for the atomic system of units. Computer methods and equipment used, as well as special computational techniques developed, in the course of this work are described in Appendix E. Finally, the reasons for the semantic break from the conventional use of the term *Hamiltonian* are given in Appendix F.

1.1 Linearity and nonlinearity in classical and quantum mechanics

After listing the many different uses of the term *linear* in physics, this section defines *resonance* as it occurs in both linear and nonlinear systems. It also shows that, contrary to some opinion, nonlinear resonance occurs in quantum mechanics as well as classical, and refers to the parts of this work where that is demonstrated.

Linearity has several different meanings in mathematics and physics. The original meaning derives from the property of the function $f(x)=ax+b$ that its graph versus the variable x has the form of a straight *line*. This is generalized to define the linearity of a function or equation *in a particular argument* to mean that the dependence on that argument is entirely via a term which is proportional to the argument. Thus $f(x, y, z)$ is linear in x if it has the form $ax+g(y, z)$. If the argument has some structure, then the proportionality factor may also. For example, $f_i(\vec{x}, \vec{y})=\Sigma_j a_{ij}x_j + g_i(\vec{y})$ is linear in $\vec{x}$. A *linear differential operator* and a *linear differential equation* are a linear function and a linear equation, respectively, whose list of arguments consists of another function and its derivatives. A *linear combination* of a list is a linear function of the elements of the list which has no term independent of those elements. Thus $f(\vec{x})=\Sigma_i a_i x_i$ is a linear combination of $\vec{x}$. This then gives rise to the concept of a *linear space* (or *vector space*), in which every element is a linear combination of a set of basis elements. It also gives rise to the idea of a *linear operator*, to which a linear combination is transparent: $L(a\cdot f + b\cdot g)=a\cdot L(f) + b\cdot L(g)$.

In classical mechanics, a *linear oscillator* is a harmonic oscillator, a *linear system* is a system which can be analyzed into harmonic oscillators, and *linear resonance* is the behavior of a harmonic oscillator under the influence of an oscillatory perturbation with frequency near the natural frequency of the oscillator. A harmonic oscillator can be defined in several ways, two of which involve a linearity:

- A harmonic oscillator is a system with a linear restoring force, $F(x)=-k_F x$.
- A harmonic oscillator is a periodic system whose energy[1] is linear in its action coordinate: $E=E_0+k_E I$.

Of these two definitions, it is the second which is more useful for explaining the phenomenon of linear resonance. Hamilton's equation for the angle coordinate says that the natural frequency of the system is independent of the action: $\omega=\partial E/\partial I=k_E$. This means that the dynamics of the system are unchanged by changes in the action values. If energy is absorbed from a perturbation with a frequency near ω, then that absorption can proceed without limit until there is a breakdown which alters the form of the energy.

In a *nonlinear oscillator*, the energy is a nonlinear function of the action, so the frequency does depend on the action: $\omega=\omega(I)$. Here, if the system has action I and is perturbed with a frequency near $\omega(I)$, then it exchanges energy with the perturbing system. But the resultant change in the value of the action changes also the value of the frequency ω. The system moves out of resonance, and so it does not keep exchanging energy indefinitely.

[1] Energy functions in classical mechanics, and energy operators in quantum mechanics, are usually called in the literature *Hamiltonians*. It is argued in Appendix F that this term is superfluous, and it is never used in this work.

The behavior in classical linear resonance is a steady increase in the amplitude of oscillation, and a resultant migration of the system through regions of higher and higher energy in its phase space. The more complicated behavior in nonlinear resonance is characterized by the existence of *resonance zones* in the phase space. Inside each such zone, the system has a pronounced oscillatory response to the perturbation. At moderate perturbation strengths this response is localized within the zone with no migration from zone to zone. Moreover, whereas in a linear system the amplitude of the response is infinite at the exact resonant frequency, the amplitude of resonant oscillation at the center of each resonance zone is *zero*. Thus, at moderate perturbation strengths, the phenomenon of nonlinear resonance has an inherent *stability*.

As the strength of the perturbation is increased, however, the resonance zones grow in size and *overlap* each other. The boundaries delineating the zones, the *KAM surfaces*, are destroyed and the phase paths of the system wander from zone to zone. This migration is sensitively dependent on the initial conditions of the system, and is therefore *chaotic*. At moderate perturbation strengths, some KAM surfaces decay while others remain intact. The migration of the system is then restrained by the surviving KAM surfaces; the behavior is said to be *locally chaotic*. At higher and higher perturbation strengths, more and more KAM surfaces are destroyed. Eventually, the system becomes free to wander throughout its entire phase space, and the behavior is called *globally chaotic*.

There has been some doubt as to whether nonlinear resonance can occur in quantum mechanics. The objection is stated by pointing out that Schrodinger's equation is linear, so that there can be no nonlinear phenomena in quantum mechanics. This point of view is in error, however, because the linearity of Schrodinger's equation is linearity in the state vectors, and the significance of that linearity is that the space of quantum mechanical states is a linear (i.e., vector) space. What is relevant to the linearity of a resonance phenomenon is not the linearity of the equation of motion, but the linearity of the energy in the action coordinate.

There does not exist a pair of operators to correspond, in quantum mechanics, to the action and angle coordinates of classical mechanics.[2] However, in the classical limit, there is a correspondence between the index of the energy eigenvalues and the classical action. This suggests a way to carry over the concepts of linear and nonlinear resonance to quantum mechanics *in the special case of large energy quantum numbers*. That is to consider linear resonance to occur in quantum mechanics when the energy eigenvalues of a system with a discrete energy spectrum form a linear function of their index: $E_n = E_0 + an$. The energy level spacing is then independent of the energy index: $E_{n+1} - E_n = a$. This means that the dynamics of the system are unchanged by changes in the energy level. If energy is absorbed in the form of photons of energy a, then that absorption can proceed without limit until there is a breakdown which alters the form of the energy. This is indeed the case for the quantum mechanical harmonic oscillator, whose energy eigenvalues are $E_n = \frac{1}{2}\hbar\omega + n\hbar\omega$.

With this understanding of quantum mechanical linear resonance, nonlinear resonance is understood to occur when the energy eigenvalues form a nonlinear function of their index, so the energy level spacing depends on the energy eigenvalue of the system: $E_{n+1} - E_n = a(n)$. If

---

[2] There is a literature of attempts to find such operators: 408WPa, 46aWHF, 636DJu, 639WHL, 645LSu, 64aERD, 677HMK, 677REP, 684ECL, 684PCa, 693BLe, 694BLe, 696ECL, 69bJJL, 69cJCG, 709EKI, 725DJS, 736YAh, 745JDo, 763JML, 795RGN, 822RAL, 836MVB, 845MVB, 847AGa, 848JHH.

the system has energy E_n, and is perturbed electromagnetically with a frequency $a(n)/\hbar$, then it exchanges photons with the perturbing system. But the resultant change in the energy level changes also the energy level spacing. The system moves out of resonance, and so it does not keep exchanging photons indefinitely.

The behavior in quantum mechanical *linear* resonance is a steady increase in the energy level of the system, similar to the situation in classical mechanics. But what is there in quantum mechanics to compare to the existence of *non*linear resonance zones in the phase spaces of classical mechanics? By studying an appropriate physical system on the border between classical and quantal behavior, extreme Stark states of hydrogen, the present work demonstrates the existence of resonance zones (actually *subspaces*) in the Hilbert space of the system. In a way that parallels the classical oscillatory behavior, the system undergoes a spreading of its probability within each zone. At moderate perturbation strengths the spreading is localized within the zone with no migration from zone to zone. Thus, at moderate perturbation strengths, the phenomenon of nonlinear resonance has, also in quantum mechanics, an inherent *stability*. (There is, however, nothing to correspond to the zero amplitude of oscillation at the precise center of the classical resonance zone.)

As the strength of the perturbation is increased, the quantum mechanical resonance zones grow in size and overlap each other, just as in classical mechanics. Since there are no phase paths, there is no parallel concept for sensitive dependence on initial conditions, and therefore no chaos in the quantum resonance picture. But the net result in the behavior is the same: the probabilistic spread of the system through a larger region of its space of states.

The patterns of resonance zones in the two classical versions of the hydrogen system studied are laid out in great detail in Chapters 2 and 3. The corresponding pattern in quantum mechanics is the subject of Chapter 4. The existence of the quantum mechanical resonance zones is demonstrated in Section 4.4. They are found to correspond closely to the pattern found for the classical approach in action-angle coordinates (Chapter 3). Section 4.5 presents some data on the overlap of neighboring zones under the increase of the perturbation strength.

1.2 Integrable, nonintegrable, and quasi-integrable classical systems

This section is a discussion of the important concept of *integrability*.

The evolution of a classical system is system is given by a 1-dimensional path in the system's phase space. The dimensionality of the phase space is twice the number of the system's freedoms. The phase path may, in time, fill the entire phase space, or it may be constrained to a lower-dimensional subspace. If the path space is so reduced in dimensionality, this is explained by the existence of *isolating constants* of the system's motion. Each isolating constant reduces the dimensionality of the path space by one.[3]

[3] A *nonisolating constant* is a constant which does not impose such a constraint. For example, the initial conditions of an orbit are nonisolating constants.

For example, the simple harmonic oscillator has one freedom (the "coordinate") and one isolating constant (the energy). The phase space is 2-dimensional, but the phase path is constrained to a 1-dimensional curve, an ellipse, therein.

An *integrable* system is one with at least as many isolating constants as freedoms. For such a system, therefore, the dimensionality of the path space is no more than the number of freedoms. In this case, the system's Hamilton-Jacobi equation can be separated and thereby integrated [801HGo, 451], hence the name.

If a system has less isolating constants than freedoms, then it is *nonintegrable*. There is a very special case of a nonintegrable system, called *quasi-integrable*. In this case, there is a controllable parameter and there are one or more quantities which within some range of the parameter behave approximately like isolating constants. Furthermore, there are enough of these quantities to bring the total number of (exact and approximate) isolating constants up to at least the number of freedoms. So, within the said range of the parameter, the system behaves as if it were integrable; outside that range, it behaves nonintegrable.

Integrable and nonintegrable behavior are distinguished empirically by a technique called the *Poincare section*[4]. This is a plot of points on a 2-dimensional surface where a trajectory in a higher-dimensional phase space crosses the surface, recording all crossings in the same direction. If the system under study is integrable, then the Poincare sections for all orbits in its phase space form nested families of closed, continuous curves. If the system is nonintegrable, then the points of each orbit fall randomly all over the 2-dimensional surface, the points arising from different orbits intermingling throughout. In the intermediate case of quasi-integrability, some regions of the surface are filled with nested families of curves, while the rest of the surface shows a randomly scattered array of points. The relative proportions of the Poincare section containing closed curves versus random dots depends on the control parameter.

The combination of a nonlinear oscillator and a time-dependent perturbation is an example of a quasi-integrable system. The strength of the perturbation is the controllable parameter. The KAM surfaces are the reduced-dimensional path spaces of the system. At moderate values of the perturbation strength, the Poincare sections turn up cross sections of the KAM surfaces as closed curves. At higher strength, the KAM surfaces are destroyed and the Poincare sections appear as random scatterings of dots.

The existence of a resonance structure in the Hilbert space of a perturbed nonlinear oscillator suggests that there may be a concept in quantum mechanics analogous to integrability in classical mechanics. This is an open question at this time. There has been some interesting work on this problem by Reichl and Haoming [902LER].

[4] This is also called a *surface of section*, or a *Poincare surface of section*.

1.3 The hydrogen atom in classical and quantum mechanics

This section lays out the dynamics of the unperturbed hydrogen atom in a context that is valid in both classical and quantum mechanics.

Expressions for the energy[5]

An isolated hydrogen atom is a Kepler system, with energy (given the subscript "u" for *unperturbed*):

$$E_u = \frac{\vec{p}^2}{2m} - \frac{q^2}{r},$$

where $\vec{p}$ is the momentum of the electron relative to the proton, r is the distance between the two particles, m is the reduced mass of the system, and q is the electric charge of the proton. In classical mechanics, $\vec{p}$ and r are real-valued functions of time, and so E_u is likewise. In nonrelativistic quantum mechanics, $\vec{p}$ and r are Hermitian operators in the Hilbert space of states of the atom, and so, again, E_u is likewise. In both theories, m and q are simply numerical constants.

This energy is simplified by adopting atomic units [Appendix D.1], which will be used throughout this work. In these units, the reduced mass, m, and the proton charge, q, are set equal to 1. In addition, in quantum mechanical expressions, Planck's constant is set equal to 2π, i.e., $\hbar = 1$. The energy of the isolated hydrogen atom then becomes:

$$E_u = \frac{\vec{p}^2}{2} - \frac{1}{r}.$$

In spherical coordinates, this energy is [classical: 801HGo, (3-15), (10-49), (10-54); quantal: 770LDL, 103^+]:

$$E_u = \frac{1}{2}\left[p_r^2 + \frac{\vec{p}_{\theta,\phi}^{\,2}}{r^2}\right] - \frac{1}{r},$$

where p_r is the radial component of momentum and $\vec{p}_{\theta,\phi}$ is the angular momentum. Again, these quantities are real-valued functions of time in classical mechanics, and Hermitian operators in quantum mechanics. It is possible to also break down the angular momentum into its components:

$$E_u = \frac{1}{2}\left[p_r^2 + \frac{p_\theta^2}{r^2 \sin^2\phi} + \frac{p_\phi^2}{r^2}\right] - \frac{1}{r},$$

[5] Energy functions in classical mechanics, and energy operators in quantum mechanics, are usually called in the literature *Hamiltonians*. It is argued in Appendix F that this term is superfluous, and it is never used in this work.

but while this expression is still equally valid in both classical and quantum mechanics, the correspondence between real-valued functions of time and Hermitian operators no longer holds because ϕ is not an operator.

Symmetries of the energy

The Kepler motion has three isolating constants: the energy, E_u, the angular momentum, $\vec{L} \equiv \vec{r} \times \vec{p}$, and the periapsis vector[6], $\vec{A} \equiv \vec{p} \times \vec{L} - \vec{r}/r$. Since $\vec{L}$ and $\vec{A}$ have three components each, this adds up to seven isolating constants. However they are subject to two constraints [classical: 801HGo, (3-83), (3-87), quantal: 770LDL, >(36.34)]:

$$\vec{A} \cdot \vec{L} = 0 \qquad \text{and} \qquad A^2 = 2EL^2 + 1 ,$$

so there are five independent isolating constants.

Since the Kepler system has more isolating constants (five) than freedoms (three), it is *integrable* [§1.2] and, in fact, has two more constants than it needs to be so. While the discussion up to this point has been equally valid whether the atom is in a bound or ionized state, advantage can be taken of those two additional constants if the restriction is made to bound states only.

In classical mechanics, the restriction to bound states renders the system time-periodic, permitting a transformation of the phase space to action-angle coordinates. In quantum mechanics, it renders the energy spectrum discrete. In both theories, the existence of two additional constants reduces the system to one freedom with one independent constant[7] [classical: 801HGo, (10-117), quantal: 770LDL, >(36.35)]:

$$E_{u_{\text{classical}}} = -\frac{1}{2I^2} \qquad E_{u_{\text{quantal},n}} = -\frac{1}{2n^2} .$$

In classical mechanics, I is the principal action coordinate, $I \equiv I_r + I_\theta + I_\phi$; in quantum mechanics, n is the *principal quantum number*, the index of the energy eigenvalues.

---

[6] This is called variously the Runge-Lenz, the Lenz or the Laplace vector. It is called here the *periapsis vector* because its constant direction is from the center of attraction to the periapsis.

In quantum mechanics, the definition is adjusted because $\vec{p}$ and $\vec{L}$ do not commute: $\vec{A} \equiv \frac{1}{2}(\vec{p} \times \vec{L} - \vec{L} \times \vec{p}) - \vec{r}/r$.

[7] In classical mechanics, this is because the frequencies of all the angle coordinates are equal. In quantum mechanics, it is because the energy spectrum is degenerate. (Goldstein uses the word *degeneracy* to describe the classical case also [801HGo, >(10-117)], but this contradicts his earlier usage of the word with the weaker meaning of commensurate frequencies [801HGo, >(10-100)].)

Classical dynamics of unperturbed bound states

In classical mechanics, the dynamics of the atom is obtained from Hamilton's equations. If the angle coordinate is called ξ, then:

$$\left\{ \begin{array}{l} \dfrac{d\xi}{dt} = \dfrac{\partial E_u}{\partial I} = \dfrac{1}{I^3} \\ \\ \dfrac{dI}{dt} = -\dfrac{\partial E_u}{\partial \xi} = 0 \end{array} \right\} .$$

The action is constant in time, while the angle increases linearly with a speed (i.e., angular frequency) inversely proportional to the third power of the action. Since the action is non-negative, so is $d\xi/dt$. Thus the system point follows a circle in (I, ξ)-polar coordinates in the counterclockwise direction. The phase space is densely filled with a concentric family of such circular orbits, one for each value of I. The fact that I is constant implies that, even though $\vec{p}$ and r vary with time, E_u is constant.

Quantum dynamics of unperturbed bound states

In quantum mechanics, the energy states are *stationary*: there is no evolution if the atom is not perturbed. If the initial state is a superposition of negative-energy states, as every bound state is:

$$|t=0\rangle = \sum_n c_n |n\rangle ,$$

then the atom remains in that superposition indefinitely.

The level splitting for the atom is given by the Balmer formula:

$$E_{n+1} - E_n = \frac{1}{2}\left[\frac{1}{n^2} - \frac{1}{(n+1)^2}\right] \underset{n\to\infty}{\to} \frac{1}{n^3},$$

which, for large values of the principal quantum number, approaches the same form as the frequency of the orbital motion in classical action-angle coordinates, with $I \to n$.

1.4 Harmonically driven Stark states of hydrogen (HSH)

This section brings the microwave perturbation of the Koch and Bayfield experiments into the dynamics of the atom under investigation. It then makes the restriction to extreme Stark states (the 1-dimensional approximation). This yields the model that is the focus of this work, the *harmonically driven Stark states of hydrogen*, or *HSH*, atom.

The complex behavior that makes hydrogen interesting arises under a perturbation that destroys constants of its motion. In this case, the system is no longer integrable, but it is *quasi-integrable* [§1.2].

The perturbation studied here is a monochromatic, linearly polarized, electromagnetic wave. The energy of interaction is just the scalar product of the electric vector of the wave with the dipole moment of the atom so that the total system is modeled by:

$$E = E_u + \vec{F}\cdot\vec{x}\cos(\omega t)\,, \qquad \textit{HH energy}$$

where E_u is the unperturbed energy, $\vec{F}$ and ω are the peak field strength and angular frequency of the wave, and $\vec{x}$ is the separation vector of the proton and electron. The sign of the second term is arbitrary because it can be reversed by a shift in the origin of time. A phase term in the argument of the cosine is likewise not necessary, as its effect can also be absorbed into the definition of t. This is the *harmonically driven hydrogen*, or *HH*, model. See Appendix B.1 for a discussion of several simplifying assumptions and approximations implicit in this model.

In classical mechanics, $\vec{x}$ is a real-valued vector function of time; in quantum mechanics, it is a Hermitian vector operator in the atom's Hilbert space. In a fully quantal analysis (i.e., in quantum electrodynamics), $\vec{F}$ would also be an operator, but the approach taken here is semiclassical in that $\vec{F}$ is treated, along with ω, as a real-valued parameter of the system.

The excited states used to produce the experimental data in Figure 1.1 were prepared by laser excitation in the presence of a static electric field. (See Figure 5.1.) These states are therefore *extreme Stark* or *1-dimensional* states[8]. In these states, the classical orbit or the quantum mechanical orbital of the electron lies almost along a straight line and the electron remains predominantly on one side of the proton. The electrostatic field is not active in the region of the microwave perturbation; the Stark states are the states of the unperturbed atom. (The Stark states are assumed to be stable on the time scale of the experiment, and to undergo transitions only to other such Stark states [§B.2].) The polarization of the microwave is lined up with the Stark axis of the atom. Then the energy of the perturbed system can be modeled as:

$$E = E_u + F x \cos(\omega t)\,. \qquad \textit{HSH energy}$$

[8] For further discussion of the motivation for going to a 1-dimensional model, see 83bRVJ, 387 ¶2 and 872RBl, 84 ¶2.

Thus the system to be studied is a hydrogen atom in an extreme Stark state, harmonically driven by a monochromatic, electromagnetic wave linearly polarized along the direction of the Stark stretching. This is the *harmonically driven Stark states of hydrogen*, or *HSH*, model. Again, further reducing the energy to this form involves several implicit assumptions and approximations; these are discussed in Appendix B.2.

As often happens when a model is simplified, the HSH energy actually models a broader range of phenomena than just harmonically driven Stark states of hydrogen. It has appeared in the literature describing the behavior of a perturbed surface-state electron (an electron bound to the surface of liquid helium by its image charge) [827RVJ, 837RBl, 83bRVJ, 841RBl, 852RBl], and of a perturbed particle in an infinitely deep square well [859WAL, 861LER, 862LER, 874LER, 878WAL, 87cWAL] (in which case, however, E_u is not the hydrogen energy discussed above).

2 Classical HSH dynamics in the physical phase space

This chapter studies the HSH atom in the ordinary, "physical" phase space of classical mechanics. This is the space spanned by the relative separation of the proton and electron and their relative momentum. Section 2.1 reviews the dynamics of the unperturbed atom in this perspective. The effect of the microwave perturbation on the phase paths is shown in Section 2.2. Section 2.3 goes to the *extended* physical phase space, and explains the nonlinear resonance zones in terms of infinite families of concentric dynamical tori in this space. The use of Poincare sections to study the families of tori is shown in Section 2.4. The important data on the effect of increasing the strength of the perturbation are in Section 2.5. It is these data that are used to show, later in Section 5.2, that the widths of the stable regions in the experimental ionization data are explained by the growth of resonance zones.

2.1 The motion of the unperturbed 1-dimensional hydrogen atom

This section reviews the dynamics of the unperturbed atom in the physical phase space.

The energy of the unperturbed 1-dimensional hydrogen atom is, in atomic units [Appendix D.1]:

$$E_u(x,p) = \frac{p^2}{2} - \frac{1}{x}.$$

Hamilton's equations for this energy are:

$$\left\{ \begin{array}{l} \frac{dx}{dt} = \frac{\partial E_u}{\partial p} = p \\ \\ \frac{dp}{dt} = -\frac{\partial E_u}{\partial x} = -\frac{1}{x^2} \end{array} \right\}.$$

The electron is always accelerating toward the proton. In a state with positive momentum, the electron moves away from the proton with decreasing speed. If the energy is positive, this goes on forever; this is an ionized state. If the energy has a negative value, then the atom is in a bound state and the electron moves away until it reaches apapsis (the point of maximum distance from the proton), and then turns around and approaches the proton with increasing speed. In this simplified 1-dimensional model, the electron hits the proton with infinite speed, bouncing off of it again with infinite speed.

The kinematics of this system are studied in Appendix D.3 as a limiting case of the 2-dimensional Kepler problem. It is shown there that the motion of the atom is along an infinitesimally wide ellipse whose foci coincide with the periapsis and apapsis of the orbit. The proton therefore lies *at* the periapsis of the orbit, and the apapsis is equal to the major axis of the ellipse, designated $2a$.

This conservative, 1-dimensional system has one isolating constant of the motion [§1.2]. That constant can be specified in terms of any one of many physical quantities, such as the energy of the atom, E_u, the semi-major axis of the orbit ellipse, a, the action coordinate, I (defined and discussed at length in Chapter 3), or the frequency of the orbital motion[1], ω_{atom}. These constants are related by [801HGo, (10-133), (3-75)]:

$$E_u = -\frac{1}{2a} = -\frac{1}{2I^2} = -\frac{\omega_{atom}^{2/3}}{2}.$$

The action is the most convenient constant to use to characterize the orbits, primarily because it corresponds to the principal quantum number in quantum mechanics.

The phase paths of the atom in its 2-dimensional phase space have the simple form shown in Figure 2.1:

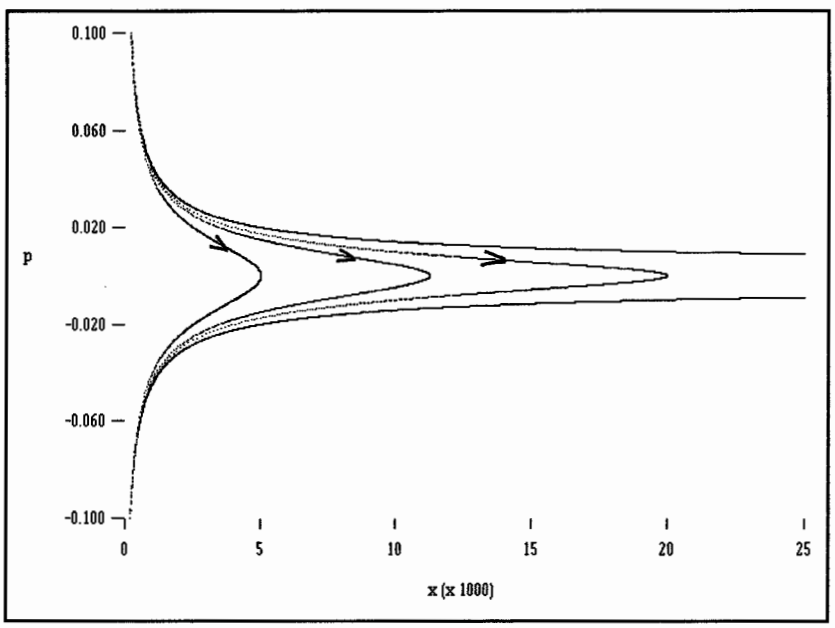

Figure 2.1. Three phase paths of an unperturbed 1-dimensional hydrogen atom. The orbits shown have apapses of 5,000, 11,250, and 20,000 atomic units (or $2.6 \cdot 10^{-5}$, $0.60 \cdot 10^{-4}$, and $1.1 \cdot 10^{-4}$ cm), corresponding to atoms with action values (principal quantum number) 50, 75 and 100, respectively.

The curves extending off to $x = \infty$ are the orbit of an atom with $E_u = 0$. These curves form the boundary between bound and ionized states of the atom. All of the 2-dimensional plots in this chapter show this boundary.

This illustrates the basic underlying motion of the HSH atom in the limit of no perturbation.

[1] The unperturbed orbital frequency is designated here with the subscript "atom" to distinguish it from the frequency of the perturbation, for which the symbol ω is used without a subscript.

2.2 The HSH motion in the phase space of the unperturbed atom

This section shows the effect of the microwave perturbation on the hydrogen phase paths.

The HSH energy is obtained by adding to the energy of 1-dimensional hydrogen the perturbation of an electromagnetic wave polarized along the axis of the atom:

$$E(x,p,t) = \frac{p^2}{2} - \frac{1}{x} + F x \cos(\omega t) .$$

If the perturbing wave is strong and of high-frequency (large F and ω), then there are two results of the exchange of energy between the atom and the electromagnetic field, as shown in Figure 2.2. On a small scale, the orbits waver about their original shapes. On the scale of an entire orbit, the net exchange of energy causes the apapsis (the farthest distance of the electron from the proton) to drift from its original value:

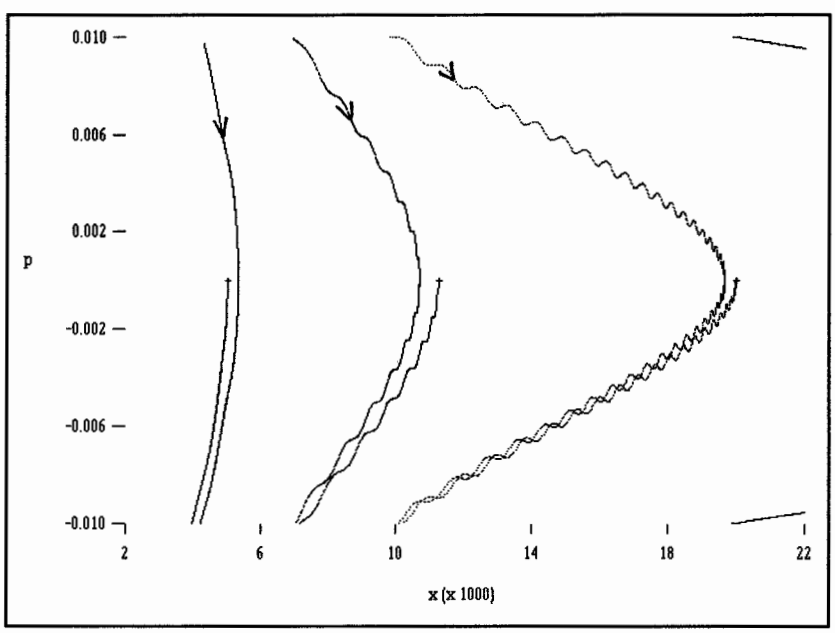

Figure 2.2. A close up view of the three orbits in Figure 2.1, now perturbed by an electromagnetic wave of peak field strength $F=1.0\cdot10^{-8}$ (51 V/cm) and frequency $5.0\cdot10^{-5}$ (ν=329 GHz). The cross-hairs, "+", mark the initial condition for each orbit plotted.

The short curves in the right-hand corners of the graph are the ionization boundary (orbit for E_u=0).

In this plot, the perturbation has peak field strength $F=1\cdot10^{-8}$ and frequency $\omega=5\cdot10^{-5}$. For comparison, the following table shows the Coulomb field strength and orbital frequency of the three orbits:

Parameters of various hydrogen orbits		
Action	Coulomb field strength at ½-apapsis	Orbital frequency
I	$-1/I^4$	Average $\omega=1/I^3$
50	$-1.6\cdot10^{-7}$ (822 V/cm)	$0.80\cdot10^{-5}$ (ν=53 GHz)
75	$-3.2\cdot10^{-8}$ (162 V/cm)	$2.4\cdot10^{-6}$ (ν=16 GHz)
100	$-1.0\cdot10^{-8}$ (51 V/cm)	$1.0\cdot10^{-6}$ (ν=6.6 GHz)

Thus the perturbation ranges in strength from about an order of magnitude weaker to about the same as the Coulomb force, and has from just under one to 1½ orders of magnitude higher frequency than the Kepler motion.

If the perturbation frequency is now brought down to within the domain of the orbital frequencies, then the wavering of the orbits' shapes and the drift of their apapses come approximately into phase. This yields a much more pronounced effect, to the point of ionization of higher energy orbits, as is seen in Figure 2.3. This effect can be described as resonance between the electromagnetic wave and the orbital motion of the electron. However, this is nonlinear resonance, and is much more complicated than its linear counterpart. (See the discussion of linear and nonlinear resonance in Section 1.1.)

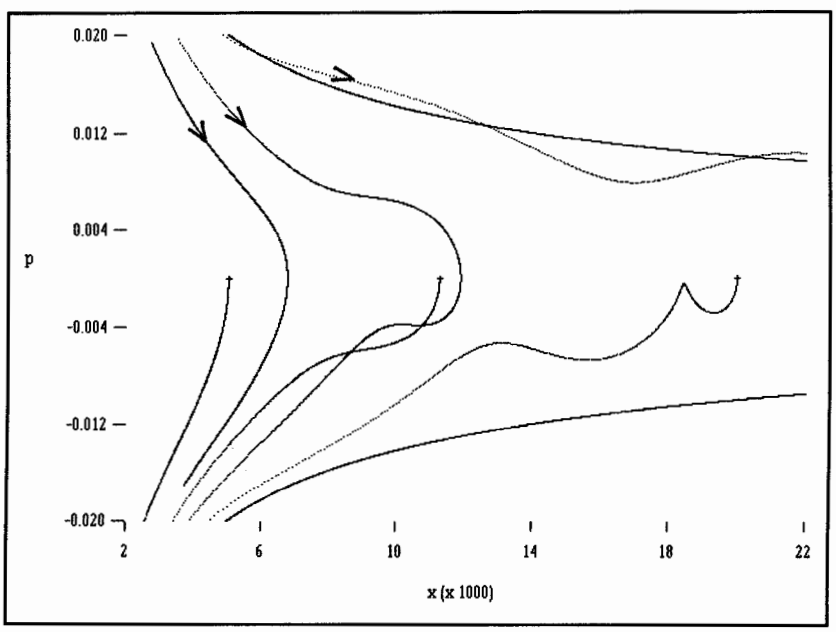

Figure 2.3. The same three orbits again, here perturbed by an electromagnetic wave of the same field strength, but reduced frequency $\omega=5.0\cdot10^{-6}$ (ν=33 GHz).

As in all the 2-dimensional plots in this chapter, the orbit for $E_u=0$ is shown. Here, one of the perturbed orbits is seen to straddle this boundary between bound and ionized states of the atom.

The high perturbation strength and frequency used in the above plots have a dramatic effect on the dynamics of the electron. And these values of the parameters are not out of

reach in the laboratory. Experiments[2] lead by Bayfield and by Koch since 1974 have investigated hydrogen atoms with principal quantum numbers as high as 98, perturbed by microwaves up to $\omega=0.55\cdot10^{-5}$ ($\nu=36$ GHz) and up to $F=1.9\cdot10^{-7}$ (10^3 V/cm). Generally, those experiments have measured *ionization*, while the analysis here is of the *bound* resonance behavior. For this reason, the analysis is carried out from here on with the moderate parameter values $F=1.947\cdot10^{-10}$ (1.000 V/cm) and $\omega=1.509\cdot10^{-6}$ ($\nu=9.923$ GHz). These values correspond to the frequency and the lower end of the field strength range used by Koch in the experiments whose results are shown in Figures 1.1 and 5.2. After a complete analysis at these parameters is presented, a few data are also given for three higher field strengths [§2.5]. The numerical data are then compared to the laboratory results in Section 5.2.

The behavior of the HSH atom with the chosen parameter values is shown in Figure 2.4.

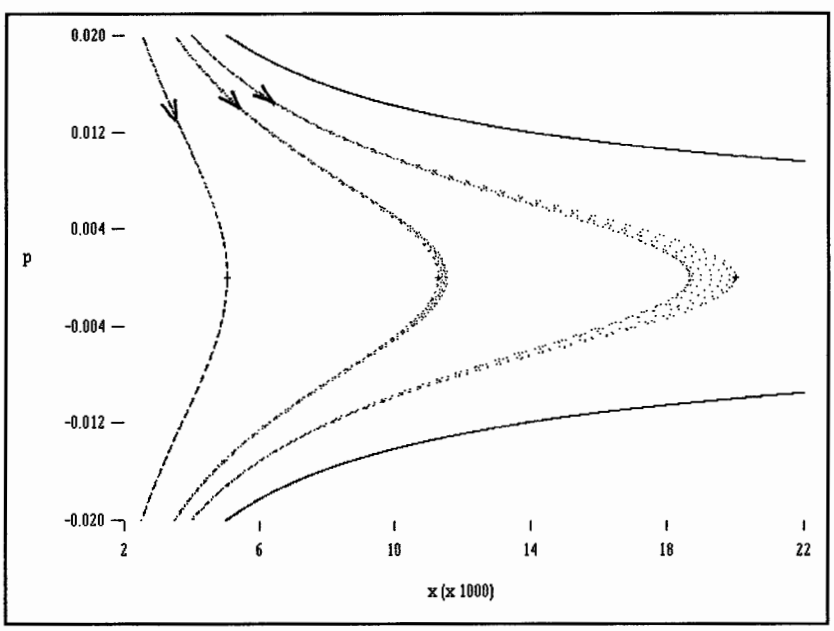

Figure 2.4. The three orbits of the previous plots, perturbed by a weaker and slower electromagnetic wave, $F=1.947\cdot10^{-10}$ (1.000 V/cm) and $\omega=1.509\cdot10^{-6}$ ($\nu=9.923$ GHz). Each orbit oscillates within a region near its initial condition.

The monotonic increase of the width of these regions with the energy of the orbits is a coincidence of the particular set of initial conditions chosen, and is *not* the case in general.

Each orbit drifts back and forth within a narrow region near its initial conditions.

[2] For references to all the experiments mentioned in this paragraph, see Section 5.2.

2.3 The extended phase space

This section discusses the HSH atom in its *extended* physical phase space, and explains the nonlinear resonance zones in terms of infinite families of concentric dynamical tori in this space.

As each orbit in Figure 2.4 drifts back and forth within its particular region, it crosses itself repeatedly. This indicates that the p-x space cannot be the phase space of the perturbed system. Indeed, the application of the electromagnetic wave introduces an additional freedom to the 1-dimensional hydrogen atom, so that the phase space of the perturbed atom is 4-dimensional. Appendix D.2 presents the mathematics behind the enlargement of the phase space to account for the perturbation.

The coordinates of the extended phase space are $p, x, -E$ and t. A 3-dimensional representation of the orbits can be obtained by ignoring the $-E$ coordinate and plotting p, x, and t. With t scaled by ω, the resulting representation of each orbit lies on an, albeit strangely shaped, torus. This representation can be thought of as resulting from plotting the ordinary 2-dimensional orbits while at the same time rotating the 2-dimensional phase space about its p axis with angular frequency ω. For an example, Figure 2.5 shows this construction for one of the orbits in Figure 2.4.

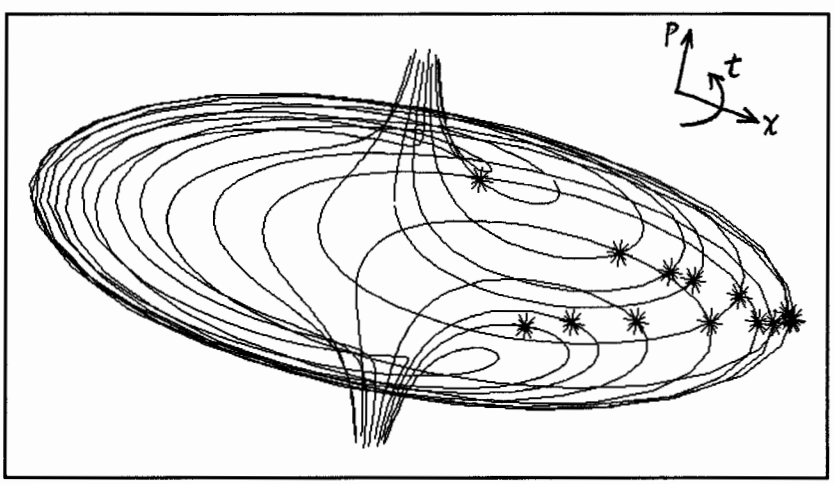

Figure 2.5. The outermost orbit in Figure 2.4, plotted in its energy subspace of the extended phase space. The orbit lies on a torus with no "donut hole", and with longitudinal circumferences extending to $p = \pm\infty$. The sense of motion is: down at the top, spiralling around counterclockwise, and out through the bottom. The asterisks are those points lying in one copy of the original 2-dimensional phase space; they are strobe points, and form a Poincare section [§1.2] of the orbit. This plot may be thought of as made by replotting the outermost orbit in Figure 2.4 while rotating the 2-dimensional phase space about its p axis, which becomes the central axis of the torus.

The apparent rounded shape at the equator on the right side of the picture is an optical illusion caused by seeing intersections of lines belonging to the upper and lower hemi"spheres" of the torus. The downward-spiraling orbits in the lower hemisphere appear to go up, across, and then down, and so seem to form a rib-like structure, thereby suggesting the rounded appearance to the brain. The actual shape of the torus can be inferred from the placement of the asterisks, which show it to have considerable thickness in the mid-region, and come to a rather sharp edge at the equator. With some practice and effort, this correct shape can be seen in the left side of the picture.

With this picture of the motion, the oscillatory drift seen in the orbits of Figure 2.4 can be seen to be due simply to a smooth variation of the equatorial radius of the torus.

An orbit on a torus is characterized by the frequencies of its two orthogonal motions. For the case at hand the two motions are the underlying orbital motion of the atom, with frequency $\omega_{atom}=1/I^3$, and the advance of time[3], with frequency ω. If these frequencies are commensurate, so that $\omega/\omega_{atom}=I^3\omega$ is a rational number, then the motion does not fill the torus, but degenerates into a closed loop wrapped around it. Several examples are shown in Figure 2.6.

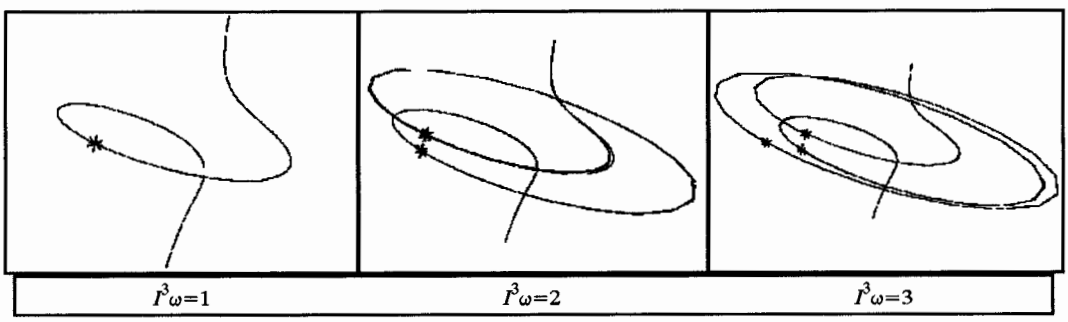

Figure 2.6(a). Trajectories of the HSH atom in its energy subspace of the extended phase space, for three special cases where the ratio of frequencies is an integer. The asterisks are strobe points, those points appearing when t is an integer multiple of the perturbation period, $2\pi/\omega$. Although each orbit appears to be a single curve spiralling around from top to bottom, each such curve is actually traversed several times in the calculation, showing that the motion is periodic.

All of the toroidal plots of Figures 2.5 and 2.6 have been rotated to an orientation that shows their features most clearly. There is no physical significance to the differences in orientation among these plots. The system of axes for this set of figures is the same as that shown in Figure 2.5.

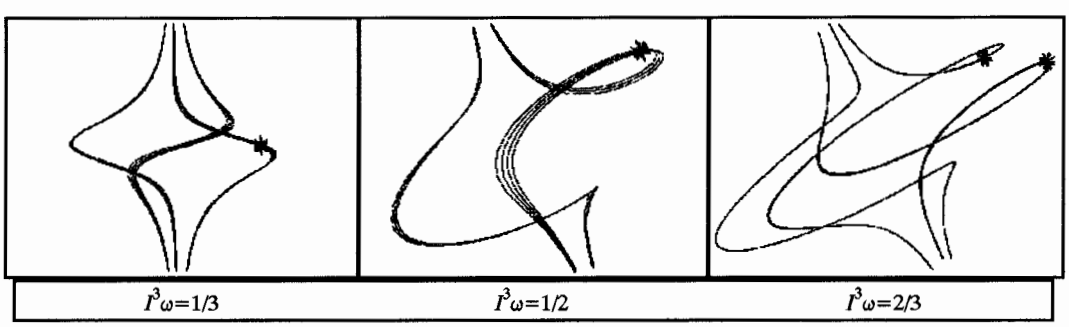

Figure 2.6(b). Trajectories of the HSH atom in its energy subspace of the extended phase space, for three special cases where the ratio of frequencies is less than 1. The motion is very nearly periodic, but some imprecision in the initial conditions has caused some of the orbits to "fan out" with each successive pass. This fanning out means that the orbit actually lies either on an interstitial torus enclosing the periodic orbit with the stated winding number, or on a nearby KAM torus.

[3] In the extended phase space, the advance of time qualifies as a component of motion because time is treated in this context as an independent freedom. The role that is usually played by time, that of a measure of the progress of motion, is served by the new parameter called ζ in Appendix D.2.

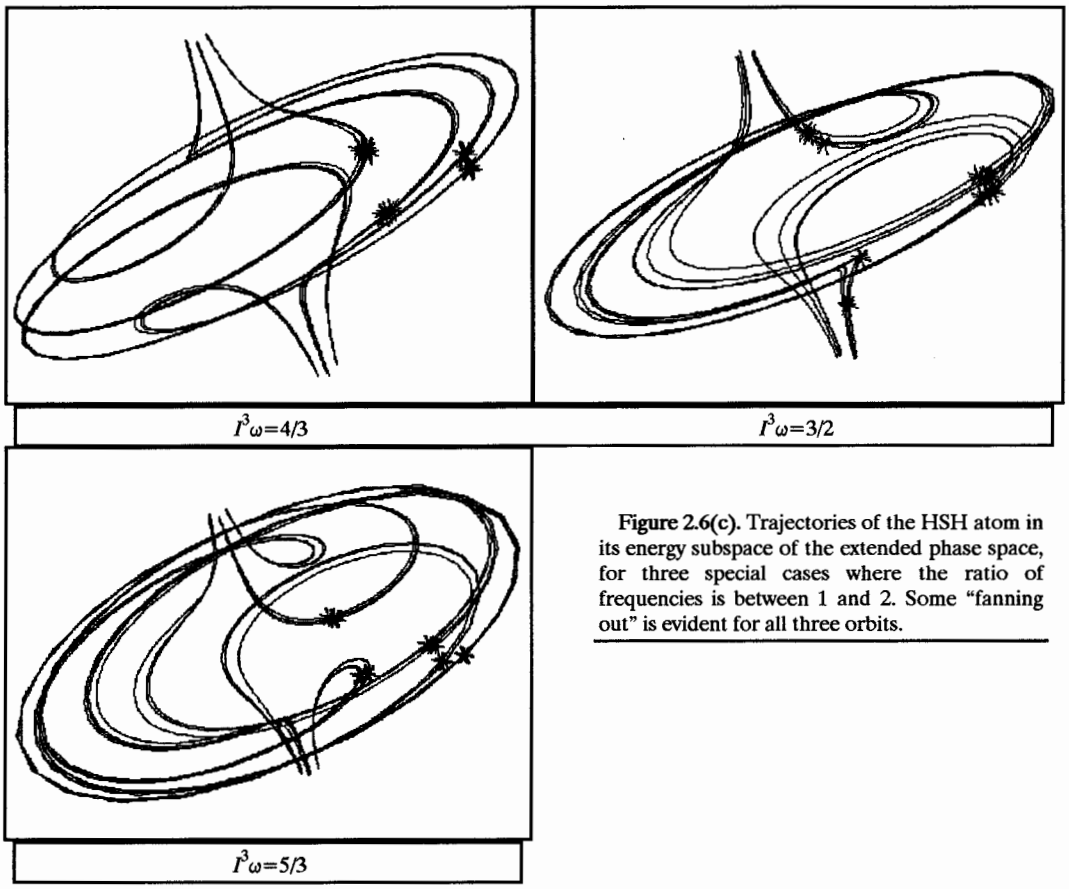

Figure 2.6(c). Trajectories of the HSH atom in its energy subspace of the extended phase space, for three special cases where the ratio of frequencies is between 1 and 2. Some "fanning out" is evident for all three orbits.

There are several common features to notice about these plots. If the ratio of the frequencies is called s/r, then the system point executes s circuits of the t coordinate and r circuits of the p before coming back to its initial state. The circuits in t show up in each plot as s lateral spirals, the circuits in p as r vertical strands reaching up and down. The ratio s/r is called the *winding number* of the orbit.

The asterisks in these plots are *strobe points*, the phase points of the system at integer multiples of the period of the t coordinate. They make up the intersection of each orbit with a single copy of the original 2-dimensional phase space of the unperturbed system. A 2-dimensional plot of the strobe points alone is a *Poincare section* [§1.2]. Since a system with commensurate frequencies is periodic (It retraces its steps along an orbit like those shown in Figure 2.6.), the system returns to the same strobe points over and over again in the Poincare section. For a winding number of s/r, there are s repeated points in the Poincare section of a periodic orbit. This is verified for all (except one[4]) of the plots in Figure 2.6 by noticing that the number of asterisks (which are all really several asterisks plotted at the same point) is equal to the numerator of the ratio $I^3\omega$. The Poincare sections are studied in great detail in Section 2.4.

[4] The exception is $I^3\omega=3/2$, but the exception is a matter of appearance only: There really are three clusters of asterisks as there should be. Two of them are seen very near the equator of the torus. The third consists of the other asterisks which are running both up one strand and down another on the neck of the torus. This third cluster, which spans the singularity at $x=0$, is so spread out because the time scale expands exponentially in this region.

Geometrically, a Poincare section constructed of strobe points slices through the torus with a half-plane of constant t mod $2\pi/\omega$. One could also make a Poincare section that slices through the torus at equal values of p instead. For a winding number of s/r, this would have r repeated points. One can imagine making such a construction, for example, by slicing through the r strands extending upwards or downwards in any one of the plots in Figure 2.6.

Look back now at Figure 2.5. The winding number for this orbit is 1.509 (since $I^3\omega = 100^3 \cdot 1.509 \cdot 10^{-6}$). This is close to 3/2, but is more precisely 1,509/1,000. The Poincare section for this orbit therefore has 1,509 repeated points. The strobe points form what appears to be, as more and more points are plotted, a solid curve, tracing the outline of the torus in the p-x plane. In the limit as the winding number approaches any irrational number this curve becomes truly continuous. Such a curve is called a *KAM curve*, and the torus it forms is a *KAM torus*. Since irrational numbers are not representable in the floating point representation used in these calculations, an actual KAM torus cannot be shown. However, the torus in Figure 2.5 is an approximation of one.

The orbits that follow the unperturbed tori fall, therefore, into two classes, as follows:

	1	2
Relationship of frequencies of unperturbed atomic orbit and of perturbation:	commensurate (ratio is rational)	incommensurate (ratio is irrational)
Periodicity of orbit in extended phase space:	periodic (closed curve on torus)	aperiodic (fills the torus)
Strobe plot yields:	set of discrete points (repeated points)	continuous curve (KAM curve)

In the limit $F=0$, every point on an orbit with a commensurate frequency is a repeated point. This means that a strobe plot starting anywhere on such an orbit yields a set of discrete points that includes that point. But when the strength of the perturbation is not zero, the points on the commensurate orbits become specialized. $2s$ of the points on an orbit with winding number s/r become s pairs of repeated points, one elliptic and one hyperbolic[5]. A strobe plot starting at one of these points still yields a set of discrete points, but if the plot is started at any other point on a commensurate orbit, the result is a set of s closed curves encircling the s elliptic points.[6,7]

[5] At an *elliptic*, or *stable*, point, a small change in the initial conditions results in an orbit whose Poincare section is a small, closed curve (approaching an ellipse in the limit as the deviation from the point goes to zero) encircling the point. This is a condition of stability for the system because small deviations in initial conditions are not magnified in the time evolution.

At a *hyperbolic*, or *unstable*, point, a small change in the initial conditions involves a bifurcation: the Poincare section of the resulting orbit evolves in one direction or the other toward a neighboring elliptic point on the same orbit. This is a condition of instability, i.e., of sensitive dependence on initial conditions.

[6] These statements assume that the strobe times are $t_n = 2n\pi/\omega$, so that the Poincare section always slices the torus with same half-plane. The effect of strobing at times $t_n = t_0 + 2n\pi/\omega$ is to slice with a half-plane rotated with respect to the half-plane for $t_0 = 0$. This shifts the location of the repeated points around on the unperturbed orbit.

[7] A lucid explanation of this differentiation of repeated points is given in 830AJL, §3.2b.

In the extended phase space, the orbits whose Poincare sections are sets of closed curves encircling sets of elliptic points have the following structure. *Surrounding each stable periodic orbit* there arises (and grows with the strength of the perturbation[8]) *an infinite family of concentric tori.* These new tori are called here *interstitial tori* because each infinite family of them lies in between a pair of tori for two aperiodic orbits, the two tori bracketing the torus of the periodic orbit. In the limit of zero perturbation strength, a whole family of interstitial tori occupies the space of the original torus for a periodic orbit. But the new tori are topologically distinct from the original tori on which both the periodic and aperiodic orbits lie. This is because each family of interstitial tori follows a periodic orbit, winding around the space of the original torus on which that orbit lies with the same winding number as the orbit. This structure is illustrated in Figure 2.7:

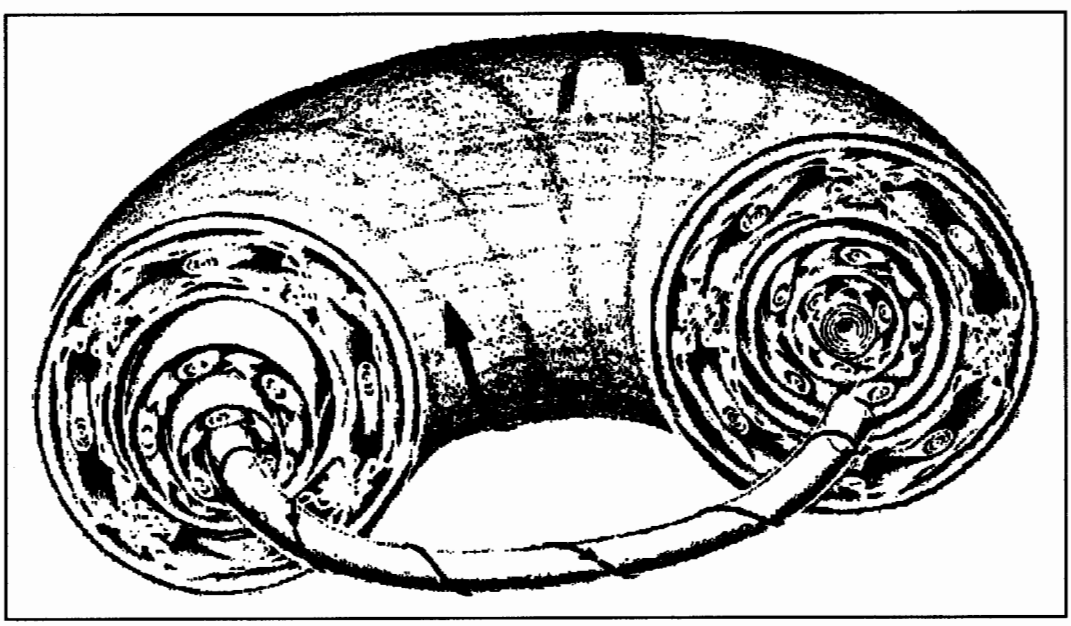

Figure 2.7. Artistic rendition of the toroidal structure of the phase space of a quasi-integrable system, such as the HSH atom. This picture shows cross sections of the *original* tori which arise from the deformation of the unperturbed orbits, and the *interstitial* tori winding around in between the original tori. [780MVB, Figure 8.3-3]
This picture is drawn in action-angle coordinates, which are considered in Chapter 3. The families of tori in the physical phase space have different shapes from, but the same topology as, those shown here.

All of the strobe points shown in Figure 2.6 are elliptic points. But notice that in some of the plots, particularly those where the winding number is not an integer, a small deviation from the intended initial conditions has caused the orbit to fan out instead of exactly repeating the course of a single curve. This "fanning out" indicates that the orbit being plotted is not actually the periodic orbit intended, but lies either on one of the interstitial tori surrounding that periodic orbit or on a nearby KAM torus.

The fanning out of the nearly periodic orbits also helps to explain the importance of the interstitial tori to the dynamical integrity of the phase space. If the initial conditions are such that the action is slightly higher than that for the intended periodic orbit, then the electron is moving slightly faster than anticipated and the orbit fans out in the forward direction (the

[8] The growth of the interstitial tori with the strength of the perturbation is explained in the theory of the pendulum approximation [§3.4].

direction of decreasing p). If the action is slightly lower, then the electron is slower and the orbit fans out in the backwards direction (increasing p). These conditions define two regions whose juxtaposition would constitute a dynamical discontinuity. The interstitial tori serve as an interface between the two regions.

In the limit of infinitesimal perturbation strength, the interstitial tori occupy infinitesimal volume in the phase space. With increasing perturbation strength, however, these tori grow to assume an equal dynamical importance with the original tori.

In this growth, the orbits on the interstitial tori fall into the same classification as the orbits on the original tori. The two classes are:

- Periodic. These have a rational winding number, describe a closed curve on their torus, and appear in Poincare section as a set of repeated points. And
- Aperiodic. These have an irrational winding number, fill their torus, and appear in Poincare section as a continuous curve. The torus in this case is called a KAM torus and the Poincare section a KAM curve, just as for the original tori.

In this way, each family of interstitial tori is a microcosm replicating the topological structure of the original phase space prior to the growth of the interstitial tori. This is an example of self-similarity, a common phenomenon in systems exhibiting nonlinear resonance.

The 3-dimensional plots are not helpful for viewing the interstitial tori because the software used does not have the ability to hide one structure when it goes behind another, and the plots become an indecipherable mess of lines. This discussion continues therefore, in Section 2.4, using Poincare sections, which convey all the dynamical information about the tori in the original 2-dimensional phase space of the unperturbed atom.

In the growth of the interstitial tori, neighboring families inevitably grow into each other's regions. This is known as *overlap*. When this happens, the KAM tori become destroyed and orbits from both families wander stochastically throughout the region defined by both families of tori. This introduces a third type of orbit. The first two types, periodic and aperiodic, are together categorized as *regular*, meaning that the evolution is predictable over long times. The third type, however, is:

- Chaotic. The orbit is not confined to a torus at all, so there is no winding number. The Poincare section is a random scattering of dots in a region which may be confined (localized chaos) or may extend throughout the phase space (global chaos).

Again, these chaotic orbits arise from the destructive interaction of the interstitial tori as they grow with increasing perturbation strength. The development of chaotic orbits with increasing perturbation strength is seen in the Poincare sections in Section 2.5.

The presence of both regular and chaotic orbits in the phase space identifies the HSH atom as a *quasi-integrable* system [§1.2]. An *integrable* system has only regular orbits, while the orbits of a fully *nonintegrable* system are all chaotic. A quasi-integrable system has a parameter (F in the case of HSH) which determines the degree of chaos in the system. For very small values of this parameter, the orbits appear to be all regular, although extreme magnification of any region of the phase space will always show evidence of chaotic behavior. As the value of the parameter is increased, more and more orbits become chaotic until, at very large values, there are no regular orbits. This progression is shown in Figures 2.8 and 2.10.

2.4 Poincare sections

This section uses a Poincare section [§1.2] of the HSH phase space to study its families of dynamical tori.

Figure 2.8 is a Poincare section of the extended HSH phase space, showing all of the orbits seen in Figure 2.6, plus several more.

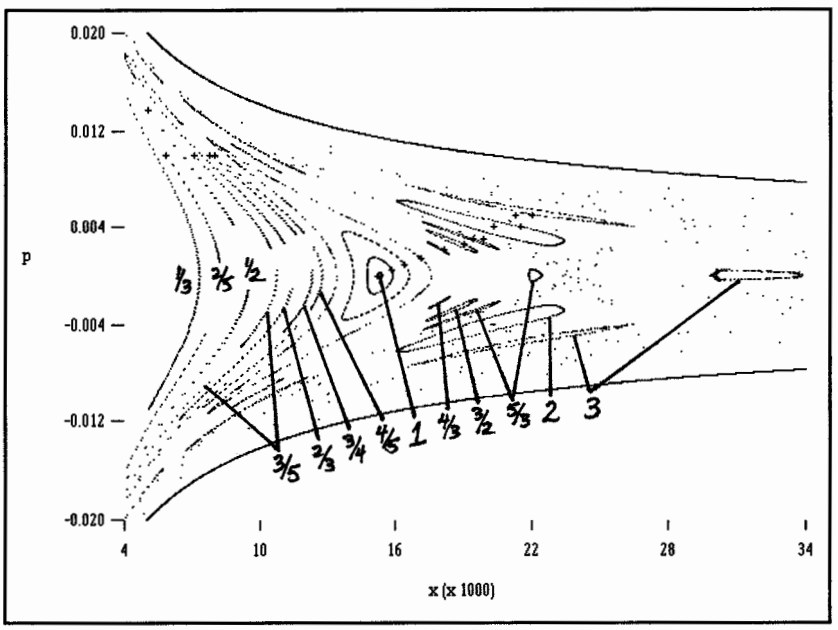

Figure 2.8. Strobe plot of HSH phase paths for various initial conditions. The perturbing electromagnetic wave has peak field strength $F=1.947\cdot10^{-10}$ (1.000 V/cm) and angular frequency $\omega=1.509\cdot10^{-6}$ ($\nu=9.923$ GHz). This is a Poincare section of all of the orbits shown in Figure 2.6, plus several others. The fraction labeling each island chain indicates the winding number of the corresponding orbit on its torus, as measured in the generation of this plot.

The outer curve is the ionization boundary (orbit for $E_u=0$).

The orbits in this plot are labeled with their winding numbers, s/r. These are *not* the theoretical winding numbers $I^3\omega$ discussed in Section 2.3, although it is shown below that they are equal. The winding numbers shown were measured during the construction of the plot, as follows:

- The numerator, s, counts the number of islands in the chain, i.e., the number of closed curves formed in the Poincare section of the orbit. This corresponds to the number of lateral spirals in the plots in Figure 2.6. Some of the islands span the singularity at $x=0$; for example, although the Poincare sections for $s/r=2/5$ and 1/2 look quite similar in this plot, the former consists of two separate islands, while the latter consists of the two ends of a single island whose midregion is at the singularity.[9]

[9] This is observed unambiguously in the plotting of the Poincare sections. In the case of the 2/5 orbit, the strobe points appear in each island sequentially, thereby tracing out both islands simultaneously. For the 1/2 orbit, the strobe points trace out first the upper lobe, then they go off-screen in the positive p direction, then they come back

- The denominator, r, is the "hit order" of the strobe points as they appear in the islands, antimod[10] the number of islands. In other words, as the dots appear on the computer screen, they hit every r'th island. This is measured clockwise around the 1-dimensional phase space, because that is the sense of the unstrobed motion of the phase point.

For $s/r=1$, the Poincare section of the exactly periodic orbit (the single elliptic point just to the left of center in the plot) is shown as well as the sections of three orbits on interstitial tori enclosing the periodic orbit (the three closed curves concentric with the elliptic point). For $s/r=2$, the Poincare sections for the periodic orbit (a pair of elliptic points) and one nearby orbit (the pair of closed curves surrounding the two elliptic points) are shown. For all other winding numbers, a single orbit near the periodic one is shown.

In addition to the regular orbits whose Poincare sections are closed curves, there are also orbits whose evolution is chaotic and whose Poincare sections consist of random scatterings of dots. Two such orbits are included in Figure 2.8.

An analysis of the regular orbits in Figure 2.8 is given in the following table.

Locations and extents in action of resonance islands for $F=1.9\cdot10^{-10}$ and $\omega=1.5\cdot10^{-6}$

Winding number for island chain (s/r)	Theoretical action ($[s/(r\omega)]^{1/3}$)	Measured action		
		Average	Width	Excursion
1/3	60.5	60.3	0.0	0.2
2/5	64.2	64.1	0.0	0.3
1/2	69.2	69.1	0.6 or more	1.1
3/5	73.5	73.5	0.1	1.1
2/3	76.2	76.0	0.1	1.2
3/4	79.2	79.2	0.1	2.3
4/5	80.9	80.9	0.1	2.9
1	87.2	87.4	11.9	11.9
4/3	96.0	95.9	0.8	2.5
3/2	99.8	100.1	1.9	2.8
5/3	103.4	103.4	2.3	4.3
2	109.8	110.1	8.4	8.4
3	125.7	126.0	8.0	8.1

The columns of this table present the following data on each chain of islands:

- The first column gives the winding number of the island chain, measured as described above.

---

onto the screen from the negative p direction, and trace out the lower lobe. They then go back off-screen in the negative p direction and repeat the cycle in the opposite direction. This ordering means that the entire structure is a single island.

[10] By "antimod" is meant the inverse of the modulo function. Since this is multi-valued, its application requires some discretion. For example, 2 antimod 3 $\in$ {2, 5, 8, ...}. So if there are three islands, and the hit order is 2, then $s/r \in$ {3/2, 3/5, 3/8, ...}. Figure 2.6 shows island chains for both $s/r=3/2$ and 3/5, and a 3/8 chain was observed but not included in this plot. The ambiguity of the antimodulo function is resolved by referring to the measured average of I for the orbit, and requiring that $I^3\omega=s/r$.

- The next two columns give the theoretical and (average) measured values of the action for the points in the island chain. In Section 2.3, an orbit was found to wind around in the extended phase space with winding number s/r if its action value, I, satisfied $I^3\omega=s/r$. These two columns test the hypothesis that the action and winding number are related by this formula.
- The last two columns give two different measures of the extent, in action, of the island chain. These measures are illustrated in Figure 2.9.
  - The *width* of an individual island is the largest difference in action value of *points appearing opposite each other* on the island. The width of a chain of islands is the largest width of all of its islands.
  - The *excursion* of an island chain is the overall difference in action encountered in traversing the whole chain.

The correct value of both the width and the excursion are obtained from measuring the outermost set of closed curves among the concentric curves forming the island (the *separatrix*). In compiling the data for the above table, and for the similar table in Section 2.5, it was always the objective to generate an island chain as close to the separatrix as possible for measurement. This is often quite difficult.

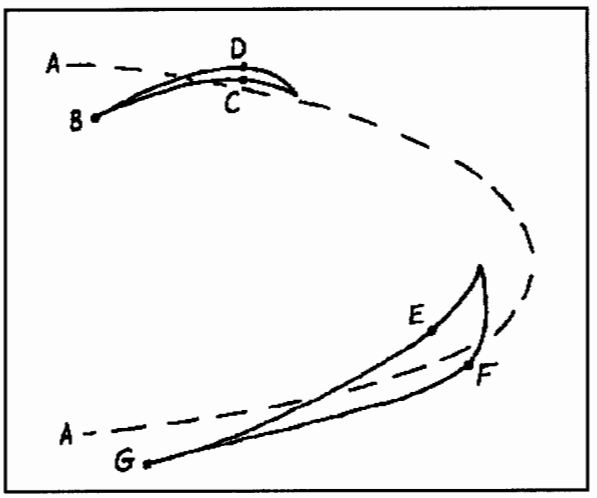

Figure 2.9. The two different measures of extent in action of a chain of resonance islands. The dotted line, A, is the line of constant action for the average value of the action in the chain. The pairs of points $\{C, D\}$ and $\{E, F\}$ appear opposite each other at the widest parts of the two islands. The point G has the largest value of action for this chain, the point B the smallest. The *width* of the chain is the largest width of all of its islands, i.e., I_F-I_E for this example. The *excursion* is the difference between the largest and smallest values of action in all of its islands, i.e., I_G-I_B here.

The combination of shapes shown here is an atypical exaggeration of the shape of an island chain, in order to express the meanings of *width* and *excursion*.

The excellent agreement between the theoretical actions (column 2) and the average measured actions (column 3) confirm what has been claimed by Jensen and others for many years: that the resonance zones in the HSH phase space are centered on the values of action given by rational values of $I^3\omega$.

The widths and excursions are important for observing the effect of increasing the strength of the perturbation. This is the subject of Section 2.5.

2.5 Higher perturbation strengths

This section presents Poincare sections of the HSH phase space for a series of perturbation strength. This yields important data on the effect of increasing the strength of the perturbation. These data are used to show, later in Section 5.2, that the widths of the stable regions in the experimental ionization data are explained by the growth of resonance zones.

In order to determine the effect of the perturbation strength on the HSH behavior, the same series of Poincare sections as in Figure 2.8 was attempted for three higher values of the microwave peak field strength, F. The results are shown in Figures 2.10.

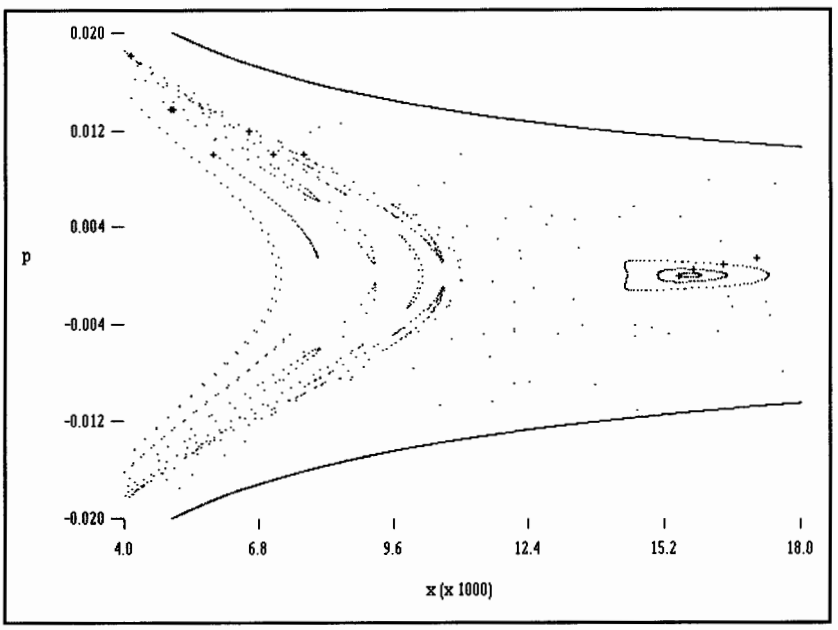

Figure 2.10(a). Strobe plot of HSH phase paths for various initial conditions, with $F=1.095\cdot10^{-9}$ (5.623 V/cm). This plot is equivalent to Figure 2.8, except for the increased perturbation strength and an expanded scale on the x axis.

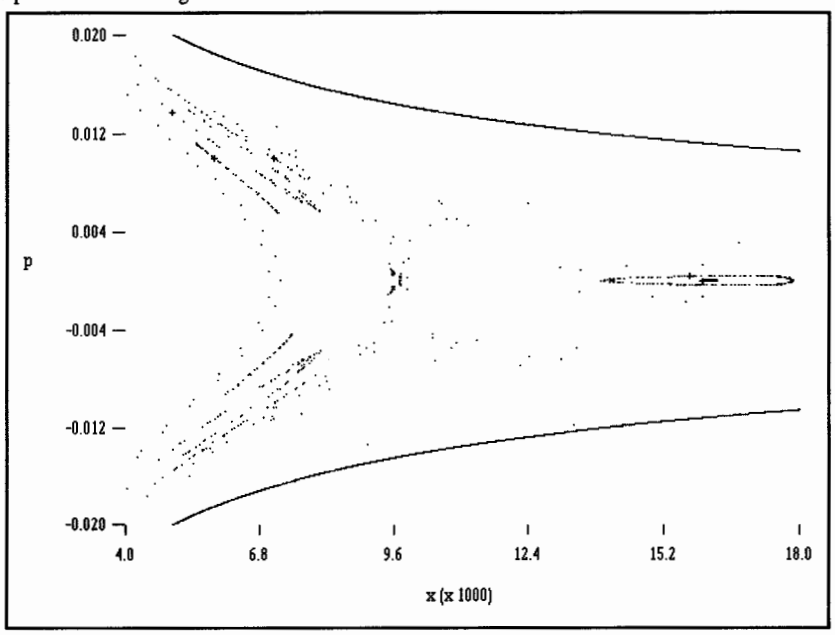

Figure 2.10(b). Strobe plot of HSH phase paths for various initial conditions, with $F=1.947\cdot10^{-9}$ (10.00 V/cm).

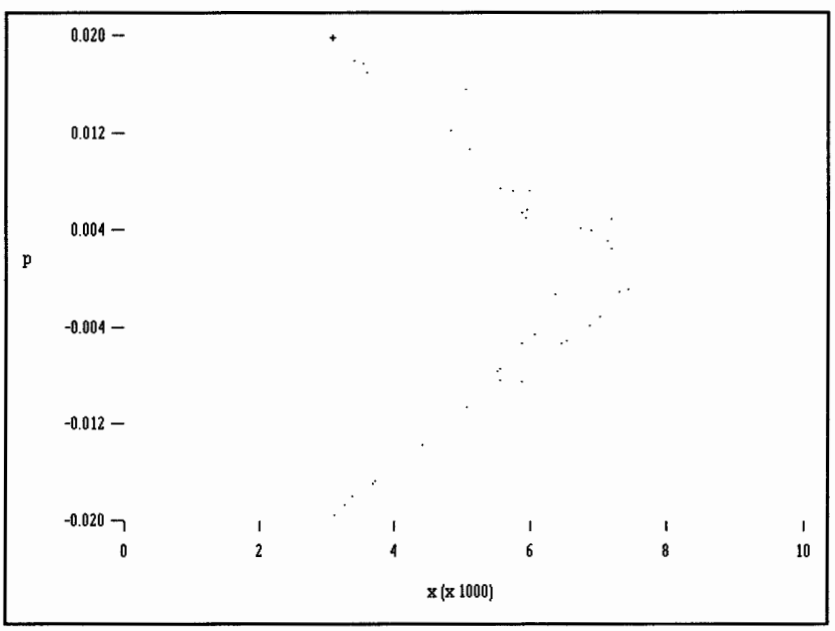

Figure 2.10(c). Strobe plot of HSH phase path with $F=0.6156\cdot10^{-8}$ (31.62 V/cm) for the only initial conditions that yield a nearly regular orbit.

The perturbation strengths used in these plots were chosen for comparison with the experimental data in Figure 1.1. The threshold field strengths are reported there as $\log_{10}F$, with F measured in volts/centimeter. The correspondences are:

The microwave peak field strengths used in the simulations			
Figure	F (atomic units)	F (V/cm)	$\log_{10}F$ (V/cm)
2.8	$1.947\cdot10^{-10}$	1.000	0.000
2.10(a)	$1.095\cdot10^{-9}$	5.623	0.750
2.10(b)	$1.947\cdot10^{-9}$	10.00	1.000
2.10(c)	$0.6156\cdot10^{-8}$	31.62	1.500

The results of these simulations are summarized in the following table. In each column for a single value of the perturbation strength, F, the three subcolumns correspond to the right three columns in the table in Section 2.4. The data in the column for $F=1.9\cdot10^{-10}$ just reproduces the data in that table.

Locations and extents in action of resonance islands for $\omega=1.5\cdot10^{-6}$ and various perturbation strengths												
	Measured action (average, width, excursion)											
s/r	$F=1.9\cdot10^{-10}$			$F=1.1\cdot10^{-9}$			$F=1.9\cdot10^{-9}$			$F=0.62\cdot10^{-8}$		
1/3	60.3,	0.0,	0.2	60.4,	0.3,	1.4	60.7,	0.6,	3.0	60.7,	4.0,	11.1
2/5	64.1,	0.0,	0.3	64.1,	0.0,	1.6	63.6,	0.1,	1.0			
1/2	69.1,	0.6,	1.1	69.6,	4.0,	6.3	70.0,	8.9,	14.2			
3/5	73.5,	0.1,	1.1	73.6,	0.3,	6.1	73.6,	0.7,	9.8			
2/3	76.0,	0.1,	1.2	76.3,	1.8,	8.1						
3/4	79.2,	0.1,	2.3	78.9,	1.0,	10.7			chaotic			
4/5	80.9,	0.1,	2.9		chaotic							
1	87.4,	11.9,	11.9	88.7,	8.2,	8.2	89.9,	11.1,	11.1			
4/3	95.9,	0.8,	2.5									
3/2	100.1,	1.9,	2.8									
5/3	103.4,	2.3,	4.3					chaotic				
2	110.1,	8.4,	8.4									
3	126.0,	8.0,	8.1									

Based on these data, the following general statements can be made about the effect of changing the perturbation strength:

- The widths and excursions both increase with the perturbation strength. (The apparent exception for $r/s=2/5$ is due to the difficulty of measuring the excursion of a very narrow island chain. The excursion measured for $r/s=4/5$ at $F=1.9\cdot10^{-9}$ is most likely too low.)
- The lower order resonances (those for which s and r are smaller) grow faster than those of the higher order ones. The 1/2 resonance grows the fastest, followed by the 1/3, 2/3, 3/4 and 3/5, in that order. (Again, the 2/5 seems to be an exception.)
- As the resonance zones grow, more and more of them decay into the "chaotic sea".

The strange behavior of the $s/r=1$ resonance, with the width getting first smaller and then larger again, is explained by looking at Figures 2.8, 2.10(a) and 2.10(b). The size of the zone is seen to consistently shrink as F is increased. The shrinkage is caused by the outer layers of the zone decaying into chaos. But while shrinking in overall size, the remaining layers of the

resonance zone also becomes stretched out (as seen in Figure 2.10(b)), causing the increase in "width".

These data are compared with the results of laboratory experiments in Section 5.2. It is shown there that the widths in the above table explain the widths of the regions of suppressed ionization in the space of energy levels of the hydrogen atom..

3 Classical HSH dynamics in action-angle coordinates

This chapter studies the classical behavior of the HSH atom in action-angle coordinates. In this perspective, the resonance structure of the phase space is directly manifested in the system energy. This structure takes the form of an infinite family of *primary resonances* which interact to cause further infinities of higher-order resonances. Since the action coordinate corresponds to the principal quantum number in quantum mechanics, this formulation of the problem provides a bridge between the theories in the physical phase space (Chapter 2) and in quantum mechanics (Chapter 4).

Section 3.1 reviews the dynamics of the unperturbed atom in action-angle coordinates, and lays out the graphical techniques for visualizing the motion in them. Section 3.2 discusses the primary resonance structure arising under the perturbation. Advantage is taken of the direct manifestation of this structure in Section 3.3, where the dynamics of individual primary resonance zones are studied independent of the others. The important *pendulum approximation* is developed for these individual resonances in Section 3.4. The interaction of two primaries, and the resulting secondary and higher-order resonances, are described in Section 3.5.

3.1 Action-angle coordinates of the unperturbed 1-dimensional hydrogen atom

This section reviews the dynamics of the unperturbed atom in action-angle coordinates, and lays out the graphical techniques for visualizing the motion in them.

The plots in Chapter 2 are made in the physical phase space of the unperturbed 1-dimensional hydrogen atom, and in the extended phase space derived from that space. By "physical" is meant that the coordinate of the motion is the physical separation distance, x, of the electron and proton. However, as is generally the case for a periodic system, the analysis of the motion is simplified by transforming to action-angle coordinates, which are designated here as (I, ξ). The action coordinate is:

$$I \equiv \frac{1}{2\pi} \oint p\, dx ,$$

where the integral is taken over one complete period of the motion. For a bound Kepler system, the action[1] is a simple function of the physical parameters of the system [801HGo, (10-133)]:

$$I = \sqrt{mka} = k\sqrt{-\frac{m}{2E_u}},$$

[1] For the 1-dimensional Kepler problem, this is *the* action coordinate. In two or three dimensions, this is the *principal* action, corresponding to the principal quantum number in quantum mechanics.

where m is the reduced mass of the 2-body system, k is the force coefficient, a is the semi-major axis of the orbit ellipse, and E_u is the energy of the system. For the hydrogen atom, in atomic units [Appendix D.1], this reduces to:

$$I = \sqrt{a} = \sqrt{-\frac{1}{2E_u}}.$$

The action coordinate is a constant of the motion for the unperturbed system. The expression for the action can be inverted to obtain the energy function in action-angle coordinates:

$$E_u(\xi, I) = E_u(I) = -\frac{1}{2I^2},$$

for which Hamilton's equations are:

$$\left\{ \begin{array}{l} \dfrac{d\xi}{dt} = \dfrac{\partial E_u}{\partial I} = \dfrac{1}{I^3} \\ \\ \dfrac{dI}{dt} = -\dfrac{\partial E_u}{\partial \xi} = 0 \end{array} \right\}.$$

The motion for any initial condition, (ξ_0, I_0), is simply a rotation, at constant angular frequency $d\xi/dt = 1/I_0^3$, around an orbit of constant radius I_0.

In action-angle coordinates, the three orbits of Figure 2.1 appear simply as shown in Figure 3.1. In this plot, and all the polar plots in this chapter, the outermost circle is not data, but is just a border for the data area of the plot.

As does Figure 2.1 in the physical phase space, this plot illustrates the basic underlying motion of the HSH atom in the limit of no perturbation, but this time from the action-angle perspective.

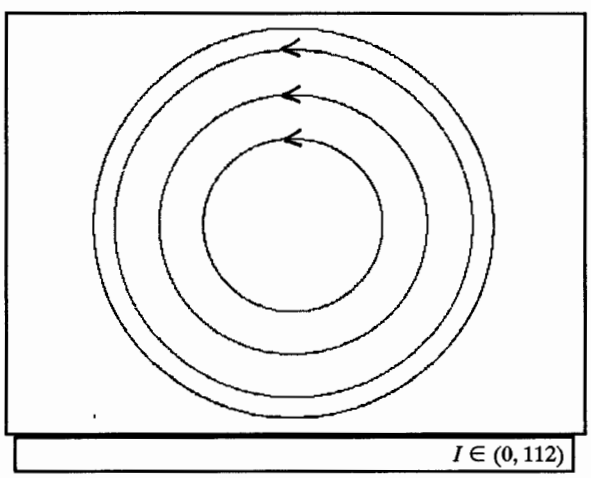

Figure 3.1. Three phase paths of an unperturbed 1-dimensional hydrogen atom, plotted in its action-angle space. The orbits shown have action 50, 75, and 100, and are thus the same orbits as those shown in Figure 2.1.

The outer circle is, as in all polar plots in this chapter, not an orbit, but just the boundary of the data region of the plot.

When the HSH perturbation is added to the energy of the 1-dimensional hydrogen atom, the resulting motion is best understood in the context of the 4-dimensional *extended phase space* [§D.2]. In that analysis, the atom moves on a 2-torus embedded in this 4-dimensional phase space. The tori form a concentric family that fills the phase space, with each of the circles in Figure 3.1, though distorted by the perturbation, appearing as a

cross-section of one such torus. The resonances which are the main focus of this chapter arise as interstitial families of mutually concentric tori, which grow between the members of the original family of tori. This structure is illustrated in Figure 2.7 in Chapter 2.

Another way to view the motion is to plot the angle coordinate itself as a function of time, as shown in Figure 3.2. Although the action coordinate is not directly plotted here, it is unambiguously represented for each orbit by the slope of the corresponding function.[2] This slope is equal to the angular frequency of the system in its action-angle phase space:

$$\frac{d\xi}{dt} = \frac{1}{I^3}.$$

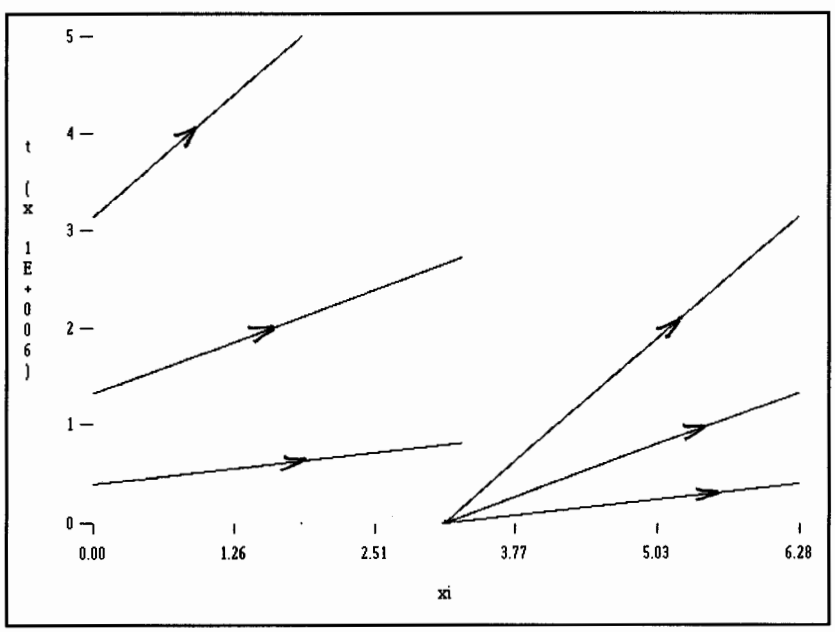

Figure 3.2. Time evolution of the angle coordinate for three orbits of the unperturbed 1-dimensional hydrogen atom. The orbits are the same as those shown in Figures 2.1 and 3.1, with action coordinates 50, 75 and 100.
For comparison with the plots in Figure 3.6, the extent of the time coordinate corresponds to the period of a perturbation with frequency $\omega = 2\pi/(5 \cdot 10^6)$.

In this plot, the angle coordinate is intrinsically periodic, while the time coordinate extends without limit in both directions. Although the unperturbed atom is time-periodic, there is no natural frequency in the phase space, because the frequency of the atom varies with the value of the action coordinate. When the perturbation is applied however, the behavior takes on, in addition to the action-dependent periodicity of the underlying motion, a time-periodic response to the electromagnetic wave. It is this double periodicity that constrains the motion to the tori mentioned in conjunction with Figure 3.1 above. Advantage can be taken of the topological property of a torus, that it is equivalent to a rectangle with opposite sides identified, to plot the motion on such a torus. This is done by plotting exactly in the manner of

[2] This coincides with the fact that this plot is essentially a *space-time diagram* for the angle coordinate of the hydrogen atom. As such, the slope of a trajectory gives the speed of the system; the speed in this case means the angular frequency of the system point in the action-angle coordinates of the phase space.

Figure 3.2, but with the time coordinate plotted modulo $2\pi/\omega$, where ω is the frequency of the perturbing wave. This technique is used in Figure 3.6, alongside the polar action-angle plots of Figures 3.4 and 3.5, to illustrate the behavior of the HSH atom.

3.2 Primary resonance structure of the HSH phase space

This section discusses the primary resonance structure arising in action-angle coordinates under the HSH perturbation.

The HSH energy is obtained by adding to the energy of 1-dimensional hydrogen the perturbation of an electromagnetic wave polarized along the axis of the atom. This can be written in the action-angle coordinates of the unperturbed atom using the results of Appendix D.3:

$$E(\xi, I, t) = -\frac{1}{2I^2} + F x(\xi)\cos(\omega t)$$

$$= -\frac{1}{2I^2} + \frac{FI^2}{2}\cos(\omega t)\sum_{M=-\infty}^{\infty} A_M \cos(M\xi) \qquad ; \left\{ \begin{array}{c} A_0 = -3 \\ A_{M\neq 0} = \dfrac{2J'_M(M)}{M} \end{array} \right\}$$

$$= -\frac{1}{2I^2} + \frac{FI^2}{2}\sum_{M=-\infty}^{\infty} A_M \cos(M\xi - \omega t)\,,$$

where $J'_M(z)$ is the first derivative of the Bessel function of the first kind, taken with respect to z and evaluated at z. The values of the first few coefficients in the expansion are [page 94]:

Coefficients in the expansion of the 1-dimensional Kepler motion

$\lvert M\rvert$	A_M
0	−3.0
1	0.650
2	0.224
3	0.118
4	0.0745
5	0.0520

The above form of the HSH energy offers an alternative perspective on the cause of the resonance structure in the HSH phase space, as seen in Figure 2.8. The perturbation takes the form of an infinite superposition of rotating cosine potentials, indexed by the integers, including a zeroth order, standing cosine potential. The M'th cosine potential in the series has amplitude $FI^2A_M/2$ and rotates (except for M=0) with angular frequency ω/M. This frequency is either positive or negative (meaning an either counterclockwise or clockwise sense of rotation), according to the relative sign of M and ω.

These rotating potentials are acting on a system which, in its unperturbed state, is itself rotating in phase space in a counterclockwise direction with angular frequency $d\xi/dt = 1/I^3$ [§3.1]. If the perturbation is weak (i.e., $FA_M \ll 1/I^4$ for all M), so that the perturbed behavior can be described in terms of moderate deviations from the unperturbed behavior, and if the system is given an initial condition such that $I \approx (M/\omega)^{1/3}$ for some M, then the rotation of the system and the rotation of the M'th cosine potential are approximately synchronized. This causes a resonant response of the system to that particular (the M'th) term of the perturbation.

The resonance phenomenon which occurs here is *nonlinear*, so it incorporates both a stabilizing feedback mechanism and a progressive breakdown of phase stability [§1.1]. The stabilizing feedback means that there is an annular[3] region around each $I=(M/\omega)^{1/3}$, called a *resonance zone*, characterized by an oscillation of I about the resonant value, $I=(M/\omega)^{1/3}$, with a concomitant oscillation of $d\xi/dt$ about $1/I^3$. Whereas in a linear resonance phenomenon, the response is infinite at the exact resonant value (hence *instability*), this oscillatory behavior means that the response is zero at $I=(M/\omega)^{1/3}$ (hence *stability*). The breakdown of stability occurs when the perturbation is strong enough that a particular trajectory resonates to more than one term of the perturbation. Heuristically, this can be seen in terms of the interaction of neighboring resonance zones as they grow closer together under the increasing strength of the perturbation.

The resonances discussed in this section are called *primary resonances*. In Section 3.5, it is shown that interactions of neighboring resonances lead again to an identical resonance structure. Structures arising from the interaction of two primaries are *secondary* resonances. Higher order structures likewise appear.

If the perturbation is weak enough, then in each resonance zone the effect of the perturbation is dominated by one particular term. That is, in each annular region satisfying $I \approx (M/\omega)^{1/3}$, the atom resonates to the M'th cosine potential in the perturbation. In each such region the other terms can be neglected, and the effective energy is:

$$E^{(M)}(\xi, I, t) = -\frac{1}{2I^2} + \frac{FI^2 A_M}{2}\cos(M\xi - \omega t)\,. \qquad \textit{Singly-resonant HSH energy}$$

In parts of the phase space that are outside of any resonance zone, the effect of this perturbation is minimal. One can use this energy to study the dynamics under each individual term of the perturbation, independent of the others. This is the subject of Section 3.3.

Under a stronger perturbation the resonance zones overlap, and so there are regions in which the atom resonates to more than one term. In these regions the condition $I \approx (M/\omega)^{1/3}$ is satisfied for more than one value of M. Then all of the corresponding terms must be included in the energy, but the others can be neglected:

$$E(\xi, I, t) = -\frac{1}{2I^2} + \frac{FI^2}{2}\sum_M A_M \cos(M\xi - \omega t)\,,$$

[3] A resonance zone is annular, in that it is a neighborhood of the circle $I=(M/\omega)^{1/3}$. But it *not* an annulus, i.e., its boundaries are not circles. The shape of the resonance zones is discussed in Section 3.4.

where the sum is over the resonant terms of the perturbation. This form of energy can be used to study the dynamics under particular combinations of perturbation terms, independent of all others. This is done for two terms in Section 3.5.

This section has discussed the existence of resonance zones, and their locations. As discussed so far, a resonance zone is an annular region defined by $I \approx (M/\omega)^{1/3}$. But there is no clue here as to the meaning of the approximation symbol in that expression, and therefore no way to calculate the radial width, nor the shape, of such a zone. These matters are discussed in Section 3.4.

3.3 The singly-resonant HSH system in classical mechanics

This section takes advantage of the direct manifestation of the resonance in the HSH energy by studying the dynamics of individual primary resonance zones independent of the others.

If the HSH perturbation is weak enough, then in each resonance zone the effect of the perturbation is dominated by one particular term. In such a region the effective energy is:

$$E^{(M)}(\xi, I, t) = -\frac{1}{2I^2} + \frac{FI^2 A_M}{2}\cos(M\xi - \omega t)\,. \qquad \textit{Singly-resonant HSH energy}$$

This energy can be used to study the HSH dynamics under each individual term of its perturbation, independent of the others.

Figure 3.3, on the right, shows the motion of the singly-resonant HSH system for $M=1$ in the neighborhood of the first primary resonance. The behavior is similar to that seen in Figure 2.4 in Chapter 2 for the full HSH in its physical phase space. The orbit executes an approximately periodic motion, wandering away from its initial configuration, and then coming almost back again.

The graphic domain of Figure 3.3 is magnified in the I coordinate, with the radial component running the range indicated under the bottom right corner.

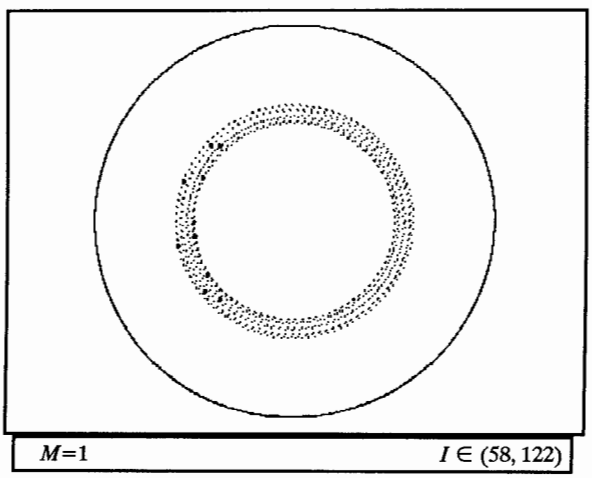

Figure 3.3. Phase path of the singly-resonant HSH system with $M=1$, $F=2\cdot10^{-10}$ (1.0 V/cm) and $\omega=2\pi/(5\cdot10^6)$ ($\nu=8.26$ GHz). The initial action value is $I=90$, just below the first primary resonance at $I=92.6$.

The large dots are strobe points of the orbit, i.e., they are the phase points of the system at integer multiples of the period of the perturbing wave, $2\pi/\omega=5\cdot10^6$.

This plot, and all the polar plots in this chapter except Figure 3.1, use a graphic distortion to increase their useful area. Since the regions of interest, those where the resonance zones are located, have fairly high values of the action, the center of the (I, ξ) polar plane is of little interest. A (large) neighborhood of the origin is therefore deleted, which amounts to a magnification of the I scale of the data. Each polar plot in this chapter shows, just below the lower right hand corner, the range of action represented by the radial component of the graph. An orbit of constant action equal to the lower number in this range would appear as a single point at the center of the plot.

The orbit shown here crosses itself several times in just the 10 periods plotted. This means that the phase space of the unperturbed atom, which is the space in which the plot is made, is *not* the phase space for this perturbed system. The correct phase space is the *extended phase space* described in Appendix D.2. In that 4-dimensional space, the orbits take the form of 2-dimensional tori. One circumference of such a torus corresponds to the underlying atomic motion of the electron with respect to the proton. This circumference is coordinatized by ξ, with intrinsic period 2π. The other circumference corresponds to the variation of this motion under the perturbation of the

electromagnetic wave. The coordinate for this circumference is t (time); its periodicity is that of the perturbation, $2\pi/\omega$.

The problem with Figure 3.3 is that it projects the entire motion around the torus onto a single plane slicing through it. This does not provide a useful or instructive view of the motion. This is the same as the problem with Figure 2.4 in the physical phase space.

There are three ways to usefully organize the data represented in Figure 3.3:

- Plot the orbit in the rest frame of the cosine potential, i.e., in a frame of reference that is rotating with the angular phase velocity of the cosine potential: ω/M. This phase velocity, or angular frequency, is the same as that with which the orbit torus winds its way through the extended phase space. This method works because the singly-resonant HSH system is integrable [§1.2]. (This is proven in Section 3.4.) This means that, while the extended phase space is useful for making the connection to the full HSH behavior, the phase space of the singly-resonant HSH system is really just 2-dimensional, and is obtained by rotating the unperturbed phase space as described above.
- *Strobe* the motion at the frequency of the perturbation, ω. As in Chapter 2, this yields a Poincare section [§1.2] by slicing through the 4-dimensional phase space with a single copy of the 2-dimensional unperturbed phase space.
- Plot the orbit on the torus. In Chapter 2, it was possible to plot the torus in three dimensions by eliminating one of the extended phase space coordinates, $-E$. Here, two coordinates, I and $-E$, can be eliminated, and the torus can be plotted in two dimensions as a rectangle. This is the method described in conjunction with Figure 3.2 above.

The results of these three techniques are shown for three different values of M in Figures 3.4, 3.5 and 3.6. The values of the perturbation peak field strength and frequency are the same here as in Figure 3.3.

Resonance zones are clearly visible in these plots. The orbit shown above in Figure 3.3 is the same orbit that yields the banana-shaped crescent in the $M=1$ frames of Figures 3.4 and 3.5 below. The first few phase points that form that crescent are shown as enlarged dots in Figure 3.3.

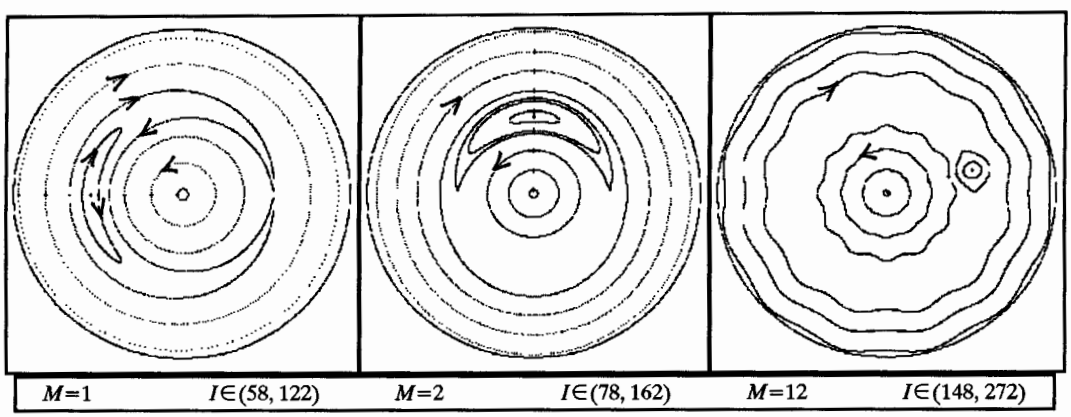

Figure 3.4. Phase paths of the singly-resonant HSH system, in a frame of reference that is rotating along with the cosine potential. The perturbation parameters are the same as in Figure 3.3. The sense of motion, indicated by arrowheads placed on the orbits, is (a) inside the resonance zone, clockwise about the center of the zone, (b) below the zone, counterclockwise about the origin, and (c) above the zone, clockwise about the origin.

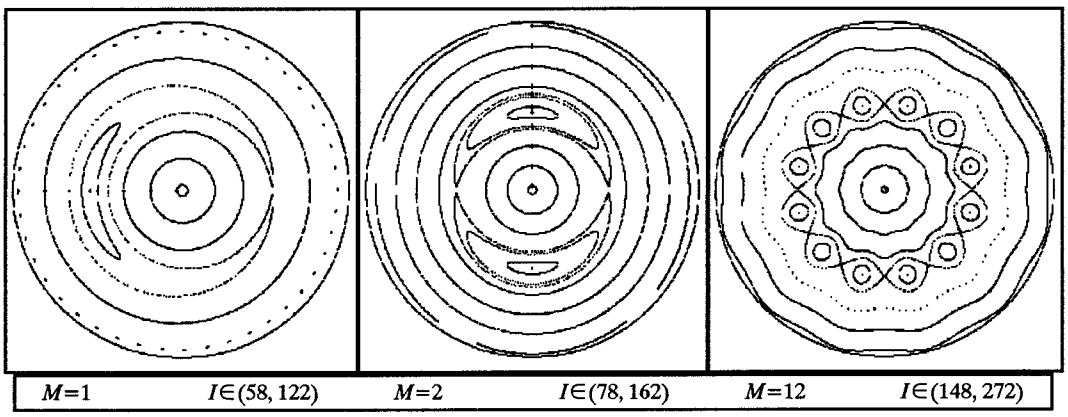

Figure 3.5. Strobe plots for the singly-resonant HSH system, for three different resonances. The perturbation parameters are the same as those used in Figure 3.3 and 3.4.

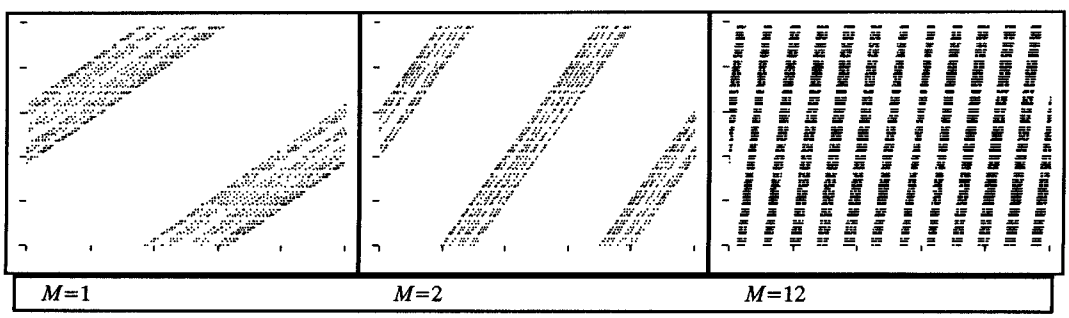

Figure 3.6. Plots of the motion of the singly-resonant HSH system on its 2-dimensional tori, for three different resonances. The perturbation parameters are the same as those used in Figures 3.3, 3.4 and 3.5. The extents of the graphs are the same as in Figure 3.2.

The plots in Figures 3.4 and 3.5 are identical excepts that the strobe plots show M copies of the M'th resonance zone, while the rotated plots only show one. This is because the strobe frequency is consistently $\omega/2\pi$. Strobe plots made at strobe frequency ω/M have exactly the same appearance as the rotated plots in Figure 3.4. On the other hand, the rotated plots could generate all M copies of the resonance zones if M different initial values of ξ were used for each initial value of I, instead of just one. (It does not work to increase the rotation frequency to ω because this does not yield a rest frame of the cosine potential.)

The rotating frame plots of Figure 3.4 are interesting to consider in the light of the theoretical considerations of Section 3.4 (*Pendulum Approximation*), because they show by inspection that in their frame of reference the singly-resonant HSH system clearly exhibits the behavior of a pendulum.

Of the three techniques, only the stroboscopic method can be applied to the HSH system with more than one term in the perturbation.

In the 4-dimensional geometry of the extended phase space, the meaning of these pictures is that a concentric family of interstitial tori has grown up in the midst of the original family of tori. (See Figure 2.7.) The family for the M'th resonance wraps around inside the stable tori M times before connecting back up with itself. This is the reason for the appearance of M families of interstitial closed curves in each plot; every set of M interstitial curves is

actually the Poincare section of a single torus. For example, in the plot for $M=12$, the twelve circles are all parts of the Poincare section of a single torus.

Alternatively, these pictures can be viewed in terms of the discrete mapping in the (I, ξ)-polar phase plane. From this point of view, the structure seen is consistent with the Poincare-Birkhoff theorem [830AJL, 168]. The unperturbed trajectory for $I=(M/\omega)^{1/3}$ is a repeated point for any value of ξ, and the trajectories on either side of it advance in opposite senses. By this theorem, the fact that the adjacent trajectories are preserved implies that there must remain in the vicinity of $I=(M/\omega)^{1/3}$ a set of pairs of elliptic (stable) and hyperbolic (unstable) repeated points.

The relationship between the discrete mapping and the extended phase space is:

- The elliptic points of the mapping are together the Poincare section of the degenerate torus[4] at the center of the concentric family of interstitial tori.
- The boundary between the original and the interstitial tori (the *separatrix*) is a torus that winds around inside the original tori just tightly enough to touch itself along a 1-dimensional curve. The hyperbolic points of the discrete mapping are together the Poincare section of this osculating curve.

It is of crucial importance to note that all of the strobe plots for the isolated resonances indicate that all orbits are confined to tori, since the strobe points for each orbit lie on definite 1-dimensional curves. This constitutes empirical evidence that the singly-resonant HSH system is integrable [§1.2], with two constants of the motion. The same conclusion is reached on theoretical grounds in Section 3.4.

The location of each resonance is the I-coordinate of the elliptic points. This is the I-coordinate of the degenerate torus at the center of the concentric family of interstitial tori. According to the theory in Section 3.2, the center of the M'th primary resonance should be at $I=(M/\omega)^{1/3}$. The width of each zone is the difference in values of I encountered in an orbit close to the separatrix. The pendulum approximation is used in Section 3.4 to predict the widths of the primaries. The following table compares the theoretical estimates of these quantities with the values measured from the plots in Figures 3.4 and 3.5:

Locations and widths of some primary resonances for $F=2\cdot10^{-10}$, $\omega=2\pi/(5\cdot10^6)$
(classical theory and classical simulations)

M	Location, I_M		Width, $2\Delta_M^{res} I$	
	Theoretical, $(M/\omega)^{1/3}$	Measured	Theoretical, $\frac{4M}{\omega}\sqrt{\frac{FA_M}{6}}$	Measured
1	92.7	92.6	14.8	15.0
2	117	116	17.4	18.4
12	212	213	24.4	25.0

The results of the simulations are seen to be in good agreement with the predictions.

[4] A degenerate torus is one in which one (or more) radius is zero. The case considered here, a singly degenerate 2-torus, is a closed, 1-dimensional curve.

3.4 The pendulum approximation for the singly-resonant HSH system

This section presents a method for calculating the shape and radial width of the primary resonance zones. This method, the *pendulum approximation*, is originally due to Zaslavskii and Chirikov [719GMZ, §2.2].

The M'th primary resonance zone is an annular neighborhood of the circle $I=(M/\omega)^{1/3}$. In this region, the amplitude of the perturbation can be approximated[5] in terms of, and the unperturbed energy can be expanded about, this resonant value of the action, $I_M \equiv (M/\omega)^{1/3}$:

$$E^{(M)}(\xi, I, t) \approx -\frac{1}{2I_M^2}\left[1 - 2\frac{\Delta_M I}{I_M} + 3\left[\frac{\Delta_M I}{I_M}\right]^2\right] + \frac{FI_M^2 A_M}{2}\cos(M\xi - \omega t),$$

where $\Delta_M I \equiv I - I_M$.

In this expression, the first term in the larger brackets contributes only an additive constant to the energy, and so has no effect on the dynamics. The second term in the larger brackets can be eliminated by a time-dependent canonical transformation which shifts the zero of momentum to I_M and boosts the coordinate into the rest frame of the resonant cosine potential. The generating function of the transformation is:

$$G_M(\xi^{(M)}, I, t) = -\frac{\Delta_M I}{M}(\xi^{(M)} + \omega t),$$

with the result [801HGo, (9-20)]:

$$\left\{\begin{aligned} I^{(M)} &= -\frac{\partial G_M}{\partial \xi^{(M)}} = \frac{\Delta_M I}{M} \\ \xi &= -\frac{\partial G_M}{\partial I} = \frac{\xi^{(M)} + \omega t}{M} \quad \Rightarrow \quad \xi^{(M)} = M\xi - \omega t \\ E^{(M)}(\xi^{(M)}, I^{(M)}) &= E^{(M)}(\xi, I, t) + \frac{\partial G_M}{\partial t} \\ &= E^{(M)}(\xi, I, t) - \frac{\Delta_M I \omega}{M} = E^{(M)}(\xi, I, t) - \frac{\Delta_M I}{I_M^3} \end{aligned}\right\}.$$

The new coordinate system is not polar, but Euclidean:

- $I^{(M)}$ takes on both positive and negative values, and

[5] Note that the approximation for the amplitude of the perturbation is of zeroth order, while that for the unperturbed energy is of second order. There is no justification for this discrepancy in the method other than that it works.

- $\xi^{(M)}$ is not periodic. (Although the new energy, $E^{(M)}$, shown below, is periodic in $\xi^{(M)}$, this coordinate is not *intrinsically* periodic as is ξ.)

The $\xi^{(M)}$ axis is formed from multiple copies of the circle $I=I_M$ cut open and laid end-to-end. The $I^{(M)}$ axis is limited in valid extent[6] by the assumption that the perturbation is small (which implies that $\Delta_M I$, and therefore $I^{(M)}$, are small). Expressed in these coordinates, the energy is:

$$E^{(M)}(\xi^{(M)}, I^{(M)}) = E_u(I_M) - \frac{3M^2}{2}\frac{I^{(M)2}}{I_M^4} + \frac{FI_M^2 A_M}{2}\cos(\xi^{(M)})$$

$$\equiv E_M - \frac{I^{(M)2}}{2m_M} + F_M\cos(\xi^{(M)}),$$

where $E_M \equiv E_u(I_M) = -1/(2I_M^2)$, $m_M \equiv I_M^4/(3M^2)$ and $F_M \equiv FI_M^2 A_M/2$. The important fact that this energy[7] is time-independent means that the singly-resonant HSH atom is, to the extent that the approximations used above are valid, integrable [§1.2]. This explains why the Poincare sections in Figure 3.5 are closed curves, and why it is possible to plot the singly-resonant orbits in the 2-dimensional phase space of Figure 3.4.

The last form of the energy shown above is the energy of a pendulum with mass (or moment of inertia) m_M and peak force (or moment of weight) F_M. This is a key feature of the HSH system, discovered by Zaslavskii and Chirikov [719GMZ, §2.2], that *the behavior under a single term of the perturbation is approximated by the behavior of an unperturbed pendulum.* This means that the singly-resonant HSH energy can be written in the action-angle coordinates of this pendulum. For conformity with the discussion in Appendix D.4, the pendulum energy is written in the form:

$$E^{(M)'}(\xi^{(M)}, I^{(M)}) = \frac{I^{(M)2}}{2m_M} + F_M\left(1 - \cos(\xi^{(M)})\right).$$

If the action-angle coordinates of the pendulum are called $(\zeta^{(M)}, J^{(M)})$, then the relationship between the original HSH energy, $E^{(M)}$, and the energy of the HSH pendulum, $E^{(M)'}$, is:

$$E^{(M)'}(J^{(M)}) = E^{(M)'}(\xi^{(M)}, I^{(M)}) = -E^{(M)}(\xi^{(M)}, I^{(M)}) + E_M + F_M,$$

The energy $E^{(M)'}(J^{(M)})$ is the inverse of the function giving the action of a pendulum with mass m_M and peak force F_M. The algebraic and graphical form of this function are discussed in Appendix D.4. This form of the HSH energy is used in Section 3.5, where interaction of neighboring resonances is considered.

---

[6] An indication of the valid range of $I^{(M)}$ is given by the rightmost column (% error) of the tables in Appendix C.

[7] This is often called the *quasienergy*.

The phase paths of a pendulum form two topologically distinct regions[8] in its phase space in which the behavior is, respectively, oscillation and rotation. In the rotational region, the trajectories have the same topology as those of the unperturbed motion in the (I, ξ)-polar coordinates of the phase space. On the other hand, the resonant response of the system to the single-term perturbation is oscillatory. (See the discussion of *stability* on page 35.) Therefore, the conjecture is made that the pendulum separatrix, the boundary between oscillatory and rotational motion, provides a natural boundary for the resonance zone.

The shape of a resonance zone can be understood by translating this conjecture back to the HSH action-angle coordinates. This means returning to polar coordinates, shifting the zero of momentum away from I_M back down to $I=0$, and boosting back to an angular frequency of $1/I_M^3$. The result for the M'th zone is a pattern of M periods of the pendulum oscillatory region bent around the circle $I=I_M$, and rotating around that circle with angular frequency $d\xi/dt=1/I_M^3$. For small M, the resonant orbits appear as rotating crescents. For larger M, they appear more circular, and form a rotating rosette pattern around the phase space. The computer simulations in Figure 3.5 demonstrate these shapes very nicely for several individual resonances. This shows that the pendulum approximation is valid, at least for the parameters of those calculations.

The half-width of a particular resonance zone is therefore just the amplitude of the corresponding pendulum separatrix, which is proportional to the maximum value of the pendulum momentum:

$$\Delta_M^{\text{res}} I = MI_{\max}^{(M)} = 2M\sqrt{m_M F_M} = 2I_M^3\sqrt{\frac{FA_M}{6}} = \frac{2M}{\omega}\sqrt{\frac{FA_M}{6}}.$$

Note that the width of a resonance zone goes as the square root of the strength, F, of the perturbation. This is significant because it means that a change in the perturbation strength has a disproportionately smaller impact on the dynamics.

This prediction of the widths of the resonance zones is compared to the outcome of the numerical simulations in the table in Section 3.3. The agreement is excellent.

[8] There are two regions, not three. The region of rotation is disjoint, lying both above and below the region of oscillation.

3.5 The doubly-resonant HSH system in classical mechanics

This section describes the interaction of two primary resonance zones, and discusses the resulting secondary and higher-order resonances. The method used here is originally due to Escande and Doveil [811DFE; 813DFE].

The interaction of neighboring resonance zones is the route to chaos in the HSH atom and similar quasi-integrable systems [§1.2]. The simplest way to study such interactions is to consider the HSH energy with two terms included in the perturbation:

$$E^{(M,N)}(\xi, I, t) = -\frac{1}{2I^2} + \frac{FI^2}{2}\left(A_M \cos(M\xi - \omega t) + A_N \cos(N\xi - \omega t)\right).$$

Doubly-resonant HSH energy

Another reason for studying this energy is that it approximately governs the behavior of the HSH system in a region of phase space in which there are two, and only two, primary resonances near each other.

If the M'th and N'th resonances are close enough, then the pendulum approximation [§3.4] can be applied arbitrarily to either one and still be valid in the region of the other. If the approximation is applied to the M'th resonance, the result is:

$$E^{(M,N)}(\xi^{(M)}, I^{(M)}, t) = E_M - \frac{I^{(M)^2}}{2m_M} + F_M \cos(\xi^{(M)}) + F_{M,N} \cos\left[\frac{N}{M}\xi^{(M)} + \frac{N-M}{M}\omega t\right],$$

where $F_{M,N} \equiv FI_M^2 A_N/2$. This is the energy of a pendulum with the parameters discussed in Section 3.4, plus a perturbation arising due to the N'th term of the HSH perturbation. The new perturbation is a rotating cosine potential in the *pendulum* phase space, $(I^{(M)}, \xi^{(M)})$, with amplitude $F_{M,N}$ and angular frequency $\frac{M-N}{N}\omega$. Note that this energy is periodic in $\xi^{(M)}$ with period $2M\pi$.

The dynamics of this system can be most easily studied by transforming to the action-angle coordinates of the unperturbed pendulum, $(J^{(M)}, \zeta^{(M)})$. The first three terms above are simply the unperturbed energy $E^{(M)}(\xi^{(M)}, I^{(M)}) = E_M + F_M - E^{(M)'}(J^{(M)})$ [§3.4]. The last term, the perturbation term, can be transformed by considering the pendulum coordinate, $\xi^{(M)}$, to be a function of the action-angle coordinates $(J^{(M)}, \zeta^{(M)})$, and then expanding the cosine in a Fourier series in $\zeta^{(M)}$. This is done assuming that the cosine has the same periodicity in $\zeta^{(M)}$ that the whole energy has in $\xi^{(M)}$, i.e., that it is periodic in $\zeta^{(M)}$ with period $2M\pi$. This is true at least in the limit as F goes to zero, in which limit $\zeta^{(M)}$ reduces to $\xi^{(M)}$.

The expansion of the perturbation term is performed using a formula given in Appendix D.5. With that result, the energy of the doubly-resonant HSH atom, in the action-angle coordinates of the M'th HSH pendulum, is:

$$E^{(M,N)}(\zeta^{(M)}, J^{(M)}, t) = E_M + F_M - E^{(M)'}(J^{(M)}) + F_{M,N} \sum_{n=-\infty}^{\infty} C_n(J^{(M)}) \cos\left[\frac{n}{M}\zeta^{(M)} + \frac{N-M}{M}\omega t\right].$$

This has the same structure as was derived for the whole HSH energy [§3.2]: an infinite superposition of rotating cosine potentials, indexed by the integers, including a zeroth order, standing cosine potential. The n'th cosine potential in the series has amplitude $F_{M,N}C_n(J^{(M)})$ and rotates (except for $n=0$) with angular frequency $\frac{M-N}{n}\omega$. This frequency may be either positive or negative (meaning an either counterclockwise or clockwise sense of rotation).

These rotating potentials are acting on a system which, in its unperturbed state, is itself rotating in its phase space in a counterclockwise direction with the angular frequency $d\zeta^{(M)}/dt$ calculated and graphed in Appendix D.4. If the perturbation is weak enough that the perturbed behavior can be described in terms of moderate deviations from the unperturbed behavior, and if the system is given an initial condition such that $\frac{d\zeta^{(M)}}{dt} \approx \frac{M-N}{n}\omega$, then the rotation of the system and the rotation of the n'th cosine potential are approximately synchronized. This causes a resonant response of the system to that particular (the n'th) term of the perturbation.

The resonances arising in the above energy are called secondary resonances, because they arise from the interactions of primary resonances. This is the base of a self-similar structure of infinitely many higher-order resonances.

3.5.1 Locating the secondary resonances

Secondary resonances arise from the same mathematical structure as primary resonances: the interaction of a rotating system (the pendulum of Section 3.4) with an infinite series of rotating cosine potentials. Resonance occurs between the M'th and N'th primary resonances when the angular frequency of the "pendulum" of the M'th primary in its action-angle space is close to the rotation frequency of one of the cosine potentials arising due to the interaction with the N'th primary. This condition is, for the n'th cosine potential [pages 45 and 97]:

$$\frac{M-N}{n}\omega \approx \frac{d\zeta^{(M)}}{dt} = \left\{ \begin{array}{ll} \pi\sqrt{\frac{F_M}{m_M}}\frac{1}{E_{1C}(k^2)} & \text{, for } k \le 1 \\ \pi\sqrt{\frac{E^{(M)'}}{2m_M}}\frac{1}{E_{1C}\left(\frac{1}{k^2}\right)} & \text{, for } k \ge 1 \end{array} \right\},$$

where E_{1C} is the complete elliptic integral of the first kind and $k \equiv \sqrt{E^{(M)'}/(2F_M)}$. Thus the condition for resonance is that the angular frequency of the pendulum (the quantities in the large brace brackets above) divided by ω be a rational number. While this resonance condi-

tion is in terms of the pendulum energy, $E^{(M)'}$, it can be expressed approximately in terms of the unperturbed action, I, by the following numerical procedure. The results are tabulated in Appendix C.

Numerical procedure

Figures D.2 and D.3 [page 97] graph the action and the angular frequency of a pendulum, both versus the pendulum energy. The data points in these two graphs can be correlated to produce a graph of angular frequency versus action. The result is:

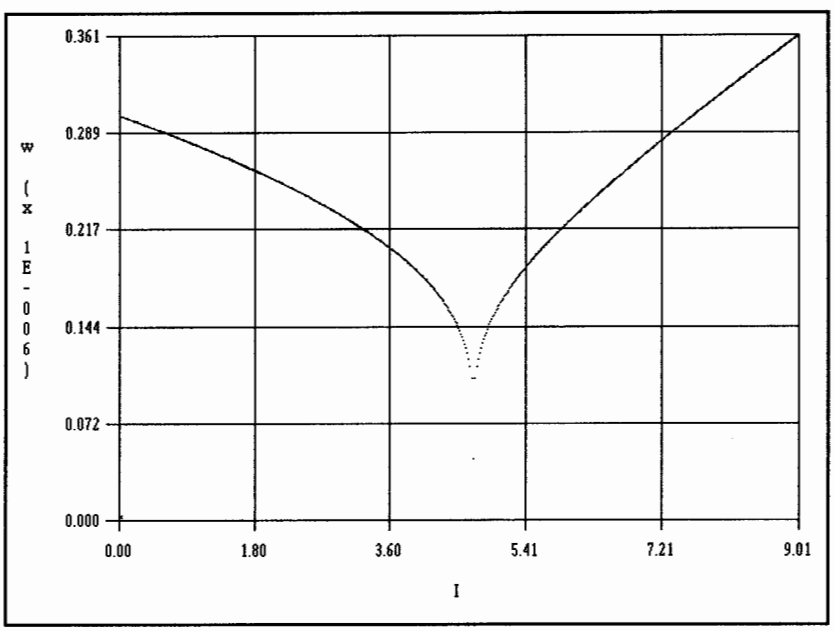

Figure 3.7. Plot of the angular frequency of a pendulum in its action-angle space, as a function of its action. This plot is made by eliminating the energy between two graphs of the type of Figures D.2 and D.3 [page 97], but with numerical values calculated for the theoretical pendulum arising in the approximation of the singly-resonant HSH with $M=1$, $\omega=2\pi/(5\cdot10^6)$ and $F=2\cdot10^{-10}$.

The axis labels, "I" and "w", representing the action and the angular frequency of the pendulum, correspond in the HSH theory to $J^{(M)}$ and $d\zeta^{(M)}/dt$, respectively.

The resonance condition is now that the values along the vertical axis of this graph, divided by ω, i.e. the values of $\dot{\zeta}^{(M)}/\omega$, are rational numbers. A routine was written to pick out each value of this quantity that is closest to a rational number with a denominator of from 1 through 5. For those values of $\dot{\zeta}^{(M)}/\omega$, the stored value of $E^{(M)'}$, which was the independent variable used to calculate the data on both axes of the above graph, gives the zero-force limit of the resonant action:

$$I^{(M)}_{F=0} \equiv \sqrt{2m_M E^{(M)'}}\,.$$

From this quantity, in turn, can be calculated the zero-force limit of the unperturbed action:

$$I_{F=0} \equiv I_M + MI_{F=0}^{(M)}.$$

The result, then, is a set of estimates of the locations, in terms of the unperturbed action coordinate, of the resonances corresponding to particular rational values of $\dot{\xi}^{(M)}/\omega$.

It is important to test the quality of these estimates. This is done, roughly, by calculating the energy in the unperturbed action-angle coordinates in two different ways, and comparing the results. One way uses the estimate of the unperturbed action:

$$E_{F=0}(\xi, I) \equiv -\frac{1}{2I_{F=0}^2},$$

while the other uses the estimate of the resonant action:

$$E^{(M)}(\xi, I) = E^{(M)}(\xi^{(M)}, I^{(M)}) + \frac{MI^{(M)}}{I_M^3} \approx -E^{(M)'} + E_M + F_M + \frac{MI_{F=0}^{(M)}}{I_M^3}.$$

The percentage error between these two values of the energy was calculated for each resonance located. In Section 3.4, where $I^{(M)}$ was introduced, it was pointed out that the valid extent of $I^{(M)}$ is limited. The error calculated between these two energies is an indication of the valid range of $I^{(M)}$.

The results of this procedure are given in the form of three tables in Appendix C, one for each of $M=1$, 2, and 3.

The tables in Appendix C list all fractional values of $\dot{\xi}^{(M)}/\omega$ with denominators from 1 through 5 for the range of pendulum energies, $E^{(M)'} \leq 50$. All numerators are included. For any particular pair of primaries, the secondary resonances correspond to fractions with the numerator $|M-N|$. For example, in the table for $M=1$, the fractions $1/n$ correspond to resonances with $N=2$, the fractions $2/n$ correspond to resonances with $N=3$, and so on. In the table for $M=2$, the fractions $1/n$ correspond to resonances with $N=1$ and 3, the fractions $2/n$ correspond to resonances with $N=4$, and so on.

Relationship to winding number

The above discussion appears to be independent of whether the secondaries are considered to arise from perturbation of the M'th primary by the N'th, or of the N'th primary by the M'th. But there is a subtle difference.

The fraction $\frac{M-N}{n}$, the angular frequency of the n'th cosine potential arising from the perturbation of the M'th primary by the N'th, is also thereby the winding number[9] of the corresponding secondary resonance orbit *in the phase space of the pendulum of the M'th*

[9] The *winding number* of a toroidal orbit is the ratio of the frequencies of the orbit in the two periodic coordinates of the torus.

primary. But in the HSH action-angle phase space, the M'th primary has itself a winding number of $1/M$. If the net winding number of the secondary in the HSH phase space is called r/s, and if $M>N$ (and so $n>0$), then the winding numbers are related by:[10]

$$\frac{M-N}{n} = \left\{ \begin{array}{ll} \left[M\frac{r}{s}\right] \bmod 1 & \text{for orbits below the } M\text{'th primary} \\ \left[M\frac{s-r}{s}\right] \bmod 1 & \text{for orbits inside or above the } M\text{'th primary} \end{array} \right\}.$$

The HSH winding number, r/s, means that the Poincare section of the orbit has s islands, and that as the Poincare section is generated the new points hit every r'th island in sequence, counting counterclockwise. The complementary winding number, $(s-r)/s$, is obtained if the hits are counted in the clockwise direction, which is the direction of motion for the pendulum phase space inside and above the separatrix. (See Figure 3.4.)

If the secondaries are now considered in the phase space of the pendulum of the N'th primary, a fraction with the same value appears for the $(-n)$'th cosine: $\frac{N-M}{-n}$. So the left hand side of the above relationship remains unchanged, but on the right side every occurrence of "M" must be replaced by "N":

$$\frac{M-N}{n} = \left\{ \begin{array}{ll} \left[N\frac{r}{s}\right] \bmod 1 & \text{for orbits below the } N\text{'th primary} \\ \left[N\frac{s-r}{s}\right] \bmod 1 & \text{for orbits inside or above the } N\text{'th primary} \end{array} \right\}.$$

This difference introduces an intriguing new complication into the HSH resonance structure. Arising from any pair of primary resonances, there are *six* infinite families of secondaries, one below, one inside and one above the separatrix of each of the two primary resonance zones. Of these families, four lie in independent regions of the phase space (below the lower primary, above the higher, and inside of each). But the other two (above the lower primary, and below the higher) occupy the same region, in between the two primary resonance zones. It is observed in the computer simulations shown in Section 3.5.2 that some of the resonances in these families coincide, but others do not. This means that a resonance zone may be a secondary from the point of view of one primary, and not from the point of view of the other.

[10] These relationships were induced empirically with the help of the plots in Section 3.5.2. They are consistent with the theoretical discussion, but are not directly deduced from it.

3.5.2 The region between the two primaries

Figure 3.8 is a strobe plot of the doubly-resonant HSH system for $M \in \{1, 2\}$. A great depth of structure is evident.

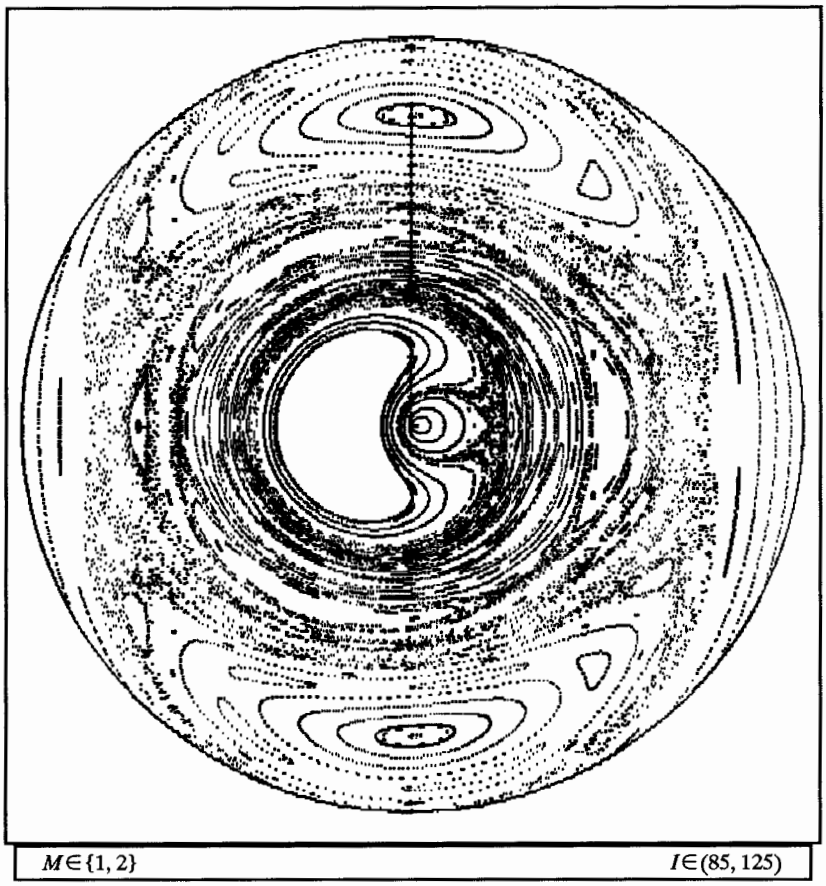

Figure 3.8. Strobe plot of the doubly-resonant HSH system for $M \in \{1, 2\}$. The other parameters are the same as for Figure 3.5: $F = 2 \cdot 10^{-10}$ and $\omega = 2\pi/(5 \cdot 10^6)$.
The vertical line in the upper hemisphere of the plot is a line of cross-hairs, "+", for the initial conditions of the orbits.

In this plot, the large region to the left of the center is the first primary resonance zone, and the two large regions at the top and bottom are the second primary. These regions correspond to those seen in the first two of plots in Figure 3.5. There are also many secondary and higher-order resonances, which are seen more clearly in Figure 3.9. Surrounding the stable orbits of the resonance zones are the chaotic trajectories.

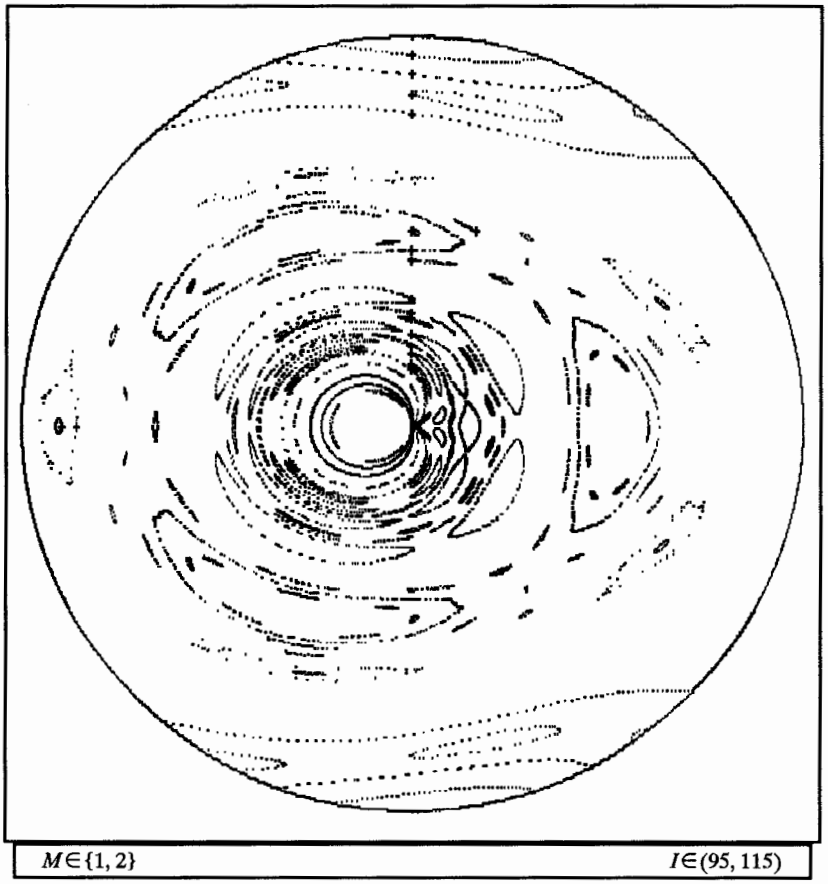

Figure 3.9. Large-scale view of the non-chaotic orbits in the region of Figure 3.8 between the two primary resonance zones. Numerous secondaries and higher-order resonances are visible.

The following table lists all of the island structures found in the region between the two primaries. Most of the structures listed are shown in Figure 3.9, although some of them are difficult to see. The denominators in the three columns on the left give the number of islands in a particular chain, and can be used to identify the corresponding structure in the plot. The numerator in the left-most column is recorded by observing the formation of the plot; the numerators in the next two columns are calculated by the indicated formulas. In columns 2 and 3, winding numbers with a numerator of 1 ($=M-N$) are shown in bold face to identify the secondary resonances. These are the resonances that arise from the interaction of the two primaries, as discussed in Section 3.5. The resonances whose winding numbers are not in bold face are of higher order, meaning that they arise from the interaction of a primary with a secondary, or a secondary with a secondary, or any other pairing of resonances except two primaries. This data shows that, as mentioned near the end of Section 3.5.1, whether a particular resonance is a secondary can depend on which primary is used as the basis for the analysis (the difference between columns 2 and 3).

Analysis of orbits between first and second primary resonances of HSH
(Orbits with r/s listed in brackets are not shown in Figure 3.9.)

Winding numbers			Location		
For HSH:	Above $M=1$:	Below $M=2$:		Predicted (Secondaries only)	
r/s	$(s-r)/s$ mod 1	$2\,r/s$ mod 1	Actual	Above $M=1$	Below $M=2$
1/1	**1/∞**	**1/1**	93.3	92.7	77.3
(8/9)	**1/9**	7/9	96.4		
7/8	**1/8**	6/8	96.8		
6/7	**1/7**	5/7	97.6		
(23/27)	4/27	19/27	97.8		
(16/19)	3/19	13/19	98.2		
(26/31)	5/31	21/31	98.3		
5/6	**1/6**	4/6	98.5		
9/11	2/11	7/11	99.1		
(22/27)	5/27	17/27	99.2		
(21/26)	5/26	16/26	99.5		
4/5	**1/5**	3/5	99.9	101.2	
7/9	2/9	5/9	100.8		
10/13	3/13	7/13	101.2		
3/4	**1/4**	2/4	102.0	102.3	
(18/25)	7/25	11/25	103.4		
(23/32)	9/32	14/32	103.5		
9/13	4/13	5/13	104.8		
2/3	**1/3**	**1/3**	106.1	104.3	102.2
9/14	5/14	4/14	107.4		
5/8	3/8	2/8	108.4		
(8/13)	5/13	3/13	109.0		
3/5	2/5	**1/5**	109.9		106.4
1/2	**1/2**	**1/∞**	117.1	109.0	116.8

This table includes the primaries as the first ($r/s=1/1$) and last (1/2) resonances in the list because their winding numbers fall into the sequences of winding numbers of the secondary resonances. This means that the primaries coincide with the outermost secondaries in this region.

In column 2, there is no winding number 1/1. This is correct because the formula $(s-r)/s$ mod 1 cannot yield the value 1. So the 1/2 secondary, which coincides with the second primary, is the upper limit of the family of secondary resonances above the first primary. In column 3, secondaries only appear with odd-denominator winding numbers. This is also correct because the formula $2\,r/s$ mod 1 cannot yield a number with an odd numerator and an even denominator.

The right three columns of the table discuss the locations of the resonances. The "actual" column lists average values of the action for each island chain, as recorded by the computer. The "predicted" columns give the values appearing for the appropriate fractions in the $I_{F=0}$ columns of the tables for $M=1$ and $M=2$ in Appendix C. Except for the secondaries which coincide with primaries, the predictions are within a few percent of the actual locations.

The winding numbers, r/s, here represent the same resonance zones as are found to have winding numbers s/r in the physical phase space in Chapter 2. The method there turns out to be superior for predicting the locations of the resonances. That method is also more general because it offers predictions for all the resonances in the table above, not just the ones called here "secondaries".

The region below the first primary

Simulations were also run to identify resonances below the first primary resonance for the doubly-resonant HSH system with $M \in \{1, 2\}$. The resonances found in this region are extremely tiny, with widths on the order of 10^{-5}. In the physical phase space, it is true that the resonances below the 1/1 resonance are smaller than some of those above, but their widths are much wider than in the action-angle space. It is conjectured here that it takes the full series of primary resonances, which are all present implicitly in the energy in the physical phase space, to bring the resonances in the lower region up to their full width.

This is an important point when making the connection to quantum mechanics. It may be that it is very difficult to reproduce the stable regions in Koch's experimental data in quantum mechanical calculations without including a very large number of terms in the HSH perturbation. This would be a very time-consuming calculation on even the fastest supercomputer.

4 Quantum dynamics of the HSH atom

This chapter gives the quantum mechanical view of the HSH dynamics. Section 4.1 reviews the dynamics of the unperturbed atom in quantum mechanics. The primary resonance structure arising under the perturbation is shown in Section 4.2. The special graphical techniques developed to visualize the quantum mechanical evolution are described in Section 4.3. In Section 4.4, the dynamics of individual primary resonance zones are studied using these techniques. A few data are presented on the overlap of neighboring resonances in Section 4.5.

4.1 Quantum dynamics of the unperturbed 1-dimensional hydrogen atom

This section reviews the dynamics of the unperturbed atom in quantum mechanics.

The energy eigenvalues of the unperturbed, bound, 1-dimensional hydrogen atom are, in atomic units [Appendix D.1]:

$$E_{u_n} = -\frac{1}{2n^2}$$

The associated states are *stationary*: there is no evolution as long as the atom is not perturbed. If the initial state is a superposition of negative-energy states, as every bound state is:

$$|t=0\rangle = \sum_n c_n |n\rangle ,$$

then the atom remains in that superposition indefinitely.

The level splitting for the atom is given by the Balmer formula:

$$E_{n+1} - E_n = \frac{1}{2}\left[\frac{1}{n^2} - \frac{1}{(n+1)^2}\right] \underset{n\to\infty}{\to} \frac{1}{n^3},$$

which, for large values of the principal quantum number, approaches the same form as the frequency of the orbital motion in classical action-angle coordinates, with $I \to n$.

4.2 Primary resonance structure of the HSH Hilbert space

This section derives the primary resonance structure arising in the Hilbert space of the 1-dimensional hydrogen atom under the HSH perturbation.

The HSH energy is obtained by adding to the energy of 1-dimensional hydrogen the perturbation of an electromagnetic wave polarized along the axis of the atom:

$$\hat{E}|n\rangle = \left[-\frac{1}{2n^2} + F\hat{x}\cos(\omega t)\right]|n\rangle .$$

The projection of the separation operator, $\hat{x}$, on the energy states is, using the results of Appendix D.6:

$$\begin{aligned}\hat{x}|n\rangle &= \sum_{M=-\infty}^{\infty} |n+M\rangle\langle n+M|\hat{x}|n\rangle \\ &= \frac{1}{2}n^2\left[A_0|n\rangle + \sum_{M=1}^{\ll n} A_M\left(|n+M\rangle + |n-M\rangle\right)\right] .\end{aligned}$$

The upper bound on the sum over M is required by the condition on the use of the A_M's in Appendix D.6, that $|M| \ll n$. The monotonic drop in A_M with increasing M would provide an effective cutoff for the sum anyway, so the need for an upper bound is justified.

Combining the projection of the separation operator on the energy states with the unperturbed energy yields for the projection of the HSH energy on the unperturbed energy states:

$$\begin{aligned}\hat{E}|n\rangle &= -\frac{1}{2n^2}|n\rangle + \frac{Fn^2}{2}\cos(\omega t)\left[A_0|n\rangle + \sum_{M=1}^{\ll n} A_M\left(|n+M\rangle + |n-M\rangle\right)\right] \\ &= -\frac{1}{2n^2}|n\rangle + \frac{Fn^2}{4}\cdot \\ &\quad \cdot\left[A_0\left(e^{i\omega t}+e^{-i\omega t}\right)|n\rangle + \sum_{M=1}^{\ll n} A_M\begin{bmatrix} e^{i\omega t}|n+M\rangle + e^{i\omega t}|n-M\rangle + \\ e^{-i\omega t}|n+M\rangle + e^{-i\omega t}|n-M\rangle \end{bmatrix}\right] \\ &= -\frac{1}{2n^2}|n\rangle + \frac{Fn^2}{4}\sum_{M>>-n}^{\ll n} A_M\left[e^{i\omega t}|n+M\rangle + e^{-i\omega t}|n-M\rangle\right] .\end{aligned}$$

In classical action-angle coordinates, the energy of this system gives rise to resonance between the rotation of the unperturbed system and the rotation of a set of cosine potentials.

In quantum mechanics, resonance is explained in terms of the splitting between energy levels. In the above energy, the kets $|n\pm M\rangle$ represent transitions up and down by M levels, where M is an integer much smaller in magnitude than n. The microwave perturbation is in resonance with the atom if its photon size is a multiple by some M of the level splitting of the atom:

$$\lim_{n\to\infty}\left[E_{n+1}-E_n\right] = \frac{1}{n^3}.$$

So the resonance condition is, for large n, $n^3\omega \approx M$, where $|M| \ll n$. This is identical to the resonance condition in the classical case, except that the classical theory does not put a limit on the magnitude of M.

The projection of the HSH energy on the unperturbed energy states can be used in Schrodinger's equation and integrated on a computer to simulate the quantum mechanical HSH behavior. As in classical action-angle coordinates, in order to study the behavior due to individual resonances and their interactions, the energy used includes a single term or a selected set of terms from the resonance sum:

$$\hat{E}|n\rangle = -\frac{1}{2n^2}|n\rangle + \frac{Fn^2}{4}\sum_M A_M\left[e^{i\omega t}|n+M\rangle + e^{-i\omega t}|n-M\rangle\right],$$

where the sum is over the terms included in the calculation. This is the form of energy used in the simulations presented in this chapter. Those simulations demonstrate a phenomenon very similar to the classical HSH behavior in that there are regions of confinement of probability in the space of energy levels[1]. The locations and widths of these regions match those predicted by the pendulum approximation for the resonance zones in the classical theory in action-angle coordinates. Furthermore, these regions expand and merge as the strength of the HSH perturbation is increased, as do the resonance zones in the classical theory.

It is very important that these results are as described. The HSH atom is on the boundary between the quantal and classical domains. So both theories must predict the same behavior.

There is another way to understand the resonance behavior in quantum mechanics, in terms of quantizing the classical behavior. Inside of a classical resonance zone of a singly-resonant HSH atom, the system point is oscillating as a pendulum, undergoing regular variations in I and ξ [§3.4]. It is in a bound state, governed by the pendulum energy. The unperturbed action, I, is no longer a constant of the motion, but the pendulum action, $J^{(M)}$, is. When this system is quantized, the stationary states are the energy eigenstates of this pendulum, which are superpositions of the unperturbed energy eigenstates. In the simulations in this chapter, n is the energy index of, and labels the stationary states of, the *unperturbed* atom. When the system is started with a definite value of n, it is not in a stationary state of the perturbed system, and the probability must spread. The region within which the probability spreads is the region of the potential well of the pendulum.

[1] In quantum mechanics, a *region* in a parameter space, such as in the space of energy levels, corresponds to a *subspace* in Hilbert space.

4.3 Graphic representation of the evolution

Special graphical techniques were developed to visualize the quantum mechanical evolution of the HSH atom. These techniques are described in this section.

In all cases, the initial state given to the computer was a zero-phase definite-energy state, i.e., a state in which the real part of the amplitude was 1 for one energy state, and in which the corresponding imaginary part as well as the amplitudes for all other energy-values were all zero. The number of energy states included in the integration was a monotonically increasing variable controlled by the program; in essence, the space of energy levels was programmed to expand in step with the spreading of probability. The probability distribution was saved at regular intervals, and various other diagnostic and metric data were also recorded by the program. The calculation would continue either for a preset number of intervals, or until the space of energy levels had ceased to expand (according to a programmed formula), so that the atom could be presumed to have reached a steady state.

A sample of the data output at a single time-step is shown at the right. This shows the energy configuration of the atom at a particular time after the turn-on of the perturbation. A complete calculation consists of a sequence of many such frames.

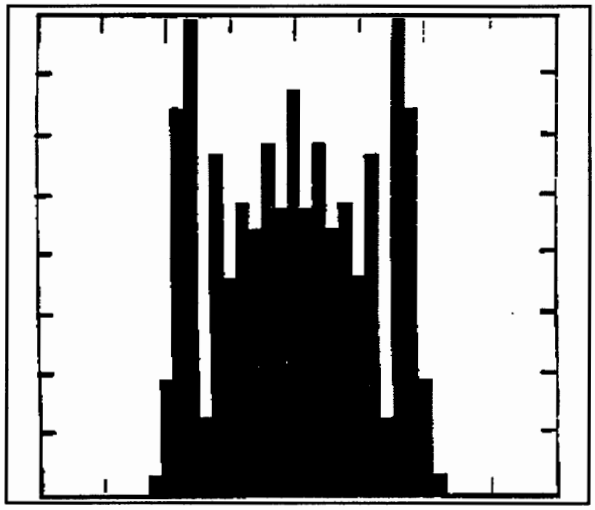

Figure 4.1. Probability distribution of an approximation to the singly-resonant HSH system (based on the pendulum approximation [§3.4]) with $M=1$, $F=0.95\cdot10^{-9}$ (4.9 V/cm) and $\omega=80^{-3}$ ($\nu=13$ GHz). The initial state is $n_0=80$; the state shown is for $t=6.8\cdot10^{6}$ ($1.6\cdot10^{-10}$ sec).

The horizontal axis is $n\in[60, 100]$. The vertical axis is $P\in[0, 0.08]$.

The configuration shown in a single time-frame may or may not be representative of the evolution of the atom. In order to understand what is going on, it is necessary to get a unified picture of the entire sequence of frames. The simplest way to do this is to plot the frames side by side in repeated rows on a page. This still makes it difficult to get the flavor of the motion. Another technique which was tried was to flash the sequence of frames on the computer screen in quick succession so as to show the evolution of the atom as a movie in energy-probability space. This was a lot of fun, but the moment-by-moment fleeting of the image prevented the formation of an overall impression. Another problem with the movies was the difficulty of comparing two or several time series with each other.

A method was found for representing the entire evolution of an atom, from the turn-on of the perturbation through steady-state, in a single, static picture. The technique is to use color to represent the magnitude of probability; this frees up one of the two dimensions on the plotting surface to be used to represent time. The result is the type of plots shown in Figure 4.2. Any vertical slice through one of these figures contains the same information as the probability plot for one time-frame, although with much lower resolution since there are

only nine colors. This technique makes it possible to see many aspects of the motion that are not evident from inspecting series of individual frames. It is also easy to compare numerous time series for different values of a variable parameter, such as initial state, and quickly observe the effect that the variation has on the motion.

Ultimately, however, when there are very many time series to be compared to each other, the evolution plots exhibit the same weakness as the representation by individual time-frames. In order to really *see* evidence of the quantum resonance zones, it is necessary to further collapse a series of evolution plots into a single picture. As can be seen in the example evolution plot above, the essential features of the probability distribution remain fairly stable after steady-state is reached, yet with some oscillation in time. This suggests that the essential information about a single evolution is preserved if the entire plot is collapsed by averaging the probabilities for each energy eigenvalue over the time after steady-state is reached. This reduces each evolution plot to a vertical slice so that a series can be juxtaposed to form a new type of plot, in just the same way as the color representations of time-frames are juxtaposed to make an evolution plot.[2]

If the parameter which varies between the vertical slices is the initial state of the atom, the result is what is called here a distribution plot, with an example being Figure 4.3. Both the vertical and horizontal axes are measured in the index of the energy eigenvalue. A value on the horizontal axis denotes the initial condition of one particular calculation. A value on the vertical axis denotes a possible state in the energy-index space of each calculation. The color of the plot at the intersection of these two values indicates the extent to which a calculation has predicted the spread of probability from the initial energy state to a state with the energy index indicated on the vertical axis.

A common color scheme is used in all evolution and distribution plots in this chapter. This is shown at right. The number $1.5 \cdot 10^{-5}$ is the threshold for storage of probabilities[3]. At each time step, probabilities were stored for all states inside the region whose outermost states have at least that probability. Black grid lines are drawn only outside this region. In addition, in the distribution plots, a black dot is printed above and below the edges of this region for each initial state. This envelope delineates between states with recorded probability and those outside the recorded region. The envelope is not needed in the evolution plots because their edge states are always above the threshold, and so always have a color other than white. The distribution plots can have edge states below the threshold, because in these plots the probabilities are time averages.

Probability color scheme for evolution and distribution plots

Probability:		
More than	Up to	Color
0	$1.5 \cdot 10^{-5}$	white
$1.5 \cdot 10^{-5}$	$2.5 \cdot 10^{-4}$	yellow
$2.5 \cdot 10^{-4}$	0.001	blue
0.001	0.01	green
0.01	0.03	pink
0.03	0.065	orange
0.065	0.1	purple
0.1	0.5	brown
0.5	1	black

[2] It is also possible to collapse the evolution plots by various other procedures besides taking the time average, such as taking the maximum, or minimum, or standard deviation, over the steady state period. This can be helpful by providing alternate views of the same data.

[3] This number is the reciprocal of 65535, the largest integer that can be stored in two data bytes. For economy in storage of data, double precision (8 bytes) probabilities were scaled by this factor and stored as integers.

It may be asked if the information in the evolution and distribution plots might not be conveyed more simply (and less expensively) and with greater resolution in a 3-dimensional relief plot, instead of in color. This was tried, but it was found that while relief plots are useful for smooth surfaces, they do not adequately represent data with sharp or clustered peaks and troughs because one peak can hide another nearby peak or trough, and a trough can hide the depth of another trough nearby.

The rest of this chapter presents data for the first five isolated resonances and various combinations. These data are presented in the form of the evolution and distribution plots just described.

In all runs, the perturbation frequency was chosen arbitrarily to be the resonant frequency for $M=1$ and $n=80$, i.e., $\omega=80^{-3}=1.9\cdot10^{-6}$ ($\nu=13$ GHz). In all series of calculations, (except two, where this difference is noted), the peak field strength was $F=0.95\cdot10^{-9}$ (4.9 V/cm).

The distribution plots for combined resonances, in Section 4.5, have gaps indicating that simulations were not run for all initial states. These gaps interfere with the formation of conclusions that might be readily made if complete series were represented. They also can be a strain on the eye when trying to view the data as a coherent unit. The reason for the gaps is the enormity of data that each complete distribution plot represents. The calculation of a single, complete, distribution plot for an isolated resonance takes either several weeks on the very fast PC used in this project, or a good part of a day on the Cray. The combined resonances run slower and thus take even more time. This is the reason for the gaps in the plots for combined resonances, and is also the reason that more variety of frequencies and field strengths, as well as more combinations of resonances, are not presented.

4.4 The singly-resonant HSH system in quantum mechanics

This section studies the dynamics of individual primary resonance zones using the graphical techniques described in Section 4.3.

The first primary resonance

Figure 4.2 consists of evolution plots for the singly-resonant HSH system with $M=1$, for seven different initial states, n_0. A resonance zone is clearly exhibited.

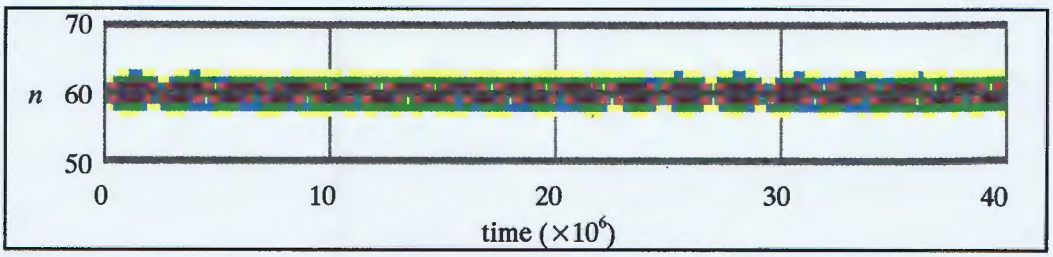

Figure 4.2(a). Evolution plot for the singly-resonant HSH system with $M=1$ and $n_0=60$.

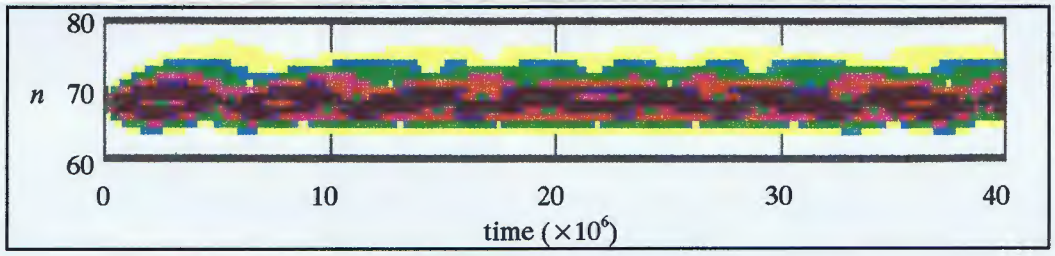

Figure 4.2(b). Evolution plot for the singly-resonant HSH system with $M=1$ and $n_0=68$.

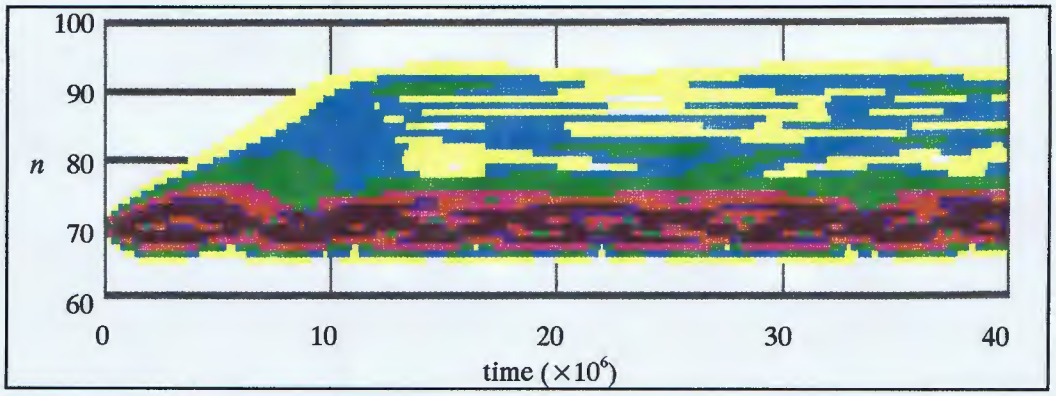

Figure 4.2(c). Evolution plot for the singly-resonant HSH system with $M=1$ and $n_0=70$.

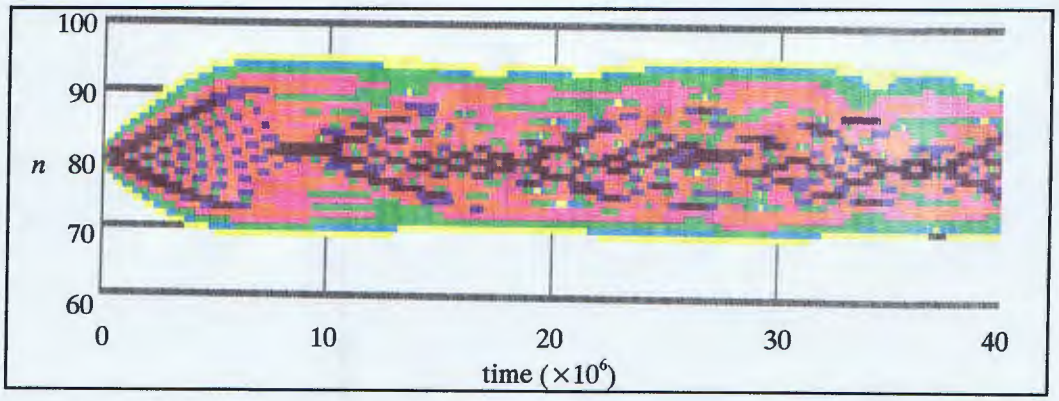

Figure 4.2(d). Evolution plot for the singly-resonant HSH system with $M=1$ and $n_0=80$.

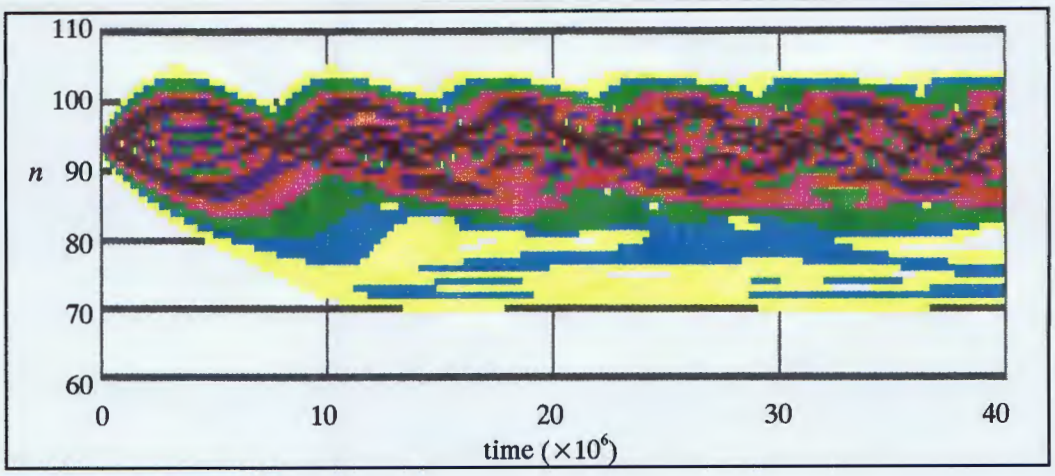

Figure 4.2(e). Evolution plot for the singly-resonant HSH system with M=1 and n_0=94.

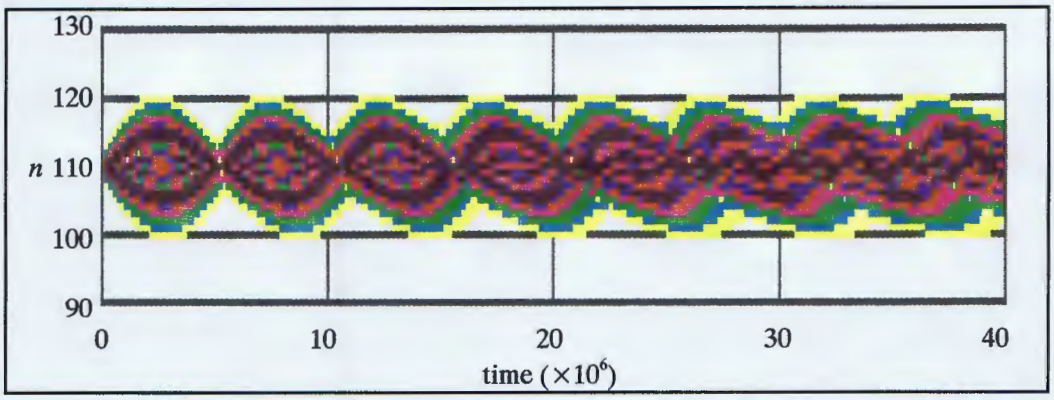

Figure 4.2(f). Evolution plot for the singly-resonant HSH system with M=1 and n_0=110.

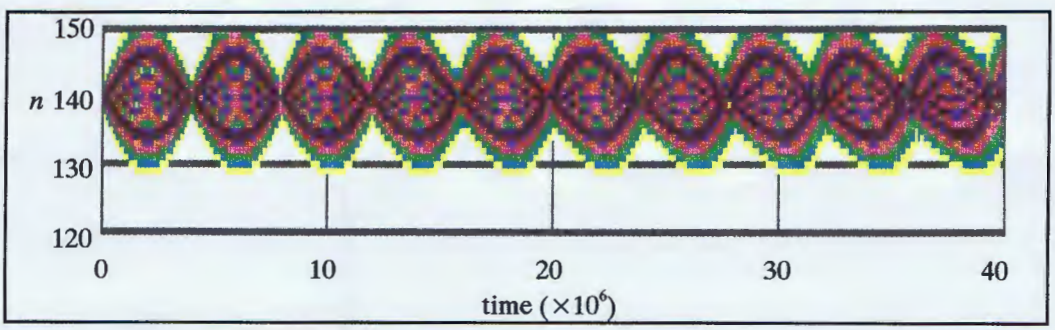

Figure 4.2(g). Evolution plot for the singly-resonant HSH system with M=1 and n_0=140.

For n_0=80 (Figure 4.2(d)), the predicted center of the resonance, the probability spreads out evenly both above and below the initial state. After spreading out to fill the region from about n=69 to 95, the probability stays in this region, yet with some oscillation in its structure. The region through which the probability has spread is identified as the resonance zone.

Below the resonance zone (n_0=60 and 68, Figures 4.2(a) and 4.2(b)), the behavior is similar to that for n_0=80, but with a much smaller spread. Above the zone (n_0=110 and 140, Figures 4.2(f) and 4.2(g)), the behavior is similar for a short time, but then the spreading undergoes a pronounced oscillation in time. The amplitude and frequency of the oscillation are higher for higher initial values of the energy index.

An interesting hybrid behavior occurs for initial states on the edges of the resonance region (n_0=70 and 94, Figures 4.2(c) and 4.2(e)). The predominant behavior is very much like that outside the region, including the pronounced oscillation on the upper edge. But this is accompanied by a thin spreading of probability into, and throughout, the resonance zone. There is an equilibrium established between the two subregions; after the initial spreading, there is no further leakage from the heavily populated subregion on the edge of the resonance zone into the thinly populated area of the rest of the zone.

As discussed in Section 4.2, the overall behavior demonstrated by these seven graphs is summarized and amplified by combining an entire series of the same sort of graph into a single distribution plot. The result is shown here:

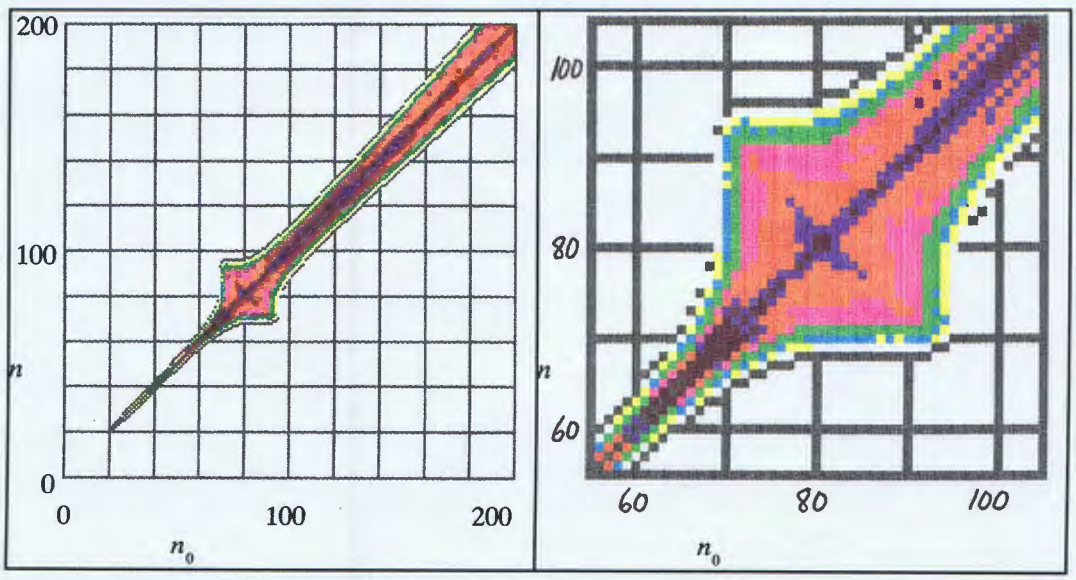

Figure 4.3. Distribution plot for the singly-resonant HSH atom with M=1. On the left is shown the series of initial states from n_0=20 to 200. On the right is an expanded view of the vicinity of the resonance zone. This scheme of pairing a large scale plot with a close up view of the resonance zone is used in all the distribution plots.

For initial states below the resonance zone, the spreading of probability is seen to be very small. Above the resonance, there is a greater degree of spreading, which increases slowly and roughly linearly with initial value of the energy index. The resonance zone shows up as a distinctive square pattern. The probability spreads out to fill the square area in a manner which is almost completely independent of the initial state of the atom.

This quantum resonance zone has an almost exact symmetry about the line n=n_0. To see how exact it is, note the two little yellow holes in the blue edge of the left side of the square, and the corresponding holes in the blue edge of the bottom of the square. This symmetry is

remarkable in that the origin of those little yellow holes is of a very different nature along the two different edges of the square. On the bottom edge, the holes mean that the probability of an atom prepared with an initial energy index of either 87 or 89 spreads downward to almost, but not quite the same extent as that of an atom prepared at the adjacent energy indices. On the left edge, they mean that the probability of an atom prepared with an initial energy index of 70 takes a shallow dip in value at energy indices 87 and 89. As appealing as the symmetry is, however, it is not perfect. For example, the amulet-like shape at the center of the square is one purple dot shy of perfect symmetry about $n=n_0$.

While the resonance zone is square in shape and has a nearly exact symmetry about its $n=n_0$ diagonal, it is definitely asymmetrical about the other diagonal. This is seen most graphically in the amulet-like shape at the center of the square, which seems to be pointing in the down-left direction. Or it can be seen numerically by measuring the geometrical center of the square to be at $n=81.5$, while the actual peak in the probabilities, in both the horizontal and vertical directions, is at $n=80$.

This plot is a compact representation of a large amount of data. It comprises vertical slices for time series for each of 181 initial states, with the probabilities in each slice being obtained by averaging over several hundred, and in many cases upwards of a thousand, time-frames.

Higher primary resonances

The same techniques were applied to plotting the second through fifth primary resonances. Essentially the same behavior was found as that shown above for the first resonance. The outstanding difference in the higher resonances is that in the M'th resonance calculation, the Schrodinger equation only couples every M'th energy state. Those states not coupled to the initial state by Schrodinger's equation must remain unoccupied, and so appear as white in the plots. This gives the evolution plots a striped appearance. The evolution plot for $M=2$ and $n_0=100$ is shown here:

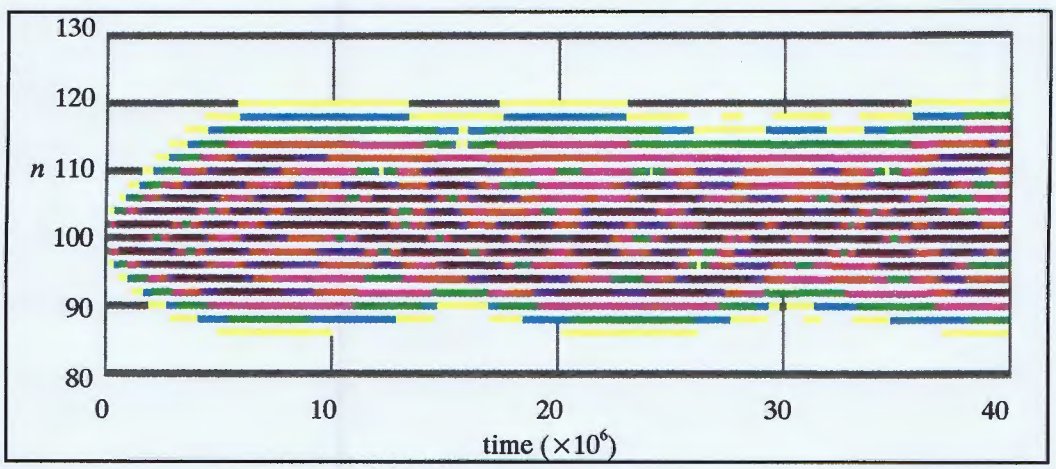

Figure 4.4. Evolution plot for the singly-resonant HSH system with $M=2$ and $n_0=100$.

No more evolution plots are presented here, in favor of the more compact distribution plots. In the distribution plots, the unoccupied states cause a checker-board-like appearance. Figures 4.5 and 4.6 are the plots for the second and third resonances:

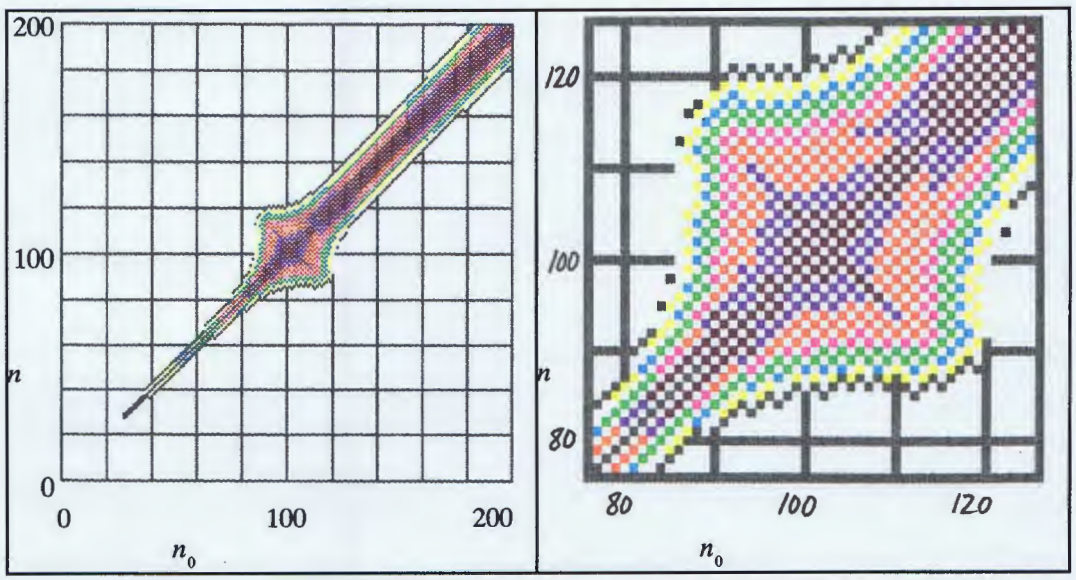

Figure 4.5. Distribution plot for the singly-resonant HSH atom with $M=2$.

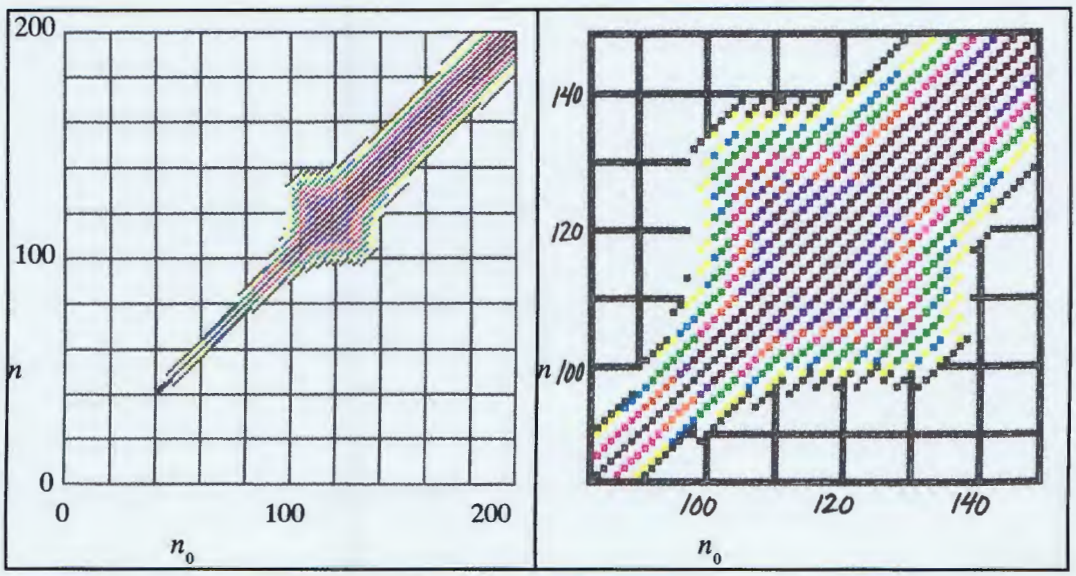

Figure 4.6. Distribution plot for the singly-resonant HSH atom with $M=3$.

These plots exhibit the same basic behavior as was found for the first primary resonance: the overall moderate spreading and the existence of a square region in which the spreading is pronounced, almost independent of the initial state, symmetrical about the line $n=n_0$, and asymmetrical about its other diagonal.

Simulations were also run for the fourth and fifth resonances. Not enough runs were made to present a useful distribution plot, so these data are not shown here. The results were, however, consistent with all the behavior described above for the first three isolated resonances.

The locations and widths of the isolated resonance zones

Since the resonance zones are not symmetrical about both diagonals, there is no physical significance to their geometrical centers. Rather, the location of a resonance zone is identified as the location of the local maximum of the probability near the geometrical center. In all cases for which complete data is available (i.e., for the first three resonances), this peak has the same energy index along both the horizontal and vertical axes, so this location is unambiguous. The sparse data available for the fourth and fifth resonances also suggest a location for the resonance, although these results are not as definitive.

The widths are not so easy to determine. The distribution plots show probability dropping from its peak values near the centers of the resonances to very low values at the edges of the recorded regions. But if the threshold of recording were lowered, the edges of this region would be pushed back farther. So where is the edge of a resonance? The evolution plots offer a clue. The probability for an initial state near the center of a resonance is oscillatory in a central subregion, and appears to decay outside this subregion. (See Figures 4.2(d) and 4.4.) This is the hallmark of a confined system in quantum mechanics, with the edges of the confinement region being identified by the change from oscillation to decay.

There is no unambiguous way to point to a boundary between oscillation and decay. Subjectively, in the two plots referred to above, the oscillatory behavior seems to be carried by the color purple. From the color scheme chart, it is seen that the subregion defined by having any purple in it is the subregion outside of which the probability never climbs above about a half of one percent. Furthermore, for both the $M=1$ and $M=2$ plots, the subregion thus defined occupies 56% of the total width of the recorded region. On this basis, the width of the resonance zones is identified as 0.56 of the width of the recorded region, i.e., of the width of the distinctive square areas in the distribution plots.

The following table compares the classical theoretical estimates (with $I \to n$) of the locations and widths of the resonances with the values measured from the evolution and distribution plots:

Locations and widths of some primary resonances for $F=0.95\cdot10^{-9}$, $\omega=80^{-3}$ (classical theory and quantum mechanical simulations)				
M	Location, n_M		Width, $2\Delta_M^{res} n$	
	Theoretical, $(M/\omega)^{1/3}$	Measured	Theoretical, $\frac{4M}{\omega}\sqrt{\frac{FA_M}{6}}$	Measured
1	80	80	21	16
2	101	101	24	20
3	115	116	27	22
4	127	126	28	26
5	137	135	29	28

The results of the simulations are seen to be in good agreement with the predictions, although the resonance zones seem to be somewhat narrower than predicted.

4.5 The doubly-resonant HSH system in quantum mechanics

The significance of the resonance zones is that their overlap is the route to chaotic behavior in the classical theory of quasi-integrable systems [§1.2]. So a very significant question is: "Is there a quantum mechanical process analogous to the overlap of classical resonance zones?" This section answers this question in the affirmative by demonstrating the overlap of neighboring quantum mechanical HSH resonance zones.

In classical mechanics, as the resonance zones grow due to an increase in perturbation strength, their mutual interactions also increase and the separatrices defining the zones break down [§2.5]. Orbits that lie outside of, and in between, two neighboring zones may remain intact under a moderate perturbation, confining chaotic behavior to within the region of each resonance zone. Under a stronger perturbation, more orbits break down and the chaos spreads throughout the phase space.

Figure 4.7 shows the distribution plot for the combined first and second primary resonances, with the same frequency and field strength as used for the isolated resonances above:

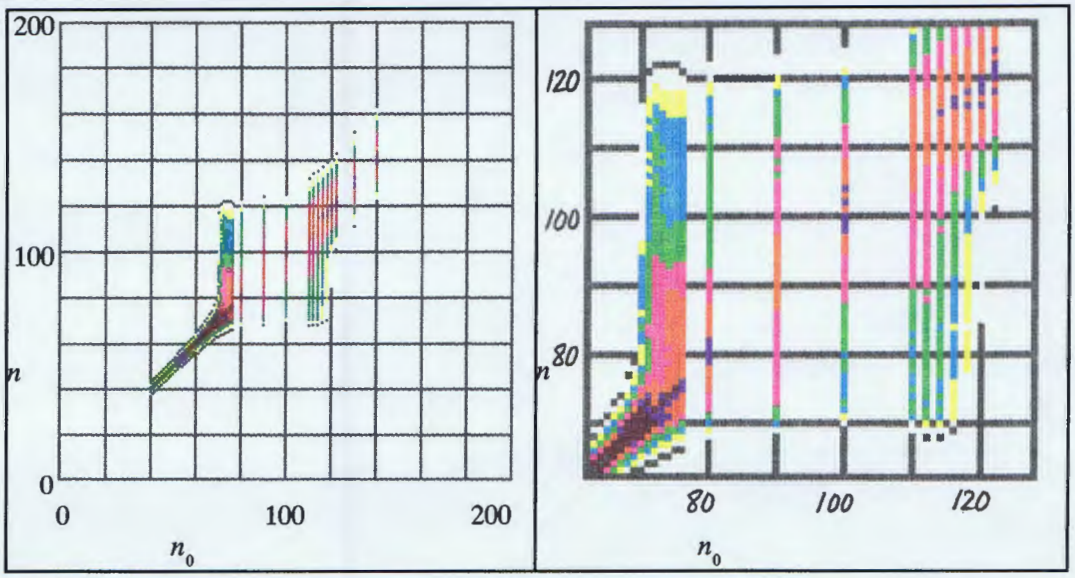

Figure 4.7. Distribution plot for the doubly-resonant HSH atom with $M \in \{1, 2\}$. The other parameters are the same as for all previous plots in this chapter.

Although incomplete due to high computation costs [page 59], this plot shows a definite overlap of the resonance regions. The square area extends from about 70 to 120, which energy indices correspond to the lower edge of the first primary resonance zone and the upper edge of the second. For an initial state in either resonance zone, the probability spreads throughout both zones. In most parts, the probability still stays primarily in the original zone, with only very little spreading into the other zone. For n_0=90, however, which is midway between the locations of the two zones, the probability is fairly evenly spread out.

There are two tests that one would want to conduct to verify that this does indeed have the character of a resonance overlap. First, increasing the field strength should cause the spreading between the zones to increase. Second, at lower field strengths the zones should shrink and pull apart, affording no exchange of probability between them. The first test will have to wait for further study. The second, however, has been performed with positive results. Below is shown a partial distribution plot for all the same parameters as that above, except that the field strength is reduced by a factor of 5:

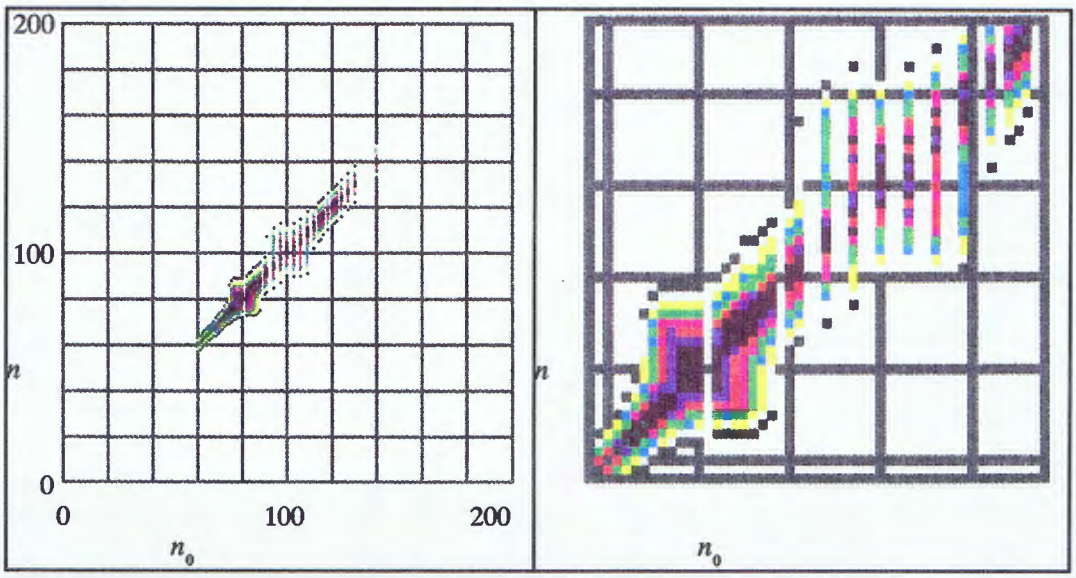

Figure 4.8. Distribution plot for the doubly-resonant HSH atom with $M \in \{1, 2\}$, and with the perturbation field strength reduced by a factor of 5 over the other plots in this chapter.

As anticipated, the resonance zones are now separate, with no spreading of probability from one into the other.

5 Discussion: Nonlinear resonance in the hydrogen atom

This concluding chapter is a combined discussion of the theoretical and experimental findings. Section 5.1 reviews the theoretical results of the previous three chapters in a unified context. Then, in Section 5.2, these results are compared with specific laboratory data found in the literature. Finally, Section 5.3 offers suggestions for carrying on the work in this field.

5.1 Summary of the theoretical results

This section reviews the theoretical results of the previous three chapters in a unified context.

In both classical and quantum mechanics, harmonically driven Stark states of hydrogen (HSH) exhibit nonlinear resonance between the orbital motion of the atom and the microwave perturbation. It is shown in Section 3.2 that in classical mechanics, the resonance occurs when the angular frequency, in action-angle space, of the unperturbed atom is close to the frequency of one or more of an infinite number of rotating cosine potentials representing the perturbation. In quantum mechanics, resonance arises when the energy level spacing of the unperturbed atom is close to an integer multiple of the microwave photon size, as is shown in Section 4.2.

This resonance structure is manifested in the evolution of the atom by the existence of *resonance zones*, which are regions of stability in the space of states of the atom. This is shown for the physical phase space in Figure 2.8, for action-angle coordinates in Figure 3.8, and for the Hilbert space in Figure 4.3. The resonance zones grow with the strength of the HSH perturbation. As they grow, neighboring zones crowd into each other, a phenomenon known as *overlap*. The result is that a system starting out in one zone is free to migrate within the larger total region of the overlapping zones. In classical mechanics this migration is by the evolution of the orbit, in quantum mechanics it is by the spreading of probability.

These results demonstrate that, despite totally different mathematical foundations, both classical and quantum mechanics do demonstrate the existence and overlap of resonance zones. Moreover, the locations and sizes of these zones are the same in both theories. In classical mechanics these are zones in the atom's phase space, and may be plotted in either the physical or action-angle coordinates. In quantum mechanics they are zones in the space of the atom's energy levels, which correspond to subspaces in its Hilbert space.

In classical mechanics, the behavior inside a primary resonance zone approximates that of a pendulum. This is shown theoretically in Section 3.4, and by numerical simulation in Figure 3.4. If the system is given an initial condition inside one of these zones, then it exhibits the typical oscillatory motion of a pendulum within this region.

When this dynamics is taken over to quantum mechanics, the oscillatory motion of the pendulum goes over into a spreading of probability. The stationary states of the perturbed system are the energy eigenstates of the pendulum, not of the unperturbed atom. If the sys-

tem is started with a definite energy index of the *un*perturbed atom, and this index corresponds to a classical action inside a resonance zone, then the system probability spreads through a region, corresponding to the classical resonance zone, in the space of the *unperturbed* energy indices. This behavior is demonstrated in the simulations in Section 4.4.

The behavior in an isolated primary resonance zone is explained in classical mechanics in Section 3.4 in terms of the interaction of a single cosine term of the perturbation with the unperturbed system. This behavior is integrable [§1.2], which means that the classical equations of motion can be solved analytically. This implies that the constants of the motion are preserved under the single-term perturbation.

More than one term of the perturbation can be considered by treating additional terms as perturbations of the primary resonance zone arising due to the first term. The result in classical mechanics is a self-similar structure throughout the phase space. The behavior is no longer integrable, and constants of the motion are lost. In classical mechanics, this results in the freedom of trajectories to wander through wide regions of the phase space, as is demonstrated in the simulations in Sections 2.4 and 3.5.2. This motion is sensitively dependent on the initial conditions, and is called *chaotic*. The corresponding behavior in quantum mechanics is a wider spreading of probability, extending from one resonance zone into the next. This is shown in Figure 4.7 in Section 4.5.

In conclusion, the HSH atom is seen to exhibit nonlinear resonant behavior in both a classical and a quantal analysis. The demonstrated behavior includes both the existence and overlap of nonlinear resonance zones.

5.2 Comparison with the experimental results

This section compares the theoretical results of the previous three chapters with specific laboratory data found in the literature.

Experiments with highly excited states of hydrogen perturbed by microwaves were pioneered in the mid-1970's by James Bayfield and his student Peter Koch at Yale University [74JEB, 77JEB]. These experiments studied the dependence of ionization on the microwave field strength and frequency. The excited states studied were not Stark states. These experiments were continued and improved at Yale through the 1970's [80bPMK]. Since the early 1980's, the two founders of this field have operated separate facilities, Bayfield at the University of Pittsburgh, and Koch at the State University of New York at Stoney Brook. The first experiments with extreme Stark states were performed by Bayfield and Pinnaduwage [84JEB; 84aJEB; 85aJNB]. These were followed by experiments by Koch and colleagues [85KvL; 86PMK; 87PMK; 88EJG].

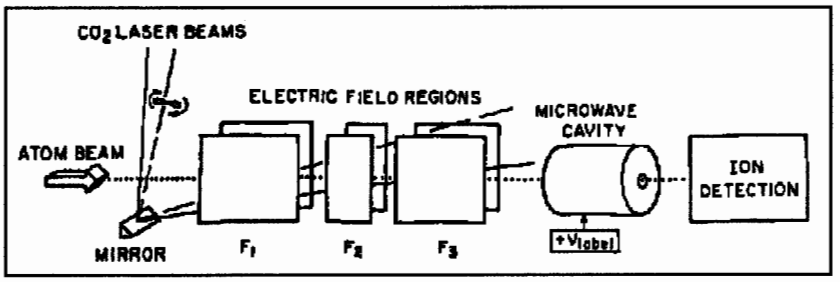

Figure 5.1 The apparatus used by Koch in experiments on the ionization of hydrogen. [83ZDRM, Figure 1, reproduced with permission of the authors.]

The central apparatus for these experiments is a microwave cavity on the order of 10 cm. long and 3 cm. in diameter. A beam of fast hydrogen atoms, prepared with a high proportion of its population in a particular highly excited state, is passed through the cavity. The excited state is prepared by a combination of selective laser excitation and the passage of the beam through a region of strong, static, electric field strength. After passage through the cavity, the beam is analyzed for ionization or energy state distribution. The experiments have used microwave field strengths up to about $F=2\cdot10^{-7}$ (10^3 V/cm), and frequencies mainly in the range of $\omega=1\cdot10^{-6}$ to $1.5\cdot10^{-6}$ ($\nu=6$ to 10 GHz). For comparison, a 1-dimensional hydrogen atom with $n=80$ has a Coulomb field strength at ½ apapsis of 125 V/cm, and a classical orbital frequency of 13 GHz. The ground state of hydrogen has a Coulomb field strength at the Bohr radius of $0.51\cdot10^{10}$ V/cm, and its classical orbital frequency is $0.66\cdot10^{7}$ GHz.

Experiments on ionization thresholds

Most of this work investigated ionization[1]. Results were usually reported in terms of 10% and 90% ionization thresholds, which are the microwave peak field strengths at which the given percentages of the population at a particular initial state becomes ionized. The results of a major series of experiments are shown in Figure 5.2.

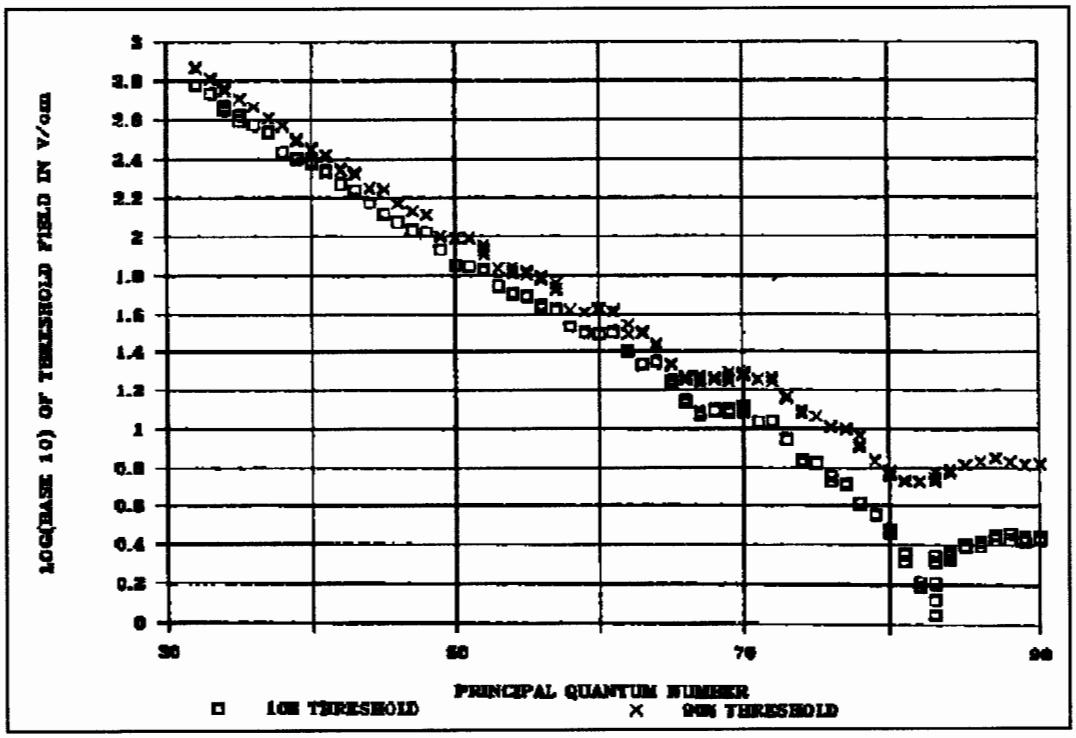

Figure 5.2. Plot of the 10% (squares) and 90% (x's) ionization thresholds versus initial energy level for hydrogen. This is the microwave peak field strength at which the given percentage of the atoms in the beam ionizes. The microwave frequency is $1.509 \cdot 10^{-6}$ (ν=9.923 GHz). [877PMK, Figure 5, reproduced with permission of the author.]

The trend, over most of the range of initial states, is for the ionization threshold to go down with increasing initial energy level, meaning that, in general, the more highly excited states are more easily ionized. This trend is broken, however, in several places, where the ionization threshold remains fairly constant (or even increases slightly!) over a range of several energy levels. These regions of suppressed ionization, or enhanced stability, are identified in the following table:

[1] The term *ionization* is used loosely in these papers, actually referring to transition of the atom into a domain of final states outside of a certain central range. Thus it may indicate either ionization, excitation or de-excitation. 84aJEB, L50 ¶2; 858KvL, 2232 ¶5].

Experimentally and numerically measured widths of HSH resonances					
Center	Corresponding winding number		Width		
n	$n^3\omega$	Closest s/r	Lab: 10%	Lab: 90%	Simulations
59½ or 60	0.32	1/3 (0.33)	3 or 4	4	4.0
62½	0.37	3/8 (0.38)	0	2	<0.1
63½	0.39	2/5 (0.40)	2	0	0.1
68½ or 69	0.49	1/2 (0.50)	4	5 or 7	8.9
71½	0.55	4/7 (0.57)	2	0 or 2	<0.1
74½	0.62	3/5 (0.60)	2	0 or 2	0.7
76½	0.68	2/3 (0.67)	0 or 2	2	1.8
87 or 88	1.01	1/1 (1.00)	>8	>10	11.1

The meanings of the columns in this table are as follows:

- Center n: The median energy level of a group of states with suppressed ionization. Such a group is any series of squares (10% data) or x's (90%) in Figure 5.2 that does not follow the overall descending trend. It is not always clear which states belong to such a group and which do not, so this specification has taken some judgement. When two values are given (as in "50 or 51") this is because the group has different centers in the 10% and 90% data. For the group at the far right, which seems to rise, fall slightly, and trail off out of range of the graph, the center is identified as the state with the peak threshold within the group.
- $n^3\omega$: This is calculated directly from the "center n" and $\omega=1.509\cdot10^{-6}$. If "center n" lists two values, then their average is used.
- Closest s/r: The lowest order rational number close to $n^3\omega$. For $n^3\omega<0.6$, the closest rationals are slightly larger than $n^3\omega$; for $n^3\omega>0.6$, they are slightly smaller.
- Widths, Lab: This is the number of states in the group, according to both the 10% and the 90% data. The smallest possible number of such states is 2. A "0" means that the data for that column do not suggest the existence of this group. The appearance of two values (as in "3 or 4") indicates that there is some ambiguity about the number of states.
- Width, Simulations: This is the largest width found for the corresponding winding number in the numerical simulations in the physical phase space, as reported in Section 2.5.

The first three columns confirm what has been claimed by Leopold and Richards [853JGL, 3382 ¶3 and Figure 4], by Jensen [860RVJ, 154 ¶1; 871MMS] and by others for many years: that the locations of the regions of stability are well predicted by the locations of resonance zones in the phase space. However, no one has previously offered an explanation of the widths of these regions, or a correspondence between the widths in the laboratory and numerical data. This is what is found here, in the last three columns of the above table.

The laboratory and numerical data are in qualitative agreement on the widths of the various resonance zones. The zones may be listed by winding number in order of decreasing width: s/r = 1, 1/2, 1/3, 2/3, ... The significance of this ordering is that the width of the zones decreases as the size of the integers in the numerator and denominator of the winding numbers increases.

No significance has been found for the excursions of the island chains, tabulated in Section 2.5 along with the widths.

In conclusion, the widths of the regions of suppressed ionization in the Koch data are explained by the expanding widths of the corresponding HSH resonance zones. The zones expand with increasing perturbation strength, and each reaches a maximum width before decaying into the chaotic sea. The widths of the regions of suppressed ionization are on the order of these maximum widths achieved by the resonance zones.

Experiments on spreading of probability

While most of the experimental work on excited states of hydrogen has investigated ionization, there are a few results reported that relate directly to the simulations presented in Chapter 4. These are measurements of the final state distribution for a beam initially prepared in a particular excited state, and perturbed in a microwave chamber. Unfortunately, none of this data has been taken with a set of parameters that would test for resonance zones. They do, however, serve as a physical check on the validity of the simulations in Chapter 4.

Below are shown a simulation and experimental results for a similar set of parameters. The color table on page 57 can be used to compare the two plots, and it is seen that the agreement is excellent. This shows not only that the numerical simulation reproduces the behavior of the actual atom, but, since the simulation only included the first three terms of the perturbation in the calculation, it also shows that, at least in this region of the parameter space, just a few terms of the perturbation can dominate the HSH behavior.

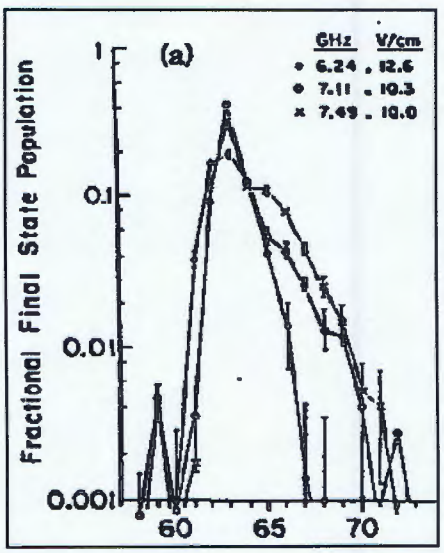

Figure 5.3(a). Energy level distribution of a beam of hydrogen atoms originally in the n=63 state, after 3000 cycles of microwave perturbation. [85aJNB, Fig. 2(a), reproduced with permission of the authors.]

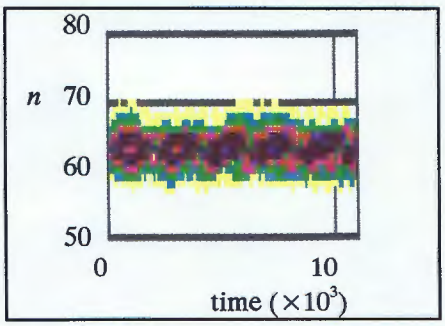

Figure 5.3(b). Evolution plot for the triply-resonant HSH atom with $M \in \{1, 2, 3\}$, and with initial state n_0=63. The other parameters are F=12.6 V/cm, and ν=6.24 GHz.

5.3 Conclusions and suggestions for future work

The conclusions of this work may be summed up as follows:

- The HSH atom does demonstrate nonlinear resonance, by the existence and overlap of resonance zones, in both a classical and a quantal analysis.
- Simulations based on the classical equations of motion do reproduce the detailed behavior observed in the laboratory. Specifically, the positions and widths of regions of stability calculated in the physical phase space match those found in the laboratory.
- Simulations based on the quantal equations of motion agree with the spreading of states observed in the laboratory, and with the size and overlap of resonance zones calculated from the classical action-angle coordinates.

Several interesting questions remain to be investigated in this field. These include:

- The quantum mechanical picture of the HSH resonance phenomenon parallels the classical picture in action-angle coordinates. But the calculations in the "physical" phase space provide a more accurate description of the motion. How might one understand the relation between the graded system of primary and higher-order resonances in the action-angle space and the single system of resonances arising in the physical space? An answer to this question might allow for the development of a more accurate quantum mechanical HSH theory. It is possible that some insight into this question may lie in the quantum KAM theory under development by Reichl and Haoming [902LER].
- More runs of the quantum mechanical simulations in Chapter 4 are needed to fill in the gaps and explore a wider space of parameters.
- More experimental data on final state distributions would be helpful in confirming the physical significance of the simulations in Chapter 4. It may be possible, although likely quite difficult, to find evidence of individual resonance zones and their overlap by probing a parameter space in which the other resonances are not important.

It is hoped that the work presented here might contribute some insight into work on these and other ongoing questions.

Appendices

The appendices provide reference information and detailed calculations.

Appendix A is a handy table of data comparing the properties of the ground state and a highly excited state of hydrogen.

Appendix B discusses the assumptions and approximation made in using the HSH model for hydrogen.

Appendix C presents the results of the numerical procedure described in Section 3.5.1 for locating the secondary resonances.

Various mathematical technicalities are handled in Appendices D. In particular, Appendix D.1 provides a useful table of conversion factors for the atomic system of units.

Computer methods and equipment used, as well as special computational techniques developed, in the course of this work are described in Appendix E.

Finally, the reasons for the semantic break from the conventional use of the term *Hamiltonian* are given in Appendix F.

A Some properties of the hydrogen atom

Quantity		Formula	Quantized ($I=n\hbar$) & Atomic units ($m=q=\hbar=1$)	Values for $n=1$ Common units	Values for $n=80$ Atomic units	Values for $n=80$ Common units
Semimajor axis	a	$\frac{I^2}{mq^2}$ [801HGo, (10-133)]	n^2	$0.53\cdot10^{-8}$ cm	6,400	$3.4\cdot10^{-5}$ cm
Average angular frequency	ω	$\frac{mq^4}{I^3}$ [801HGo, (10-118)]	$\frac{1}{n^3}$	$4.1\cdot10^{16}$ radians/sec	$2.0\cdot10^{-6}$	$0.81\cdot10^{11}$ radians/sec
Orbital frequency	ν	$\omega/(2\pi)$	$\frac{1}{2\pi n^3}$	$0.66\cdot10^{16}$ cycles/sec	$3.1\cdot10^{-7}$	$1.3\cdot10^{10}$ cycles/sec =13 GHz
Period	τ	$1/\nu$	$2\pi n^3$	$1.5\cdot10^{-16}$ sec	$3.2\cdot10^{6}$	$0.78\cdot10^{-10}$ sec
Average speed	s	circular orbit: $2\pi a/\tau$	$1/n$	$2.2\cdot10^{8}$ cm/sec $= 0.0073\,c$	0.0125	$2.7\cdot10^{6}$ cm/sec $= 0.91\cdot10^{-4}\,c$
		1-d orbit: $4a/\tau$	$\frac{2}{n\pi}$		0.0080	$1.7\cdot10^{6}$ cm/sec $= 0.58\cdot10^{-4}\,c$
Coulomb field strength (at $r=a$)	F	$-\frac{q}{a^2}$	$-\frac{1}{n^4}$	$-0.51\cdot10^{10}$ V/cm $= -1.7\cdot10^{7}$ Gauss	$-2.4\cdot10^{-8}$	-125 V/cm $= -0.42$ Gauss
Orbital energy	E_u	$-\frac{mq^4}{2I^2}$ [801HGo, (10-117)]	$-\frac{1}{2n^2}$	$-2.2\cdot10^{-11}$ erg $= -13.6$ eV	$-0.78\cdot10^{-4}$	$-3.4\cdot10^{-15}$ erg $= -0.0021$ eV
Energy splitting	ΔE_u		$\frac{1}{2}\left[\frac{1}{n^2}-\frac{1}{(n+1)^2}\right] \to n^{-3}$ $n\to\infty$	10.2 eV	$1.9\cdot10^{-6}$	$0.52\cdot10^{-4}$ eV
Wavelength (at average speed)	λ	$\frac{2\pi\hbar}{ms}$	circular orbit: $2\pi n$	$3.3\cdot10^{-8}$ cm	503	$2.7\cdot10^{-6}$ cm
			1-d orbit: $\pi^2 n$		790	$4.2\cdot10^{-6}$ cm

Note:

- The frequency of a photon with the energy of an energy splitting at high n is about the same as the average angular frequency of the electron with the same value of n.
- The de Broglie wavelength for the ground state (circular orbit only) is equal to the circumference of the orbit.
- The speed of light in atomic units is the reciprocal of the fine structure constant, $\approx$ 137. The speed of the electron in its ground state, as a fraction of the speed of light, is given by the fine structure constant, ≈ 0.0073.

B Validity of the HSH model

The harmonically driven Stark states of hydrogen model is the energy [page 11]:

$$E = E_u + Fx\cos(\omega t) \qquad \textit{HSH energy}$$

for a hydrogen atom in an extreme Stark state perturbed by a monochromatic, electromagnetic wave linearly polarized along the direction of Stark stretching. E_u is the energy of the atom in the absence of the perturbation, F and ω are, respectively, the amplitude and frequency of the electric force field of the wave, and x is the separation of the electron from the proton in the atom. In a classical analysis, E_u and x are real-valued functions, the former depending on only the initial conditions, the latter depending also on t; in a semi-classical analysis, these quantities are Hermitian operators in the complex Hilbert space of states of the atom. In either analysis, F and ω are considered to be real-valued constant parameters, and t is a real-valued independent variable.

This appendix discusses the assumptions and approximations which are implicit in the HSH energy. This is done in two parts. First Section B.1 covers the issues relating to the more general 3-dimensional model without Stark stretching [page 11]:

$$E = E_u + \vec{F}\cdot\vec{x}\cos(\omega t)\,, \qquad \textit{HH energy}$$

of which the HSH energy is a special case. Then, in Section B.2, the 1-dimensional approximation is discussed. For comparison purposes, the following energy values are helpful:

Characteristic energies of the HH atom (electron Volts)			
	ground state, $n=1$	$n=80$	$n=200$
E_u	-13.6	$-2.12\cdot10^{-3}$	$-3.40\cdot10^{-4}$
ΔE_u (up one level)	10.2	$0.521\cdot10^{-4}$	$3.37\cdot10^{-6}$
Fx, for F=50V/cm., $x=a/2$	$1.32\cdot10^{-7}$	$0.847\cdot10^{-3}$	$0.530\cdot10^{-2}$

B.1 The 3-dimensional model (HH energy)

Nonelectromagnetic interactions

Modern physical theory identifies three fundamental forces which account for all phenomena which fit into its framework. These are the gravitational, chromodynamic, and electroweak interactions. The HH energy ignores the existence of gravitational, chromodynamic, and the weak components of the electroweak interactions.

The energy of the gravitational attraction between the electron and proton in the ground state of a hydrogen atom is:

$$E_{G_{p\text{-}e}} = -\frac{G m_p m_e}{a} = -1.2\cdot 10^{-38}\text{eV},$$

which is truly negligible. The energy of the gravitational attraction between the Earth and a hydrogen atom at the Earth's surface is not so small however:

$$E_{G_{E\text{-}H}} = -\frac{G m_E m_H}{r_E} = -0.65\,\text{eV},$$

In classical mechanics, this is neglected by noticing that it is constant on the scale of the experiments and so can be absorbed into the scale of E_u. In quantum mechanics, one has to assume that the interaction affects all of the energy levels of the atom in the same way and that it can therefore again be neglected. The truth is that since there is no good quantum theory of gravity, no one really knows what affect the gravitational interaction has on the atom. On the other hand, there is no experimental evidence to suggest that there is any significant effect.

There is no chromodynamic interaction between a proton and an electron, so the only possible effect of the chromodynamic forces is in the structure of the proton. In quantum electrodynamics, this structure is taken into account in the calculation of the Lamb shift, to which it makes a small contribution. See the discussion of the Lamb shift below.

The proton and electron do engage in the weak interaction. To gain a qualitative sense of the importance of this interaction, one can think of it as a Yukawa potential mediated by the W-particle:

$$E_W(r) = g_W \frac{e^{-m_W r c/\hbar}}{r}.$$

A qualitative measure of the range of this interaction is $\hbar/(m_W c)=2\cdot 10^{-16}$ cm. This shows that the weak interaction is exponentially infinitesimal on the scale of the proton-electron separation.

Relativistic effects (fine structure)

When account is taken of special relativity, the Schrodinger equation must be replaced by Dirac's equation as the equation of motion for the hydrogen atom. Three additional terms appear in the energy. These terms are due to [730ASD, (64.11,12,13)] (a) interaction between the electron s-states and the proton (contact interaction), (b) velocity dependence of the electron's inertial mass, and (c) interaction of the electron magnetic moment with the magnetic field arising in its frame of reference due to its motion in the Coulomb field (spin-orbit coupling). These effects break the degeneracy of the energy states, since they induce a shift in the energy levels which depends on the total angular momentum of the electron [730ASD, (67.14)]:

$$\Delta E_{nj} = -\frac{\alpha^2}{2n^3}\left(\frac{1}{j+\frac{1}{2}} - \frac{3}{4n}\right),$$

where α is the fine structure constant. The leading factor has magnitude $3\cdot10^{-5}$ for $n=1$, and $0.5\cdot10^{-11}$ for $n=80$, so that comparison with the table on page 77 shows that the relativistic effects may be neglected.

Magnetic interactions (including hyperfine structure)

The fine structure induced by relativistic effects is largely due to magnetic interactions. This has been discussed in the previous paragraph.

Hyperfine structure is caused by the interaction of the proton and electron magnetic moments. Its effect is necessarily smaller than that of the spin-orbit coupling, a dominant cause of the fine structure, since the proton magnetic moment is so much smaller than the electron's orbital magnetic moment. Therefore this can also be ignored.

Another magnetic interaction in the HSH is due to the magnetic term of the Lorentz force law between the electron and the perturbing electromagnetic wave. The largest magnitude of this term occurs when the motion of the electron is perpendicular to the magnetic vector of the wave (which happens to be the case in the 1-dimensional approximation). The ratio of this magnitude to the magnitude of the electric term, and so the relative importance of this interaction, is equal to the speed of the electron as a fraction of the speed of light. This is given by the fine structure constant for the ground state and goes down as $1/n$ for the excited states [Appendix A]. Thus for states in the range $n\in\{50..100\}$, the magnetic interaction between the electron and the wave is about 10^{-4} as strong as the corresponding electric interaction, and may therefore be neglected.

Quantization of the electromagnetic field (Lamb shift)

The radiative corrections due to the interaction of the electron with the vacuum, as calculated in quantum electrodynamics, shift the energy levels of hydrogen by about 1 GHz [820VBB, 551 ¶1], or about $0.7\cdot10^{-6}$ eV. While this is completely negligible for the ground state of hydrogen, comparison with the table on page 77 shows that it shifts the $n=80$ levels by about 1% of the level separation. This is not terribly significant at the current level of sophistication, but as the theory and experiments improve it will become necessary to include radiative effects in the calculations.

Dipole approximation

The perturbation term of the HH energy is based on the multipole expansion for the energy of interaction between a charge distribution and the electrostatic influence of an external system. In the special case of two oppositely charged point particles, all multipole moments are zero except the dipole moment. See the above subsection on nonelectromagnetic interactions for a discussion of the structure of the proton, which addresses the validity of treating the atom as a pair of point particles.

The multipole expansion only gives information about the electrostatic interaction. Electrodynamic effects are calculated in the radiative corrections that make up the Lamb shift. See above for a discussion of this subject.

It is assumed in deriving the multipole expansion that the contribution of the external system to the electromagnetic field is nearly uniform throughout the region of the charge distribution. This is true in the case of an HH atom perturbed by microwaves, which have wavelengths in the centimeters. As Jensen says, in the relation to the surface-state electron model, "Since the standing wavelengths of the microwave radiation are long compared with the maximum excursion ... of the ... [electron], the spatial variation of the perturbing electric fields can be neglected" [83bRVJ, <(11)].

Central force model; reduction to one-body problem

The entire analysis rests on the reduction of the two-body central-force problem to the equivalent one-body problem. This fundamental step assumes that all forces in the problem depend only on the separation of the two bodies so that all forces are directed along the line of separation [801HGo, §3-1, 71 ¶4; 770LDL, >(36.1)]. In the treatment of the 3- or 2-dimensional problem, this assumptions would be violated by the interaction with the electromagnetic wave because that force is directed along the electric vector which would not in general be collinear with the separation of the electron and proton. It would then be necessary to investigate whether the strength of this violation would invalidate the transformation to action-angle coordinates and other aspects of the theory. In the 1-dimensional approximation, however, the assumption remains valid.

Motion of the proton; acceleration of the center of mass

No assumption that the proton is stationary (or infinitely massive, as the assumption is often stated) is necessary because of the reduction of the two-body problem to the equivalent one-body problem [above]. Furthermore, as long as the reduction to the one-body problem remains valid, the motion of the center of mass remains inertial and may therefore be ignored.

Single atom versus ensemble

In writing the HH energy, the sign of the perturbation term has been considered arbitrary since it can be reversed by a shift in the origin of time. Similarly, no phase term is included in the time-dependence of the perturbation, since it could be set to zero by a shift in t. These procedures are permissible as long as the analysis considers only a single atom, which

is the case here. If an ensemble were to be considered, it would be necessary to include an independent phase for each atom, unless there was found to be a way in experiments to arrange a phase relationship among the electrons in the various atoms, which would likely be quite difficult.

B.2 The 1-dimensional approximation (HSH energy)

The state function for the hydrogen atom in paraboloidal coordinates, in the special case $n_2=m=0$, is [§D.6]:

$$\langle \rho_1,\rho_2,\phi | n\rangle \approx \frac{1}{\sqrt{\pi}\, n^2}\, e^{-\frac{\rho_1+\rho_2}{2n}}\, L_n\left[\frac{\rho_1}{n}\right],$$

where $(\rho_1+\rho_2)/2$ is the radial distance, r, from the proton. This formula shows that the probability drops exponentially with r, except on the positive x-axis, where ρ_2 is zero and the ρ_1-dependence of the Laguerre polynomial cancels the effect of the exponential. (On the negative x-axis, ρ_1 is zero.) A plot of the absolute square of this function for $n=40$ is given at right (where the x-axis is called "z"). This shows that the probability extends primarily along the positive x-axis, and drops off rapidly everywhere else.

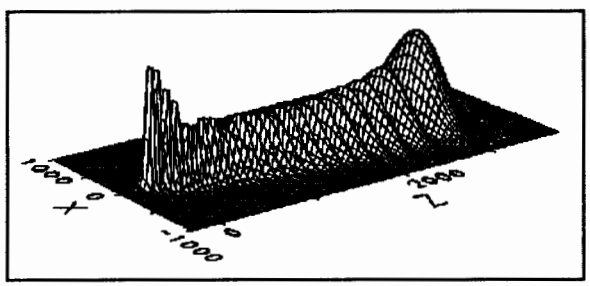

Figure B.1 Probability distribution for the extreme Stark state $|n_1, n_2, m\rangle = |39, 0, 0\rangle$, for which $n=40$. [872RBI, Figure 1, reproduced with permission of the authors.]
The z-axis in this plot corresponds to what is called the x-axis elsewhere in this work.

Shepelyansky [836DLS, §2; 872RBI, >(2.1)] sets out three arguments in favor of the 1-dimensional approximation:

- For small angular momentum Stark states[1], the probabilities of n-changing transitions calculated from the 3-dimensional model are within a few percent of those calculated from the 1-dimensional.
- The Coulomb degeneracy causes the sublevels of a single n level to act in unison.
- For small angular momentum Stark states, the time rate of occurrence of transitions in angular momentum is slow.

Bardsley and Sundaram [853JNB, 689 ¶6] also point out that the matrix elements connecting the most extreme Stark states $|n_1, n_2, m\rangle = |n-1, 0, 0\rangle$ with the less elongated states $|n-k-1, k, 0\rangle$ are diminished by a factor of n^{-k}. This provides "for highly excited states ... a strong constraint to remain on the ladder of extreme Stark states." Bayfield and Sokol [887JEB, 2008 ¶3] explain that n_1 and m should not change on account of electric dipole selection rules, and report agreement in their experimental results.

[1] It must be pointed out that the states closest to the s states of a particular energy level also have small angular momentum. These arguments do not apply to those states.

Leopold and Richards have done a classical analysis of the combined effect of a static and microwave field on an extreme Stark state of hydrogen [869JGL]. They find that a static field component is necessary to prevent the periapsis vector[2] from precessing and thereby invalidating, over time, the 1-dimensional approximation. The time during which the approximation may remain valid without a static field has a complicated dependence on the microwave frequency. Since this is a classical analysis, it may however not reflect the true behavior of the atom. Indeed, the experimental data seem to show that the 1-dimensional approximation does model the behavior of the extreme Stark states quite well.

[2] Also known as the Runge-Lenz or Laplace vector.

C Numerical estimates of locations of secondary resonances

This appendix presents the results of the numerical procedure described in Section 3.5.1 for locating the secondary resonances. Three tables are presented, one each for $M=1$, 2 and 3. All the data are for $F=2\cdot10^{-10}$ and $\omega=2\pi/(5\cdot10^{6})$. The columns in the tables have the following meanings:

$\dot{\zeta}^{(M)}/\omega$ — Ratio of angular frequencies of the pendulum in its action-angle space and of the perturbation. The frequency of the pendulum was calculated using the formula on page 97.

"as fraction": Rational number the computer was looking for when it chose this data point.

"as decimal": Value of $\dot{\zeta}^{(M)}/\omega$ at the chosen data point, as calculated from the formula.

"% error": Percent error between the data in the two previous columns.

$J^{(M)}$ — Action coordinate of the pendulum at the chosen data point. This was calculated using the formula on page 97.

$E^{(M)'}$ — Independent variable in the calculations of both $\dot{\zeta}^{(M)}$ and $J^{(M)}$.

$I^{(M)}_{F=0} \equiv \sqrt{2m_M E^{(M)'}}$.

$I_{F=0} \equiv I_M + MI^{(M)}_{F=0}$. This is the important column. It gives the locations, in terms of the unperturbed HSH action, of the resonances corresponding to the rational values of $\dot{\zeta}^{(M)}/\omega$ in the first column.

$E_{F=0}(\xi, I) \equiv -\frac{1}{2I^2_{F=0}}$.

$E^{(M)}(\xi, I)$ — calculated here as $-E^{(M)'} + E_M + F_M + \frac{MI^{(M)}_{F=0}}{I^3_M}$.

% error $\equiv 100\frac{E_{F=0} - E^{(M)}}{E_{F=0}}$.

Resonance data for $M=1$, $F=2\cdot10^{-10}$, $\omega=2\pi/(5\cdot10^{6})$									
$\dot{\xi}^{(M)}/\omega$			$J^{(M)}$	$E^{(M)'}$	$I^{(M)}_{F=0}$	$I_{F=0}$	$E_{F=0}(\xi, I)$	$E^{(M)}(\xi, I)$	%
as fraction	as decimal	% error		$(\cdot10^{-6})$			$(\cdot10^{-6})$	$(\cdot10^{-6})$	error
8/5	1.5960	-0.25	49.30	50.00	-49.58	43.09	-269.30	-169.97	36.9
3/2	1.5003	0.02	46.35	44.25	-46.64	46.03	-236.02	-160.53	32.0
7/5	1.4000	-0.00	43.25	38.60	-43.56	49.11	-207.35	-151.01	27.2
4/3	1.3330	-0.02	41.18	35.05	-41.51	51.16	-191.05	-144.88	24.2
5/4	1.2503	0.02	38.62	30.90	-38.98	53.69	-173.44	-137.55	20.7
6/5	1.1998	-0.02	37.06	28.50	-37.43	55.24	-163.88	-133.20	18.7
1/1	0.9994	-0.06	30.87	19.95	-31.32	61.35	-132.84	-116.97	11.9
4/5	0.8004	0.04	24.73	13.00	-25.28	67.39	-110.11	-102.44	7.0
3/4	0.7505	0.06	23.19	11.50	-23.78	68.89	-105.35	-99.05	6.0
2/3	0.6668	0.01	20.61	9.20	-21.27	71.40	-98.08	-93.59	4.6
3/5	0.5995	-0.09	18.53	7.55	-19.27	73.40	-92.80	-89.43	3.6
1/2	0.5008	0.16	15.50	5.45	-16.37	76.30	-85.89	-83.69	2.6
2/5	0.3999	-0.02	12.40	3.70	-13.49	79.18	-79.75	-78.32	1.8
1/3	0.3319	-0.44	10.34	2.75	-11.63	81.04	-76.13	-75.03	1.4
1/4	0.2501	0.05	7.92	1.87	-9.58	83.09	-72.42	-71.57	1.2
1/5	0.2001	0.06	6.55	1.48	-8.52	84.14	-70.62	-69.86	1.1
0 (sepx)	0.0370	100	4.72	1.12	-7.41	85.26	-68.78	-68.09	1.0
1/5	0.2000	-0.02	2.15	0.60	-5.41	87.25	-65.67	-65.07	0.9
cntr	0.2398	0.00	0.00	0.00	0.00	92.67	-58.23	-57.67	1.0
1/5	0.2000	-0.02	2.15	0.60	5.41	98.08	-51.97	-51.46	1.0
0 (sepx)	0.0370	100	4.72	1.12	7.41	100.08	-49.92	-49.47	0.9
1/5	0.2001	0.06	6.55	1.48	8.52	101.19	-48.83	-48.43	0.8
1/4	0.2501	0.05	7.92	1.87	9.58	102.25	-47.83	-47.50	0.7
1/3	0.3319	-0.44	10.34	2.75	11.63	104.30	-45.97	-45.81	0.3
2/5	0.3999	-0.02	12.40	3.70	13.49	106.16	-44.37	-44.42	-0.1
1/2	0.5008	0.16	15.50	5.45	16.37	109.04	-42.06	-42.55	-1.2
3/5	0.5995	-0.09	18.53	7.55	19.27	111.93	-39.91	-41.01	-2.8
2/3	0.6668	0.01	20.61	9.20	21.27	113.94	-38.52	-40.14	-4.2
3/4	0.7505	0.06	23.19	11.50	23.78	116.45	-36.87	-39.29	-6.5
4/5	0.8004	0.04	24.73	13.00	25.28	117.95	-35.94	-38.90	-8.2
1/1	0.9994	-0.06	30.87	19.95	31.32	123.99	-32.53	-38.26	-17.6
6/5	1.1998	-0.02	37.06	28.50	37.43	130.10	-29.54	-39.13	-32.5
5/4	1.2503	0.02	38.62	30.90	38.98	131.64	-28.85	-39.59	-37.2
4/3	1.3330	-0.02	41.18	35.05	41.51	134.18	-27.77	-40.55	-46.0
7/5	1.4000	-0.00	43.25	38.60	43.56	136.23	-26.94	-41.53	-54.1
3/2	1.5003	0.02	46.35	44.25	46.64	139.31	-25.76	-43.31	-68.1
8/5	1.5960	-0.25	49.30	50.00	49.58	142.25	-24.71	-45.36	-83.6

Resonance data for $M=2$, $F=2\cdot10^{-10}$, $\omega=2\pi/(5\cdot10^6)$									
$\dot{\xi}^{(M)}/\omega$			$J^{(M)}$	$E^{(M)'}$	$I^{(M)}_{F=0}$	$I_{F=0}$	$E_{F=0}(\xi, I)$	$E^{(M)}(\xi, I)$	%
as fraction	as decimal	% error		$(\cdot10^{-6})$			$(\cdot10^{-6})$	$(\cdot10^{-6})$	error
2/1	1.9998	-0.01	38.91	49.20	-39.03	38.68	-334.11	-134.63	59.7
9/5	1.7995	-0.03	35.02	39.90	-35.15	46.45	-231.75	-120.45	48.0
7/4	1.7500	0.00	34.05	37.75	-34.19	48.37	-213.71	-117.09	45.2
5/3	1.6662	-0.03	32.42	34.25	-32.57	51.62	-187.67	-111.55	40.6
8/5	1.5998	-0.01	31.13	31.60	-31.28	54.19	-170.28	-107.29	37.0
3/2	1.4996	-0.03	29.18	27.80	-29.34	58.07	-148.27	-101.05	31.9
7/5	1.3994	-0.04	27.23	24.25	-27.40	61.94	-130.30	-95.06	27.0
4/3	1.3335	0.02	25.95	22.05	-26.13	64.49	-120.22	-91.26	24.1
5/4	1.2496	-0.03	24.32	19.40	-24.51	67.73	-108.99	-86.58	20.6
6/5	1.1995	-0.04	23.34	17.90	-23.54	69.66	-103.03	-83.86	18.6
1/1	1.0006	0.06	19.47	12.55	-19.71	77.32	-83.62	-73.70	11.9
4/5	0.8008	0.10	15.59	8.15	-15.89	84.98	-69.24	-64.49	6.9
3/4	0.7507	0.09	14.61	7.20	-14.93	86.89	-66.23	-62.34	5.9
2/3	0.6669	0.04	12.98	5.75	-13.34	90.07	-61.64	-58.89	4.5
3/5	0.5990	-0.17	11.66	4.70	-12.06	92.62	-58.28	-56.24	3.5
1/2	0.4981	-0.39	9.70	3.35	-10.19	96.38	-53.82	-52.52	2.4
2/5	0.4021	0.53	7.85	2.30	-8.44	99.87	-50.13	-49.28	1.7
1/3	0.3347	0.39	6.55	1.70	-7.26	102.24	-47.83	-47.19	1.3
1/4	0.2501	0.04	4.96	1.12	-5.88	105.00	-45.35	-44.87	1.1
1/5	0.2001	0.05	4.07	0.86	-5.17	106.41	-44.16	-43.74	1.0
0 (sepx)	0.0321	100	2.77	0.61	-4.35	108.06	-42.82	-42.45	0.9
1/5	0.2001	0.04	0.84	0.22	-2.63	111.49	-40.22	-39.90	0.8
cntr	0.2235	0.00	0.00	0.00	0.00	116.75	-36.68	-36.37	0.8
1/5	0.2001	0.04	0.84	0.22	2.63	122.02	-33.58	-33.29	0.9
0 (sepx)	0.0321	100	2.77	0.61	4.35	125.45	-31.77	-31.52	0.8
1/5	0.2001	0.05	4.07	0.86	5.17	127.10	-30.95	-30.74	0.7
1/4	0.2501	0.04	4.96	1.12	5.88	128.51	-30.28	-30.10	0.6
1/3	0.3347	0.39	6.55	1.70	7.26	131.27	-29.02	-28.96	0.2
2/5	0.4021	0.53	7.85	2.30	8.44	133.63	-28.00	-28.07	-0.2
1/2	0.4981	-0.39	9.70	3.35	10.19	137.13	-26.59	-26.92	-1.3
3/5	0.5990	-0.17	11.66	4.70	12.06	140.88	-25.19	-25.91	-2.9
2/3	0.6669	0.04	12.98	5.75	13.34	143.44	-24.30	-25.35	-4.3
3/4	0.7507	0.09	14.61	7.20	14.93	146.62	-23.26	-24.81	-6.7
4/5	0.8008	0.10	15.59	8.15	15.89	148.53	-22.66	-24.56	-8.4
1/1	1.0006	0.06	19.47	12.55	19.71	156.18	-20.50	-24.15	-17.8
6/5	1.1995	-0.04	23.34	17.90	23.54	163.84	-18.63	-24.69	-32.5
5/4	1.2496	-0.03	24.32	19.40	24.51	165.78	-18.19	-24.97	-37.3
4/3	1.3335	0.02	25.95	22.05	26.13	169.02	-17.50	-25.59	-46.2
7/5	1.3994	-0.04	27.23	24.25	27.40	171.56	-16.99	-26.19	-54.2
3/2	1.4996	-0.03	29.18	27.80	29.34	175.44	-16.24	-27.30	-68.1
8/5	1.5998	-0.01	31.13	31.60	31.28	179.32	-15.55	-28.66	-84.3
5/3	1.6662	-0.03	32.42	34.25	32.57	181.89	-15.11	-29.70	-96.5
7/4	1.7500	0.00	34.05	37.75	34.19	185.14	-14.59	-31.16	-113.6
9/5	1.7995	-0.03	35.02	39.90	35.15	187.06	-14.29	-32.10	-124.6
2/1	1.9998	-0.01	38.91	49.20	39.03	194.82	-13.17	-36.52	-177.2

Resonance data for $M=3$, $F=2\cdot10^{-10}$, $\omega=2\pi/(5\cdot10^6)$									
$\dot{\xi}^{(M)}/\omega$			$J^{(M)}$	$E^{(M)'}$	$I^{(M)}_{F=0}$	$I_{F=0}$	$E_{F=0}(\xi,I)$	$E^{(M)}(\xi,I)$	%
as fraction	as decimal	% error		$(\cdot10^{-6})$			$(\cdot10^{-6})$	$(\cdot10^{-6})$	error
9/4	2.2501	0.00	33.41	47.45	-33.49	33.19	-454.01	-117.31	74.2
11/5	2.1995	-0.02	32.66	45.35	-32.74	35.43	-398.22	-114.27	71.3
2/1	2.0004	0.02	29.71	37.55	-29.79	44.28	-255.02	-102.77	59.7
9/5	1.8002	0.01	26.73	30.45	-26.83	53.17	-176.86	-91.94	48.0
7/4	1.7504	0.02	25.99	28.80	-26.09	55.38	-163.02	-89.37	45.2
5/3	1.6673	0.04	24.76	26.15	-24.86	59.07	-143.30	-85.17	40.6
8/5	1.6001	0.00	23.76	24.10	-23.87	62.05	-129.86	-81.87	37.0
3/2	1.4998	-0.01	22.27	21.20	-22.38	66.50	-113.07	-77.11	31.8
7/5	1.4000	0.00	20.79	18.50	-20.91	70.92	-99.41	-72.56	27.0
4/3	1.3334	0.00	19.80	16.80	-19.93	73.87	-91.63	-69.62	24.0
5/4	1.2504	0.03	18.57	14.80	-18.70	77.54	-83.16	-66.08	20.5
6/5	1.2001	0.01	17.82	13.65	-17.96	79.77	-78.58	-64.00	18.6
1/1	1.0004	0.04	14.86	9.55	-15.02	88.58	-63.72	-56.21	11.8
4/5	0.8010	0.12	11.90	6.20	-12.11	97.34	-52.78	-49.19	6.8
3/4	0.7491	-0.12	11.13	5.45	-11.35	99.60	-50.40	-47.49	5.8
2/3	0.6657	-0.14	9.89	4.35	-10.14	103.23	-46.92	-44.87	4.4
3/5	0.6023	0.37	8.95	3.60	-9.22	105.98	-44.52	-42.97	3.5
1/2	0.4999	-0.01	7.43	2.55	-7.76	110.36	-41.05	-40.09	2.4
2/5	0.3980	-0.50	5.93	1.70	-6.34	114.63	-38.05	-37.45	1.6
1/3	0.3311	-0.67	4.94	1.25	-5.44	117.34	-36.31	-35.86	1.2
1/4	0.2500	-0.01	3.77	0.82	-4.41	120.43	-34.48	-34.14	1.0
1/5	0.2000	0.02	3.08	0.63	-3.85	122.10	-33.54	-33.25	0.9
0 (sepx)	0.0306	100	2.01	0.42	-3.16	124.18	-32.42	-32.17	0.8
1/5	0.1999	-0.03	0.36	0.09	-1.48	129.21	-29.95	-29.73	0.7
cntr	0.2126	0.00	0.00	0.00	0.00	133.65	-27.99	-27.78	0.8
1/5	0.1999	-0.03	0.36	0.09	1.48	138.09	-26.22	-26.01	0.8
0 (sepx)	0.0306	100	2.01	0.42	3.16	143.12	-24.41	-24.24	0.7
1/5	0.2000	0.02	3.08	0.63	3.85	145.20	-23.72	-23.57	0.6
1/4	0.2500	-0.01	3.77	0.82	4.41	146.87	-23.18	-23.06	0.5
1/3	0.3311	-0.67	4.94	1.25	5.44	149.96	-22.24	-22.20	0.2
2/5	0.3980	-0.50	5.93	1.70	6.34	152.67	-21.45	-21.52	-0.3
1/2	0.4999	-0.01	7.43	2.55	7.76	156.94	-20.30	-20.58	-1.4
3/5	0.6023	0.37	8.95	3.60	9.22	161.32	-19.21	-19.79	-3.0
2/3	0.6657	-0.14	9.89	4.35	10.14	164.07	-18.57	-19.39	-4.4
3/4	0.7491	-0.12	11.13	5.45	11.35	167.70	-17.78	-18.97	-6.7
4/5	0.8010	0.12	11.90	6.20	12.11	169.97	-17.31	-18.77	-8.4
1/1	1.0004	0.04	14.86	9.55	15.02	178.72	-15.65	-18.45	-17.9
6/5	1.2001	0.01	17.82	13.65	17.96	187.53	-14.22	-18.86	-32.7
5/4	1.2504	0.03	18.57	14.80	18.70	189.76	-13.89	-19.08	-37.4
4/3	1.3334	0.00	19.80	16.80	19.93	193.43	-13.36	-19.54	-46.2
7/5	1.4000	0.00	20.79	18.50	20.91	196.38	-12.96	-20.00	-54.3
3/2	1.4998	-0.01	22.27	21.20	22.38	200.80	-12.40	-20.85	-68.2
8/5	1.6001	0.00	23.76	24.10	23.87	205.25	-11.87	-21.89	-84.4
5/3	1.6673	0.04	24.76	26.15	24.86	208.23	-11.53	-22.69	-96.8
7/4	1.7504	0.02	25.99	28.80	26.09	211.92	-11.13	-23.80	-113.7
9/5	1.8002	0.01	26.73	30.45	26.83	214.13	-10.90	-24.52	-124.9
2/1	2.0004	0.02	29.71	37.55	29.79	223.02	-10.05	-27.89	-177.5
11/5	2.1995	-0.02	32.66	45.35	32.74	231.87	-9.30	-31.99	-244.0
9/4	2.2501	0.00	33.41	47.45	33.49	234.12	-9.12	-33.15	-263.4

D Mathematical issues and details

D.1 Atomic units

The equations throughout most of this work are simplified by the use of atomic units.[1]

The basic atomic units	
The unit for:	is:
mass	the reduced mass of the proton-electron system, m
electric charge	the charge of the proton, q
action (only in quantum mechanics)	the reduced Planck's constant, $\hbar$

These units are useful specifically when dealing with the hydrogen atom.

Any quantity can be converted to atomic units by setting $m=q=\hbar=1$. For example, the energy of the hydrogen atom:

$$E_u = \frac{\vec{p}^2}{2m} - \frac{q^2}{r},$$

becomes, in atomic units:

$$E_u = \frac{\vec{p}^2}{2} - \frac{1}{r}.$$

The following table gives the conversion factors between atomic units and the most common scientific units for all physical quantities discussed in this work.

[1] Many references define the atomic unit of mass as the mass of the electron. The definition given here, as the reduced mass of the proton-electron system, is more correct and no less convenient to use. Values given in the table of conversion factors differ in the fourth significant digit from figures quoted on the basis of the other definition.

Conversion factors for atomic units		
To convert from atomic units for:	to:	multiply by:
mass (the reduced mass of the proton-electron system)	grams	$m \equiv \frac{m_p m_e}{m_p + m_e} = 0.910458 \cdot 10^{-27}$ gm
electric charge (the charge of the proton)	Coulombs	$q = 1.60219 \cdot 10^{-19}$ C
	esu	$= 4.80324 \cdot 10^{-10}$ esu
length (the "Bohr radius", the classical radius of the ground state of hydrogen)	centimeters	$a \equiv \frac{\hbar^2}{m q^2} = 0.529465 \cdot 10^{-8}$ cm
angular frequency (the angular frequency of the ground state of hydrogen)	radians/second	$\frac{m q^4}{\hbar^3} = 4.13189 \cdot 10^{16}$ rad/s
	frequency in GigaHertz	$\frac{m q^4}{2\pi \hbar^3} \cdot 10^{-9} = 0.657610 \cdot 10^7$ GHz
time (1/(2π) times the period of the ground state of hydrogen)	seconds	$\frac{\hbar^3}{m q^4} = 2.42020 \cdot 10^{-17}$ sec
electromagnetic field strength (the Coulomb force at the Bohr radius)	Volts/centimeter	$\frac{q}{a^2} c \cdot 10^{-8} = 0.513665 \cdot 10^{10}$ V/cm
	Gauss	$\frac{q}{a^2} = 1.71340 \cdot 10^7$ Gauss
energy (twice the energy of the ground state of hydrogen)	ergs	$\frac{m q^4}{\hbar^2} = 4.3574 \cdot 10^{-11}$ erg
	electron Volts	$= 27.199$ eV

D.2 The extended phase space for a system with a 1-dimensional, time-dependent energy

Any 1-dimensional, time-dependent energy is formally equivalent to a 2-dimensional, time-independent one obtained by going to an *extended phase space* [830AJL, 14] in which time and the original energy become a canonical pair of dynamical coordinates. The transformation to the new phase space is generated by:

$$G(q_1, q_2; \bar{p}_1, \bar{p}_2) = G(q, t; p, -E') = pq - E't$$

where E' is the *value* of the original 1-dimensional, time-dependent energy function, $E(q, p,$, this value treated here as an independent variable. Under this generating function, the old and new coordinates are related by [801HGo, (9-17)]:

$$\bar{q}_1 = \frac{\partial G}{\partial \bar{p}_1} = \frac{\partial G}{\partial p} = q \qquad \bar{q}_2 = \frac{\partial G}{\partial \bar{p}_2} = \frac{\partial G}{\partial(-E')} = t$$

$$p_1 = \frac{\partial G}{\partial q_1} = \frac{\partial G}{\partial q} = p \qquad p_2 = \frac{\partial G}{\partial q_2} = \frac{\partial G}{\partial t} = -E'$$

and the new energy is:

$$\bar{E}(\bar{q}_1, \bar{q}_2; \bar{p}_1, \bar{p}_2) = \bar{E}(q, t; p, -E') = E(q, p, t) + \frac{\partial G}{\partial t} = E(q, p, t) - E' ,$$

By this construction, the new energy, $\bar{E}$, is guaranteed to be a time-constant, and it in fact happens to be constantly equal to zero.

Hamilton's equations in the extended phase space, in terms of a new parameter of the motion, ζ, yield the original pair of Hamilton's equations, plus an additional pair:

$$\left\{ \begin{array}{l} \dfrac{dp}{d\zeta} = -\dfrac{\partial \bar{E}}{\partial q} = -\dfrac{\partial E}{\partial q} \\ \dfrac{dq}{d\zeta} = \dfrac{\partial \bar{E}}{\partial p} = \dfrac{\partial E}{\partial p} \end{array} \right\} , \qquad \left\{ \begin{array}{l} \dfrac{d(-E')}{d\zeta} = -\dfrac{\partial \bar{E}}{\partial t} = -\dfrac{\partial E}{\partial t} \\ \dfrac{dt}{d\zeta} = \dfrac{\partial \bar{E}}{\partial(-E')} = 1 \end{array} \right\} .$$

The first pair is equivalent to the original Hamilton's equations because of the fact that the second equation in the second pair implies that $\zeta = t$ (modulo a constant). The first equation of the second pair then just reiterates the definition that $E'(t) = E(q, p, t)$.

The new 4-dimensional phase space is the Cartesian product of the (p, q) phase plane with the $(-E', t)$ plane.

Everything said so far in this section applies to any 1-dimensional system with a time-dependent energy. But the true utility of this technique is for bound states of a system whose energy consists of:

- a time-*in*dependent part, plus
- a weak, time-*de*pendent perturbation which is periodic in time.

The effect of the perturbation is to superimpose an approximately time-periodic deviation on the underlying motion of the unperturbed system.

The reason the extended phase space is useful in such a case is that it is easy to make a *Poincare section* [§1.2]. For a 1-dimensional system whose energy consists of a time-independent part and a weak, time-periodic perturbation, a Poincare section of the 4-dimensional extended phase space can be taken by simply *strobing*, at the frequency of the perturbation, the motion in the *original* 2-dimensional phase space. The stroboscopic action performs the equivalent of a "Cartesian quotient" operation, pulling out one copy of the (p, q) phase plane from the 4-dimensional phase space. This technique is used to study the behavior of the HSH atom, in Section 2.4 for the "physical" phase space, and in Sections 3.3 and 3.5.2 for the action-angle space.

D.3 Cartesian coordinates of the Kepler motion

The radial distance, r, of an orbiting body from its Kepler center of attraction can be given either as a function of the body's angular displacement from periapsis, θ [801HGo, (3-64); 760LDL, (15.5..6)]:

$$r = \frac{a(1-\varepsilon^2)}{1+\varepsilon\cos(\theta)},$$

or as a function of an orbital parameter, ζ, which also parameterizes time [801HGo, (3-68, 76); 760LDL, (15.10)]:

$$\left\{\begin{array}{l} r = a(1-\varepsilon\cos(\zeta)) \\ t = \dfrac{\zeta-\varepsilon\sin(\zeta)}{\omega} \end{array}\right\},$$

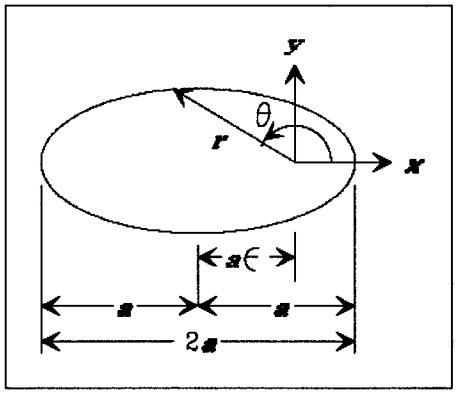

Figure D.1 Geometry of the Kepler orbit. The origin of coordinates is at the center of attraction, which is also at one of the foci of the elliptical orbit. The eccentricity, ε, gives the offset of this point from the geometrical center of the ellipse.

in which the semimajor axis, a, the eccentricity, ε, and the average angular frequency, ω, are constants of the motion[2]. Combining the formulae for r, the Cartesian coordinates of the body can be expressed in terms of the orbital parameter [760LDL, (15.11)]:

$$\left\{\begin{array}{ll} x = r\cos(\theta) & = a(\cos(\zeta)-\varepsilon) \\ y = \sqrt{r^2-x^2} & = a\sqrt{1-\varepsilon^2}\sin(\zeta) \end{array}\right\}.$$

Expansion in Fourier series

If the origin of time is taken to be at either apsidal point, then x and y are, respectively, symmetric and antisymmetric in time: $x(-t)=x(t)$ and $y(-t)=-y(t)$. So these coordinates are expanded in, respectively, Fourier cosine and sine series [413GNW, §17.2][3]:

[2] The orbital variables θ, ζ and ωt were, in "the terminology of medieval astronomy," called the *true*, *eccentric*, and *mean anomalies*, respectively [801HGo, <(3-68), >(3-76)]. The term *anomaly* referred to the deviation of a planet from the perihelion position of its orbit.

[3] Several sources refer to 750LDL, §70 for the Cartesian coordinates, but the method there for calculating the Fourier components, which uses complex Fourier series and their time derivatives, is not valid for $n=0$ and so cannot be used to provide the complete solution for $x(t)$.

$$\left\{\begin{array}{ll} x(t) = \dfrac{x_0}{2} + \displaystyle\sum_{n=1}^{\infty} x_n \cos(n\omega t) & x_n = \dfrac{a\omega}{\pi} \displaystyle\int_0^{\frac{2\pi}{\omega}} (\cos(\zeta(t)) - \varepsilon)\cos(n\omega t)\, dt \\ y(t) = \displaystyle\sum_{n=1}^{\infty} y_n \sin(n\omega t) & y_n = \dfrac{a\sqrt{1-\varepsilon^2}\,\omega}{\pi} \displaystyle\int_0^{\frac{2\pi}{\omega}} \sin(\zeta(t))\sin(n\omega t)\, dt \end{array}\right\}.$$

With the parametric expression for time given above, the calculation of the Fourier components reduces the series to:

$$\left\{\begin{array}{l} x(t) = -\dfrac{3a\varepsilon}{2} + 2a \displaystyle\sum_{n=1}^{\infty} \frac{J_n'(n\varepsilon)}{n}\cos(n\omega t) \\ y(t) = \dfrac{2a\sqrt{1-\varepsilon^2}}{\varepsilon} \displaystyle\sum_{n=1}^{\infty} \frac{J_n(n\varepsilon)}{n}\sin(n\omega t) \end{array}\right\}.$$

where $J_n(z)$ is the Bessel function of the first kind, and $J_n'(z)$ is its derivative with respect to z, evaluated at z.

This pair of equations provides an interesting picture of the Kepler motion. The constant term in the x-coordinate gives the position of a kind of center about which x oscillates. Since the geometrical center of the orbit is at $x=-a\varepsilon$, this "center of oscillation" is located half way between the geometrical center and the unoccupied focus of the ellipse. The time-dependent part of the motion is entirely harmonic, but with each harmonic term weighted by a Bessel function (for y) or a derivative of a Bessel function (for x).

Two special cases

If $\varepsilon=0$, the motion reduces to a circular orbit:

$$\left\{\begin{array}{l} x(t) = a\cos(\omega t) \\ y(t) = a\sin(\omega t) \end{array}\right\}.$$

In the opposite extreme, if $\varepsilon = 1$, the motion is along an infinitesimally wide ellipse[4]:

[4] The conic sections are usually listed with that for $\varepsilon=1$ being the parabola. In the construction where conics are considered to be the intersection of a cone with a plane, the meaning of $\varepsilon=1$ is that the plane is parallel to a straight line in the cone (a *generator* of the cone). *If* the plane *does not contain* that line, then the resulting section is a parabola. But if it does contain the line, then the plane is tangent to the cone. One can then consider a limiting process in which the plane is rotated into this position of tangency. If this process approaches tangency from $\varepsilon>1$, then the resulting section is a degenerate hyperbola, an is an infinite line. If tangency is approached from $\varepsilon<1$, then the section is a degenerate ellipse, and is a line segment. This latter case is the one at hand.

$$\left\{ \begin{array}{l} x(t) = -\frac{3a}{2} + 2a \sum_{n=1}^{\infty} \frac{J'_n(n)}{n} \cos(n\omega t) \\ \\ y(t) = 0 \end{array} \right\}.$$

Here the foci lie *on* the ellipse itself, at the very ends of the major axis, and are therefore $2a$ apart. The body does not so much go around the center of attraction, as repeatedly bounce off of it to a maximum distance of $2a$. The "center of oscillation" is at a point 3/4 of the way from the center of attraction (which coincides here with the periapsis) to apapsis. This is the orbit of the electron in the HSH atom.

Expression in terms of action-angle coordinates

Two of the constants of the Kepler motion appearing in its Fourier expansion are simple functions of the action coordinates [801HGo, (10-133..4)][5]:

$$a = \frac{I_1^2}{mk} \qquad \text{and} \qquad \varepsilon = \sqrt{1 - \left[\frac{I_2}{I_1}\right]^2},$$

in which m is the reduced mass of the two-body system, and k is the strength parameter of the Kepler force. The other constant, the average angular frequency, appears only in combination with the time. This combination is, because of the total degeneracy of the system, simply equal to the angle coordinate conjugate to I_1:

$$\xi_1 = \omega t + \xi_{1_0},$$

where ξ_{1_0}, the value of ξ_1 at $t=0$, is an arbitrary constant of integration and can be set to zero. Thus the Fourier expansion of the Cartesian coordinates in Kepler motion is easily transformed to action-angle coordinates:

$$\left\{ \begin{array}{l} x(\xi_1) = \frac{I_1}{mk} \left(-\frac{3}{2}\sqrt{I_1^2 - I_2^2} + 2I_1 \sum_{n=1}^{\infty} \frac{J'_n(n\sqrt{1-(I_2/I_1)^2})}{n} \cos(n\xi_1) \right) \\ \\ y(\xi_1) = \frac{2I_1^2 I_2}{mk\sqrt{I_1^2 - I_2^2}} \sum_{n=1}^{\infty} \frac{J_n(n\sqrt{1-(I_2/I_1)^2})}{n} \sin(n\xi_1) \end{array} \right\}.$$

[5] The notation here is slightly different from Goldstein's. The differences consist of the interchange of I_1 and I_3, and the division of his definitions of the actions by 2π.

Form needed for HSH calculation

The HSH calculation [§3.2] needs an expression for the x-coordinate for $\varepsilon=1$ in action-angle coordinates. This is obtained from the above result by setting $I_2=0$. Since in this case, ξ_2 is ignorable, there is really only one pair of relevant coordinates, so the subscripts can be dropped from I_1 and ξ_1. Also, the result is written in atomic units by setting $m=k=1$. Finally, the index of summation is changed so as not to be confused with the energy index when this expression is compared with its quantum analog:

$$x(\xi) = I^2\left[-\frac{3}{2}+2\sum_{M=1}^{\infty}\frac{J'_M(M)}{M}\cos(M\xi)\right]$$

$$= I^2\left[\frac{A_0}{2}+\sum_{M=1}^{\infty}A_M\cos(M\xi)\right] \qquad ; \left\{\begin{array}{c} A_0 = -3 \\ A_{M\neq 0} = \dfrac{2J'_M(M)}{M}\end{array}\right\},$$

$$= \frac{I^2}{2}\sum_{M=-\infty}^{\infty}A_M\cos(M\xi)\,,$$

where the last form is reached by using an antisymmetry property of the Bessel function [689MRS, (24.18), (24.4)]:

$$J'_{-M}(-z) = -J'_M(z)\,,$$

to infer that $A_{-M}=A_M$.

The values of the first few coefficients in the expansion are:

Coefficients in the expansion of the 1-dimensional Kepler motion

$\lvert M\rvert$	A_M
0	−3.0
1	0.650
2	0.224
3	0.118
4	0.0745
5	0.0520

D.4 Action-angle coordinates for the 1-dimensional pendulum

A pendulum is a system subject to a sinusoidal potential, for example:

$$E = \frac{p^2}{2m} + F(1 - \cos x) .$$

In the classic sense of a hanging object, x refers to the angular displacement of the object from the downward vertical ("θ"), m is the moment of inertia of the object about its point of suspension ("ml^2"), and F is the moment of weight of the object about that point ("mgl"). The sign of F is irrelevant to the dynamics. If F is positive, as is assumed in the following discussion, then the zero of potential is at the points of stable equilibrium at the bottom of the cosine wells in the potential.

As for any multiwell system, the behavior of the pendulum depends on whether its energy exceeds the height of the barriers between each well. If $E<2F$, then the system is trapped in a single well and oscillates in that region. If $E>2F$, then the system travels along from one well to the next; this case corresponds, for the hanging object, to the object rotating about the point of suspension.

As for most periodic systems, the dynamics of the pendulum is best described in action-angle coordinates. The action coordinate is:

$$I \equiv \frac{1}{2\pi} \oint p\, dx ,$$

where the integral is taken over one complete period of the motion. In the rotational case, $E>2F$, p can be written in terms of E and x:

$$\begin{aligned} p &= \sqrt{2m\,(E + F\,(\cos x - 1))} \\ &= \sqrt{2m\left[E - 2F \sin^2\left[\frac{x}{2}\right]\right]} , \end{aligned} \qquad \textit{rotational case}$$

and the integral taken over $x \in [0, 2\pi)$. In the oscillatory case, $E<2F$, this does not work because x does not run through this entire interval. In this case, it is helpful to make a transformation to a variable that does run over the entire interval of $[0, 2\pi)$:

$$y \equiv 2 \operatorname{invsin}\left[\sqrt{\frac{2F}{E}} \sin\left[\frac{x}{2}\right]\right] ,$$

so that

$$\sqrt{\frac{2F}{E}} \sin\left[\frac{x}{2}\right] = \sin\left[\frac{y}{2}\right] ,$$

$$p = \sqrt{2mE} \cos\left[\frac{y}{2}\right] , \qquad \textit{oscillatory case}$$

and

$$\frac{dx}{dy} = \frac{\sqrt{\frac{E}{2F}}\cos\left[\frac{y}{2}\right]}{\sqrt{1-\frac{E}{2F}\sin^2\left[\frac{y}{2}\right]}}.$$

For the rotational case, the action coordinate is therefore:

$$I = \frac{1}{2\pi}\int_0^{2\pi} p\,dx$$

$$= \frac{2\sqrt{2mE}}{\pi}\int_0^{\pi/2}\sqrt{1-\frac{2F}{E}\sin^2\left[\frac{x}{2}\right]}\,d\left[\frac{x}{2}\right]$$

$$\equiv \frac{2}{\pi}\sqrt{2mE}\,E_{2C}\left[\frac{2F}{E}\right], \qquad \textit{rotational case}$$

where E_{2C} is the complete elliptic integral of the second kind [72cMAb, (17.3.3)]. For the oscillatory case, the action is:

$$I = \frac{1}{2\pi}\int_0^{2\pi} p\frac{dx}{dy}dy$$

$$= \frac{4\sqrt{mF}}{\pi}\int_0^{\pi/2}\frac{\frac{E}{2F}\left[1-\sin^2\left[\frac{y}{2}\right]\right]}{\sqrt{1-\frac{E}{2F}\sin^2\left[\frac{y}{2}\right]}}d\left[\frac{y}{2}\right]$$

$$= \frac{4\sqrt{mF}}{\pi}\int_0^{\pi/2}\left[\sqrt{1-\frac{E}{2F}\sin^2\left[\frac{y}{2}\right]}-\frac{1-\frac{E}{2F}}{\sqrt{1-\frac{E}{2F}\sin^2\left[\frac{y}{2}\right]}}\right]d\left[\frac{y}{2}\right]$$

$$\equiv \frac{4}{\pi}\sqrt{mF}\left[E_{2C}\left[\frac{E}{2F}\right]-\left[1-\frac{E}{2F}\right]E_{1C}\left[\frac{E}{2F}\right]\right], \qquad \textit{oscillatory case}$$

where E_{1C} is the complete elliptic integral of the first kind [72cMAb, (17.3.1)].

Over the whole range of energy values, then, the action can be expressed as:

$$I(E) = \left\{ \begin{array}{ll} \frac{4}{\pi}\sqrt{mF}\left[E_{2C}(k^2) - (1-k^2)E_{1C}(k^2)\right] & \text{, for } k \leq 1 \\ \frac{2}{\pi}\sqrt{2mE}\,E_{2C}\left[\frac{1}{k^2}\right] & \text{, for } k \geq 1 \end{array} \right\},$$

where $k \equiv \sqrt{E/(2F)}$. A graph of this function is shown below for a pendulum with $m=F=1$:

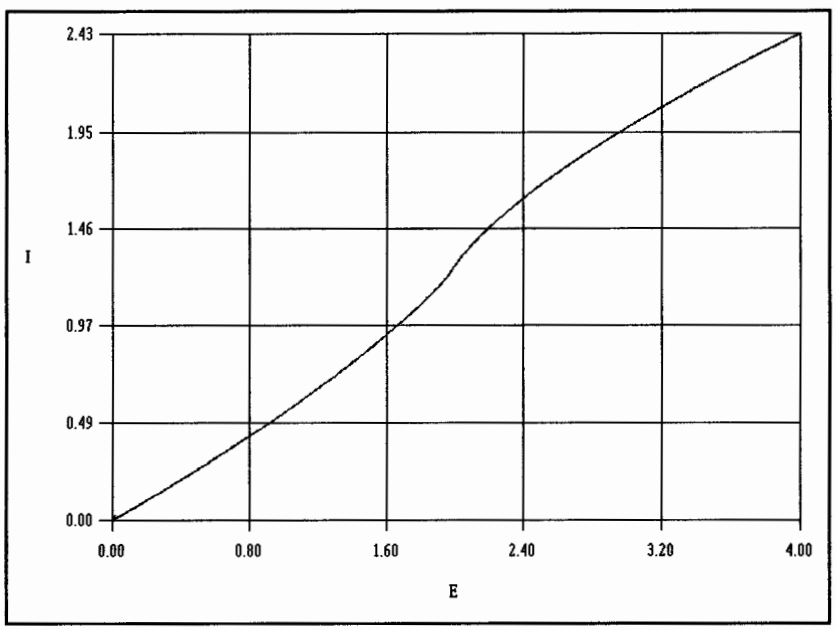

Figure D.2 Action of a pendulum as a function of its energy. The separatrix is at the midpoint of the energy range shown, with oscillation to the left and rotation to the right. The numerical values are for a pendulum with $m=F=1$.

Although this function cannot be inverted analytically, the inverse function, $E(I)$, exists and can be calculated numerically. The fact that $E(I)$ is independent of the angle coordinate implies, via one of Hamilton's equations, that the action coordinate is constant in time, which is clear anyway from the form of $I(E)$ above. The other of Hamilton's equations can be applied by taking the derivative of $I(E)$ [276ETW, §22.736]:

$$\frac{d\xi}{dt} = \frac{1}{dI/dE} = \left\{ \begin{array}{ll} \pi\sqrt{\frac{F}{m}}\,\frac{1}{E_{1C}(k^2)} & \text{, for } k \leq 1 \\ \pi\sqrt{\frac{E}{2m}}\,\frac{1}{E_{1C}\left[\frac{1}{k^2}\right]} & \text{, for } k \geq 1 \end{array} \right\}.$$

This gives the angular frequency of the system point of the pendulum in its action-angle phase space. This result is used in Section 3.5.1 to locate the secondary resonances in the pendulum approximation of the HSH. Graphically, this function has the following form:

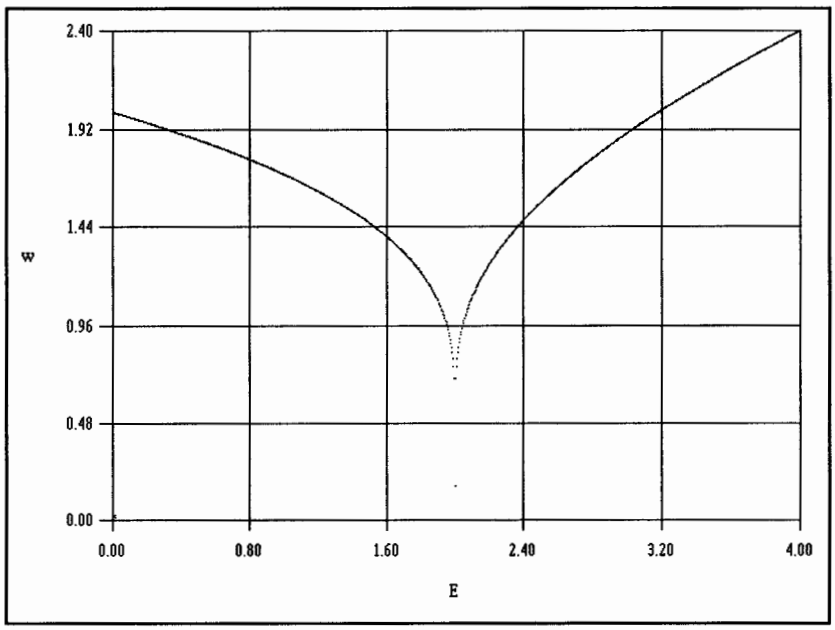

Figure D.3 Angular frequency of a pendulum in its action-angle space, as a function of its energy. The parameters of the calculation are the same as for Figure D.2. The vertical axis label, "w", represents $d\xi/dt$, the angular frequency of the pendulum in its action-angle space.

It is interesting to note that when a pendulum is at rest, its system point in its action-angle space is *not* at rest. The limit of the angular frequency as $E \to 0$ is $2\sqrt{F/m}$. On the other hand, the frequency at the separatrix, where $E=2F$, *is* zero. The frequency decreases monotonically from $2\sqrt{F/m}$ at the origin to zero at the separatrix, then rises monotonically from zero to infinity outside the separatrix.

D.5 Fourier series for the cosine of a sum

The calculation of higher-order resonances in Section 3.5 requires the expansion of

$$\cos\left[\frac{N}{M}\xi^{(M)} + \frac{N-M}{M}\omega t\right]$$

by considering the pendulum coordinate, $\xi^{(M)}$, to be a function of the action-angle coordinates, $(J^{(M)}, \zeta^{(M)})$, and assuming that the cosine is periodic in $\zeta^{(M)}$ with period $2M\pi$.

This is done using the general formula for the Fourier series for the cosine of a sum, in the argument of one of the terms of the sum, assuming that (a) the other term is independent of that argument, and (b) the cosine itself is periodic in the said argument. If the cosine to be expanded is written as $\cos[x(z)+y]$, then the expansion is in z and the assumptions are that (a) $dy/dz=0$, and (b) for some L, $\cos[x(z)+y]=\cos[x(z+2L)+y]$. The formula is:

$$\cos[x(z)+y] = \sum_{n=-\infty}^{\infty}\left[C_n^{\cos}\cos\left(\frac{n\pi}{L}z+y\right) - C_n^{\sin}\sin\left(\frac{n\pi}{L}z+y\right)\right],$$

where

$$C_n^{\mathrm{ftn}} = \frac{1}{2L}\int_0^{2L}\mathrm{ftn}\left(x-\frac{n\pi}{L}z\right)dz\,.$$

This is applied to the resonance problem by making the following identifications:

$$\left\{\begin{array}{rcl} z & \to & \zeta^{(M)} \\ x(z) & \to & \dfrac{N}{M}\xi^{(M)}(\zeta^{(M)}, J^{(M)}) \\ y & \to & \dfrac{N-M}{M}\omega t \\ L & \to & M\pi \end{array}\right\}.$$

Then

$$\cos\left[\frac{N}{M}\xi^{(M)} + \frac{N-M}{M}\omega t\right] = \sum_{n=-\infty}^{\infty} C_n(J^{(M)})\cos\left[\frac{n}{M}\zeta^{(M)} + \frac{N-M}{M}\omega t\right],$$

where[6]

[6] This is equivalent to the result given by Escande and Doveil [811DFE, (14), (C1)], except for the factor of $1/M$ ($=1/p$ in their notation) in C_n ($=V_p$), which I believe should not appear in their result. Their inclusion of an additional term, $(N/M)\zeta^{(M)}$ ($=k\theta$), in the argument of the cosine in both the sum and the integral does not affect the value of the

$$C_n(J^{(M)}) = \frac{1}{2M\pi} \int_0^{2M\pi} \cos\left[\frac{N}{M}\xi^{(M)} - \frac{n}{M}\zeta^{(M)}\right] d\zeta^{(M)}$$

$$= \frac{1}{2M\pi} \int_0^{2M\pi} e^{\left[\frac{N}{M}\xi^{(M)} - \frac{n}{M}\zeta^{(M)}\right]} d\zeta^{(M)}.$$

series. However, they have scaled $\zeta^{(M)}$ $(=\theta)$ by M $(=p)$, and that has the effect of also scaling C_n $(=V_p)$ by the same factor. So the fraction outside the integral sign in their equation (C1) should be $1/2\pi$, not $1/2M\pi$ $(=1/\tau)$.

D.6 Energy representation of the separation operator[7]

Since the isolated atom is spherically symmetric, its Schrodinger equation is separable in both spherical and paraboloidal coordinates. With these two options, the anisotropy of the separation operator makes the paraboloidal coordinate system the appropriate choice for this problem [770LDL, 128].

Expanding the matrix elements, $x_{n,n'} \equiv \langle n|\hat{x}|n'\rangle$, in paraboloidal coordinates, (ρ_1,ρ_2,ϕ), gives [770LDL, (37.4), (37.1)]:

$$x_{nn'} = \frac{1}{4}\int_0^{2\pi}\int_0^{\infty}\int_0^{\infty} x\,(\rho_1+\rho_2)\,\langle n|\rho_1,\rho_2,\phi\rangle\,\langle\rho_1,\rho_2,\phi|n'\rangle\,d\rho_1 d\rho_2 d\phi$$

$$= \frac{1}{8}\int_0^{2\pi}\int_0^{\infty}\int_0^{\infty}(\rho_1^2-\rho_2^2)\,\langle n|\rho_1,\rho_2,\phi\rangle\,\langle\rho_1,\rho_2,\phi|n'\rangle\,d\rho_1 d\rho_2 d\phi\,,$$

in which the state functions have the form [770LDL, (37.15, 16)]:

$$\langle\rho_1,\rho_2,\phi|n,n_1-n_2,m\rangle = \frac{e^{im\phi}}{\sqrt{\pi n^2|m|!^2}}\prod_{k\in\{1,2\}}\left(\sqrt{\frac{(n_k+|m|)!}{n_k!}}\;e^{-\frac{\rho_k}{2n}}\times\left(\frac{\rho_k}{n}\right)^{\frac{|m|}{2}}{}_1F_1\left(-n_k,|m|+1,\frac{\rho_k}{n}\right)\right),$$

where ${}_1F_1(a,b,z)$ is Kummer's function, one of the confluent hypergeometric functions. The energy index, n, and the paraboloidal and magnetic quantum numbers, n_k and m, are related by [770LDL, (37.13)]:

$$n - 1 = n_1 + n_2 + |m|\,.$$

In the 1-dimensional approximation, $n_2 \approx 0$ and $m \approx 0$, so $n-1 \approx n_1$ and the state functions reduce to [72cMAb, (13.1.2), (13.6.9), (22.5.16)]:

[7] Different approaches to the calculation of these matrix elements are taken in 81cSPG, §2 and 872RBl, Appendix B. The spectral properties of the matrix elements are discussed in 872RBl, Appendix C. Calculation of the 3-dimensional matrix elements is discussed in 820VBB, §52.

$$\langle \rho_1,\rho_2,\phi\,|n\rangle \approx \frac{1}{\sqrt{\pi}\,n^2}\; e^{-\frac{\rho_1+\rho_2}{2n}}\; L_n\left[\frac{\rho_1}{n}\right]$$

in terms of Laguerre polynomials. Since these state functions are real, so are the matrix elements. Notice also that the effect of choosing $n-1\approx n_2$ and $n_1\approx 0$ instead of $n-1\approx n_1$ and $n_2\approx 0$ would have been to change the argument of the Laguerre polynomial from ρ_1/n to ρ_2/n. A look at the expression for the matrix elements ($x_{nn'}$ on the previous page) confirms that this choice then determines their sign. This agrees with the fact that the sign of n_1-n_2 determines which side of the proton the electron is on.

With the above expression for the state functions, the matrix elements become:

$$x_{nn'} \approx \frac{\left[\int_0^{2\pi} d\phi\right] \int_0^{\infty}\int_0^{\infty} (\rho_1^2-\rho_2^2)\, e^{-\frac{\rho_1+\rho_2}{2}\left(\frac{1}{n}+\frac{1}{n'}\right)} L_{n-1}\left[\frac{\rho_1}{n}\right] L_{n'-1}\left[\frac{\rho_1}{n'}\right] d\rho_1 d\rho_2}{8\,\pi\, n^2 n'^2}$$

$$= \frac{\int_0^{\infty} \left[\int_0^{\infty} (\rho_1^2-\rho_2^2)\, e^{-\frac{\rho_2}{2}\frac{n+n'}{nn'}} d\rho_2\right] e^{-\frac{\rho_1}{2}\frac{n+n'}{nn'}} L_{n-1}\left[\frac{\rho_1}{n}\right] L_{n'-1}\left[\frac{\rho_1}{n'}\right] d\rho_1}{4\, n^2 n'^2}$$

$$= \frac{\int_0^{\infty} \left[\rho_1^2 - 8\,\frac{n^2 n'^2}{(n+n')^2}\right] e^{-\frac{\rho_1}{2}\frac{n+n'}{nn'}} L_{n-1}\left[\frac{\rho_1}{n}\right] L_{n'-1}\left[\frac{\rho_1}{n'}\right] d\rho_1}{2\, n\, n'\, (n+n')}$$

[689MRS, (15.76)]. This expression is symmetric in n and n', as is required by the calculation of the HSH energy [Chapter 4].

Further evaluation of the above expression requires the calculation of the integrals:

$$\int_0^{\infty} \mathrm{e}^{-bx} L_n(kx)\, L_{n'}(k'x)\, dx \qquad \text{and} \qquad \int_0^{\infty} x^2\, \mathrm{e}^{-bx} L_n(kx)\, L_{n'}(k'x)\, dx\,.$$

The first integral is a standard form [800ISG, (7.414.4)]. An expression for the second one in terms of the first can be found by differentiating the first one twice with respect to b. The resulting calculation is horrendously complicated, and has been performed using the algebraic computing language MACSyMa. The answer is quite unwieldy and does not offer sufficient insight to merit reproduction here.

The expressions for these two integrals were inserted into the expression for the matrix element, and MACSyMa was used to produce tables of matrix elements, $x_{n,n'}$, for selected values of n ranging from 6 to 100, and selected values of $n'-n$ from 1 through 15. Several attempts were made to find an analytic expression for the matrix elements, either by reducing the MACSyMa results or by matching functions to the tables produced. It was then found, quite by accident, that the tables were matched very well by:

$$x_{n,n'} = \left[\frac{n+n'}{2}\right]^2 \frac{J'_{|n-n'|}(|n-n'|)}{|n-n'|},$$

where $J'_n(z)$ is the derivative with respect to z of the Bessel function of the first kind, evaluated at z. For $n'-n=1$, the scaled error drops monotonically from 10^{-3} for $n=25$ through $0.7\cdot10^{-4}$ for $n=100$. The error grows slowly with $n'-n$, reaching about 3% for $n'-n=15$.

In the special case where $|n+n'| \gg |n-n'|$, the matrix elements can be approximated by:

$$x_{n,n\pm M} = n^2 \frac{J'_M(M)}{M},$$

with the case condition written as $|M| \ll n$. In terms of the coefficients defined in Appendix D.3,

$$x_{n,n\pm M} = \frac{1}{2} n^2 A_M.$$

This result is used in Chapter 4.

E Computational issues

E.1 Computer methods and equipment used

The plots in this work were made by a variety of methods, using a variety of equipment and a variety of compilers. The one thing that the dynamical plots have in common is that they were all made by integrating equations of motion using a 4th order Runge-Kutta algorithm in C, based on the programs ODEInt, RKQC and RK4 in *Numerical Recipes in C* [87aWHP, §15.1..2].

For the classical plots, the equations of motion were Hamilton's equations with the energy,

$$E(x,p,t) = \frac{p^2}{2} - \frac{1}{x} + Fx\cos(\omega t)$$

for the physical phase space in Chapter 2, and

$$E(\xi,I,t) = -\frac{1}{2I^2} + \frac{FI^2}{2}\sum_M A_M \cos(M\xi - \omega t)$$

in action-angle coordinates for Chapter 3. The numerical and 2-dimensional graphics routines were written in C, compiled with the MicroSoft C Optimizing Compiler, Version 6.0, and run on an Everex Tempo LX 80386SX-16 computer with an 80387 math coprocessor. The 3-dimensional graphics were generated by AcroBits AcroSpin, Version 2.0. Graphics output was captured on the VGA screen by the Catch utility of LogiTech PaintShow Plus, Version 2.21. The resulting TIFF files were then imported by Word for Windows into this document.

For the quantum plots in Chapter 4, the equations of motion were a linear system of equations representing Schrodinger's equation with the energy projection,

$$\hat{E}|n\rangle = -\frac{1}{2n^2}|n\rangle + \frac{Fn^2}{4}\sum_M A_M\left[e^{i\omega t}|n+M\rangle + e^{-i\omega t}|n-M\rangle\right]$$

The numerical routines were written in C, and compiled with MicroSoft Quick C for running on a computer built around a Hauppage 80386 Motherboard with an 80387 coprocessor, and with the Cray Standard C Compiler for running on a Cray X-MP. These routines were written to take advantage of vectorization on the Cray. The graphics routines were written in C, compiled with Quick C, and run on the Hauppage-based computer. The graphics output went to a DataProducts P-132 color printer, which overlaid the color images in boxes set up on the appropriate pages by Word for Windows.

E.2 Customizing C for scientific computing

C is the language of choice for doing state of the art computer programming. The features of C allow for the generation of the fastest, tightest executables possible without writing directly in assembly code. It also allows for the manipulation of the execution environment, giving the programmer more control over the run-time process than can be achieved with most other high-level languages.

Usually, C is seen as a "programmers language," one that nonprofessionals are best to stay away from. This is because its speed and versatility come from exposing the programmer to the raw processing power of the computer, which can be difficult to manage. However, learning how to tame that power can be rewarded with professional quality programs, and it's also fun!

I learned C for the purpose of doing the numerical simulations that form the main body of this work in Chapters 2, 3 and 4. In the meantime, I have acquired several years of experience at writing programs in C. During this time, I have developed a library of header files and utility functions that make my programming task easier. The most important concepts are contained in the header files; they are the subject of this section.

One of the best features of C is the *preprocessor*. This is a convenient tool for the redefinition of words used in programs. It allows the programmer to customize the language to his or her own specifications. This is the main purpose of the system of header files described here.

The program that performed the quantum mechanical simulations in Chapter 4 was written on a DOS computer in MicroSoft C, but the major calculations were performed on a Cray in Cray Standard C. So one of the challenges that the header library tackles is to establish portability between these two computers and compilers. In other words, the goal is to allow for code which can be compiled on either type of machine without modification.

This is not a tutorial in C; a working knowledge of the language is assumed. For programmers who are considering learning C, I recommend starting with MicroSoft Quick C, which not only provides a slick programming environment, but also comes with a tutorial, *C For Yourself*, which takes you through all elements of the language. Once you become familiar with the language, the reference of choice is *C: A Reference Manual* by Harbison and Steele. A little book that I found to be gem of wisdom, that seems to come from a lifetime of programming experience, is *The Elements of Programming Style* by Kernighan. For issues of scientific computing, there is no substitute for the amazingly comprehensive *Numerical Recipes* [87aWHP] series by Press, Flannery, Teukolsky and Vetterling.

Custom headers

The C language proper consists of only 35 words, such as *if*, *int*, and *sizeof*. The main functionality of a commercial C package is in the library of functions that come with it. The core of this library will probably conform to some standard, such as the ANSI standard, for arguments and returned values. In addition, it will probably also include functions for non-standard operations, such as graphics.

In the documentation of the library functions, you will probably be told that to use a particular function you must include a particular header file. The primary purpose of the header file is to supply a *function prototype* that gives the compiler the pattern of arguments for this function. (Alternatively, if the function is implemented as a macro, then instead of a prototype, the header file will contain the code of the macro itself.) The header may also establish new data types used by the function, and it may define aliases for constants to be passed to the function as arguments.

While it is compulsory to provide the compiler with certain information in the header files, it is not necessary to use the supplied header files themselves. What is described here is a system of header files that included in my programs instead of those supplied with either MicroSoft C or Cray Standard C. These headers customize the programming environment, while at the same time providing either compiler with the information it needs to run its library functions.

Avoiding the headers headache

In the standard procedure for writing in C, a source file starts out with a series of include commands for the headers needed. Which headers are included depends on what functions the source file calls. Every time you add a function call, you have to think about whether the appropriate header is already included. If you remove a function call, you might want to pare the include list by removing its header, but you can only do this if that header is not required by another function called in the same file.

Instead of worrying about which headers to include in the source files, it is easier to have *one* set of header files that is included in *all* source files. The following set of files, which are described individually below, provides all the functionality needed for any C program, as well as the customization mentioned above:

- keywords.h
- limits.h and float.h
- constant.h
- keystrok.h
- types.h
- variable.h
- function.h
- macros.h
- prototyp.h

Rather than including these files individually, and in order to reserve the freedom to reorganize the files, the include commands for these files are kept in a master header file. It is *that* file that is included in all of my source files.

Making C pretty: keywords.h

Personally, I like my programs to read as much like English as possible. The following list of preprocessor definitions allows a dramatic improvement in the appearance of my C code:

```
#define if          if(
#define then        )
#define is          ==
#define isnt        !=
#define set
#define to          =

#define not         !
#define and         &&
#define or          ||
#define NOT         ~
#define AND         &
#define OR          |
#define xOR         ^
#define mod         %
```

This allows the incomprehensible C gibberish:

```
if (a==0 || b!=(q%5)) x=y;
```

to be rendered as the more friendly:

```
if a is 0 or b isnt (q mod 5) then set x to y;
```

The latter version may compile a microsecond or so slower because it requires the compiler to look up several definitions. However, the resulting object code for both versions will be absolutely identical. There is no run-time disadvantage to writing C in this way.

One of the advantages of this set of symbols is that it avoids the common error of testing equality with the assignment operator, i.e., of writing "=" in place of "==" by mistake.

Aside from vocabulary, it is also easier to understand a program if you can see it all on the screen at once. I always try to write programs so that the code for each function takes up no more than one screen. There is one keyword, *unsigned*, that takes up far too much space on the screen for its significance, and tends to appear frequently. The following definitions keep declarations of unsigned integers from monopolizing the screen:

```
#define CharU       unsigned char
#define ShortU      unsigned short
#define IntU        unsigned int
#define LongU       unsigned long
```

Finally, I begin in this file a practice carried out at great length in the file function.h, described below. When a word is formed from two or more English words, I like to make the result easier to read by capitalizing the component words:

```
#define GoTo        goto
#define SizeOf      sizeof
#define TypeDef     typedef
```

Note that all of these definitions serve only to give me the freedom to use the new forms. The original symbols, such as "goto" and "==" are still in service. It's just that I choose never to use them directly.

Defining numeric data types: limits.h and float.h

These are the only *non*custom files included in the header list. They are ANSI standard files provided with every compiler to define the numeric data types.

Machine-specific constants: constant.h

Here are defined constants that are used elsewhere to determine whether the program is running in DOS on an IBM compatible or in Unix on a Cray. The list of constants and tests could be expanded almost without limit to allow for other compiling and operating environments.

```
#define Intel8086Family             1
#define CrayMachine                 2
#define MS_DOS                      1
#define Unix                        2
#define MicroSoftCompiler           1
#define CrayCompiler                2

#if defined(M_I86)
        #define CPU                         Intel8086Family
        #define OperatingSystem             MS_DOS
        #define compiler                    MicroSoftCompiler
    #elif defined(_CRAY)
        #define CPU                         CrayMachine
        #if defined(_UNICOS)
                #define OperatingSystem     Unix
            #endif
        #define compiler                    CrayCompiler
    #endif
#if not (defined(CPU) and defined(OperatingSystem))
        #error "The CPU, operating system and compiler have not all been identified."
    #endif
```

The constants M_I86, _CRAY and _UNICOS are called predefined macros, and are provided by the respective compilers.

If the machine in use is of the DOS type, then it has segmented memory addresses, and certain code and data will need to be defined as *near* or *far*. If the machine is a Cray, then any appearance of these special keywords will be ignored:

```
#if CPU is Intel8086Family and compiler is MicroSoftCompiler and not defined(NO_EXT_KEYS)
    #define near    near
    #define far     far
#else
    #define near
    #define far
#endif
```

The all-important null pointer is:

```
#define null            ((void *)0)
```

This definition appears in many of the standard header files because it is needed by many different types of function. Those files have to provide a test to see if some other file has already made the definition, but that is not necessary here because this file is only included once per source file. Those files also generally follow the convention of naming constants in all-capitals, and call this "NULL." There is no danger in breaking that convention, as long as all your source files use the name given in the definition. If you wanted to be able to also compile programs written in the standard convention, you could add "#define NULL null."

Next this file defines the color values and color indices specific to DOS machines:

```
#define cvBlack         0L
#define cvBlue          0x2A0000L
etc.

#define ciBlack         0
#define ciBlue          1
etc.
```

Not all vocabulary has to have unique meanings. Here is a definition of a pair of synonyms for the two Boolean constants, *true* and *false*, which are themselves defined later in the file types.h.

```
#define yes             true
#define no              false
```

This file also contains important physical constants, such as:

```
#define pi              3.14159265358979323846264338327950288
#define c               (2.99792458E10)
#define hBar            (1.0545887E-27)
```

If you decide to use the second definition in your own header file, be careful not to give any variables in your programs the name "c."

Finally, this file defines the often-used constants, 2π and $\pi/2$. However, the preprocessor is not equipped to do floating point arithmetic, so they are defined as variables. Alternatively, you could do the arithmetic yourself and enter the result here in a #define command. I prefer to let the computer do the arithmetic:

```
#if ThisIsTheMainSourceFile
        double TwoPi to (2. * pi);
        double PiBy2  to (pi / 2.);
    #else
        extern double TwoPi;
        extern double PiBy2;
    #endif
```

To accommodate this code, and some other similar examples below, the main source file of all the files making up the program includes the command "#define ThisIsTheMainSource-File 1."

In the definition of TwoPi and PiBy2, note the use of the customized assignment operator, "to" for "=".

Finding the right keys: keystrok.h

This file contains definitions designed to make it easy to refer to operator keystrokes other than those represented by the usual set of printable characters. This includes both the standard ASCII keys, such as:

```
#define kCtrlG          0x07
#define kRubout         0x08
#define kTab            0x09
#define kCtrlEnter      0x0a
etc.
```

and special keys specific to DOS:

```
#if OperatingSystem is MS_DOS
        #define kHome     0x4700
        #define kUp       0x4800
        #define kPgUp     0x4900
        #define kLeft     0x4b00
        etc.
    #endif
```

Code intended for execution on a DOS machine can refer to both sets. Code to be executed on the Cray must only refer to the first.

Setting up data types: types.h

This file contains all the type definitions. First, we need Booleans:

```
TypeDef enum {false, true}  Boole;
```

Next, several kinds of pairs are often useful, such as a pair of bytes, a pair of "shorts," and two precisions of complex numbers:

```
TypeDef ShortU                  PairB;
TypeDef struct {short   e1, e2;} PairS;
TypeDef struct {float   Re, Im;} ComplexF;
TypeDef struct {double Re, Im;} ComplexD;
```

A very important structure type is the one that holds data on an open stream, such as a file. The ANSI standard calls this "FILE," but I prefer "StreamType" because that is what it is:

```
TypeDef struct
    #if compiler is MicroSoftCompiler
            {CharU *pointer; int count; CharU *base, flags, handle;}
        #elif compiler is CrayCompiler
            {int count; CharU *pointer, *base; ShortU flags; CharU handle;long _ftoff;}
        #else
            #error "Sorry, but I don't recognize the compiler."
        #endif
                                StreamType;
```

Note the use of conditional compilation to account for the fact that Cray and MicroSoft define their stream structures differently. In this code, you are free to give the structure elements any names you like, but they must be listed in the order shown and have the individual types shown because already-compiled code in the Cray and MicroSoft libraries will be looking for structure elements of those types at those positions.

Finally, this file defines a special structure that is useful for holding data on the environment and other globally useful information:

```
TypeDef struct
    {Boole initialized; char calls[150]; StreamType *boss, *read, *write;
     Boole NewKeyboard; VideoType video; short pause, beep, verbosity, skip;
     }  EnvType;

#if ThisIsTheMainSourceFile
        EnvType EnvData  to {0};
    #else
        extern  EnvType  EnvData;
    #endif
```

The use of each of the elements of EnvData is quite involved, and I will not go into that here. The point of introducing this object is that it helps to have a place somewhere in memory where useful data can be accessed and updated without having to pass the address of that

location around as an argument to every function. It is best to have all of this data in one structure because that promotes a more organized style of programming than if each of these elements were an independent global variable.

Predefined global variables: variable.h

C has two standard global variables. "errno" is a standard name which will be known to the linker, so it must be used. However, it is perfectly healthy to also define and use a synonym:

```
#define ErrNo       errno
extern int near     ErrNo;
```

Both MicroSoft and Cray use an input/output buffer array called "_iob". This is not part of the ANSI standard, so other compilers may require special handling in defining these special streams:

```
#define keyboard        (&_iob[0])      /* stdin */
#define display         (&_iob[1])      /* stdout */
#define ErrorOutput     (&_iob[2])      /* stderr */
#define AuxDevice       (&_iob[3])      /* stdaux */
#define printer         (&_iob[4])      /* stdprn */

extern StreamType near  _iob[];
```

The names in comments on the right are the ANSI-styled symbols for these streams. The symbol "_iob" must be used here because it will be known to both the MicroSoft and Cray linkers. Elsewhere, the streams may be called by the names given here, "keyboard," "display," etc.

Note the use of the special keyword "near" in the declarations of both externals, ErrNo and _iob. This keyword is defined to be ignored by the Cray compiler. (See constant.h, above.)

Making function names more friendly: function.h

This is the simplest header file. All it contains is aliases for functions whose given names I don't like. Some functions are renamed just to capitalize component words that go to make up the names. Others are given new names that seem to better describe what they do. For example:

```
#define CAbs            cabs
#define CAlloc          calloc
#define CPUTime         clock
#define execute         execl
#define FClose          fclose
#define FPrintF         fprintf
#define FractionPart    modf
#define GetPID          getpid
```

```
#define InvSin      asin
#define LocalTime   localtime
#define OutByte     outp
#define remainder   fmod
#define SqRoot      sqrt
#define StrNCmp     strncmp
#define StrToDbl    strtod
#define StrToInt    atoi
```

Where the work gets done: macros.h

The wonderful thing about the #define command is that you can use it for the most trivial purpose of changing the name of a function, or you can use it define very sophisticated macros. Below are examples of some macros that I have found particularly useful.

Conditional debugging

C is famous for its speed and versatility, but those features come at the cost of exposure to dangers that other languages shield the programmer from. For example, there is no check for arithmetic overflow, so incrementing an integer too many times can lead to unpredictable results. Arrays have no defined boundaries, so errant data operations can modify the status of unexpected memory locations. The responsibility falls upon the programmer to anticipate and handle overflows and to perform array operations within the correct bounds.

Writing in C does not mean that programs cannot have error checking. It means that the decision of where and when to check for errors is left to the discretion of the programmer. The optimal way to write correct code that functions as intended and yet does not waste time checking for errors that cannot happen, is to implement a two step strategy:

- Apply stringent error checking while writing and debugging the program.
- When the program has been fully tested, reduce the checking to just handle operator error.

This variable level of error checking can be implemented by combining the preprocessor's features of macro definition and conditional compilation.

For example, it is a good idea to check all of the arguments on entry into a function, to ensure that they have values that fall within expected ranges, and to make sure that pointers are not null. Another good idea is for every *switch* statement that is expected to route through one of its *case*'s to end with a *default* statement that flags an error. It is also good practice to check the value of ErrNo every so often to see if an unexpected error has occurred[1]. However, all of these procedures will slow a program down. That is where conditional compilation comes in.

The following are examples of error-checking macros. They use a messaging system called *error* which is not described here. CheckForError issues a message if ErrNo is nonzero. CheckForNull prints a message if its argument is a null pointer (or a zero integer). CheckBoolean and CheckRange complain if their respective first arguments do not have appropri-

[1] Surprisingly, MicroSoft does not anticipate this practice. At the startup of any executable, the value of ErrNo is unpredictable [Paul E., MicroSoft technical support, 89 08 15].

ate values. And CaseError is designed to be called by a *default* statement that should never be executed.

The important thing about these macros is that they only exist if the symbol *debugging* is defined and nonzero. If *debugging* is undefined then the compiler passes over every occurrence of these macros without generating any object code. This means that you can install these macros throughout your program without concern for degrading its ultimate performance.

Once a program is debugged, it is better to turn the macros off by not defining *debugging* than to remove them from the source file. Not only is it easier, but also, when you come back to the program later to make modifications you will want to debug it again, and the macros will be sitting there ready to go to work.

```
#if debugging
    #define CheckForError(label) if ErrNo then error("ErrNo", label, ErrNo); else
    #define CheckForNull(pointer)                                          \
        if pointer is null then error("null", #pointer); else
    #define CheckBoolean(Boolean)                                          \
        if not IsEither(Boolean, 0, 1) then                                \
            error("I have '%s' = %i when it should be either 0 or 1.", #Boolean, Boolean); \
        else
    #define CheckRange(value, low, high)                                   \
        if not IsOrdered(low, value, high) then                            \
            error("range",#value,(double)(value),(double)(low),(double)(high));\
        else
    #define CaseError(variable) error("case", #variable, variable, variable)
#else
    #define CheckForError(label)
    #define CheckForNull(pointer)
    #define CheckBoolean(Boolean)
    #define CheckRange(value, low, high)
    #define CaseError(variable)  error("case: " #variable)
#endif
```

Here is another example of conditional debugging. Infinite loops are particularly frustrating for two reasons. First, the only way to break into one (unless you've left open an interrupt mechanism) is to turn off the computer. But worse, if a loop is not generating some output, then getting stuck in it is often indistinguishable from having the computer hang for any other reason, so they can be hard to diagnose. The following code is designed as a replacement for the *for* statement in C, to prevent infinite loops.

```
#if debugging
    #define loop(LoopInitializer, LoopWhile, LoopIterate, LoopAction)      \
        {double LoopCount to 0., LoopQuit to 1E5;                          \
         for ((LoopInitializer); (LoopWhile); (LoopIterate), LoopCount++) \
            {LoopAction;                                                   \
             if LoopCount > LoopQuit then                                  \
                {if error("loop",LoopCount,#LoopInitializer,#LoopWhile,#LoopIterate) \
                    is 'R' then break; else LoopCount to 0.;}              \
         } }
```

```
#else
    #if ThisIsTheMainSourceFile
            double LoopQuit;
        #else
            extern double LoopQuit;
        #endif
    #define loop(LoopInitializer, LoopWhile, LoopIterate, LoopAction)      \
        for((LoopInitializer); (LoopWhile); (LoopIterate)) {LoopAction;}
#endif
```

The first three arguments are expressions, and serve the role of the three expressions appearing in a *for* statement. The last argument is a statement, and serves the role of the body of the *for*. A semicolon is optional on the statement in the last argument, and on the *loop* macro itself. Compound expressions in the first three arguments must be enclosed in round brackets. Braces on a compound statement in the last argument are optional. The arguments are separated by commas, not by semicolons as in *for*.

The difference between *loop* and *for* is that when *debugging* is defined and nonzero, *loop* keeps track of how many times it has iterated, and issues a warning if it goes on for too long. "Too long" means, by default, more that 100,000 times; this can be reset by assigning a different value to *LoopQuit* in *LoopInitializer*, as in:

```
loop((x to 2, LoopQuit to 1E9), x < 1E6, x * x, null);
```

If the warning is issued, the loop can be continued by pressing "r" (lower case), or exited by pressing "R" (capital). (This is because of the design of *error*, which allows processing to *R*esume if "R" (either case) is pressed, and otherwise terminates processing.)

If *debugging* is not defined, then *loop* is exactly identical to *for*. There is no efficiency cost, in terms of either speed or size, for using *loop* with *debugging* off. The reason *LoopQuit* is defined as a global when *debugging* is off is so the program will not choke on code such as the example above that sets an alternate value for *LoopQuit*. If *debugging* is off, then changing the size of *LoopQuit* has no effect.

The final example of conditional debugging demonstrates checking the return value of a function and issuing a message (through *error*) if the value is not the expected one. But this particular example also perform another operation, which I encourage you to make note of if you are just getting started in C, because I found this to be a very sly and destructive source of error. If your program writes to a null pointer and you don't know about it (which can happen if the write is unintended, rather than just to a bad address) the effect is a "null pointer assignment." (*fwrite* returns the correct count.) In MicroSoft C, this will cause a run-time error message *after program termination*, and *only if the program is compiled with pointer checking on*. Otherwise the error will go undetected, and will have unpredictable effects. If the message is given, it will come without any clue as to when or where or how the bad assignment took place. Null pointer assignment bugs are very hard to find. The following code is designed to catch one common cause of them:

```
#if debugging
        #define put(stream, source, size, count)                    \
            {CheckForNull(stream);                                  \
             if fwrite(source, size, count, stream) isnt count then \
                error("put", stream, #stream, count, size, #source, #stream);}
    #else
        #define put(stream, source, size, count)   fwrite(source, size, count, stream)
    #endif
```

Logic and arithmetic

Here are three simple macros that are useful under various circumstances:

```
#define IsEither(a, b, c)          ((a) is (b) or  (a) is (c))
#define IsBoth(a, b, c)            ((a) is (b) and (a) is (c))
#define until(expression)          while (not (expression))
```

The first two work only with integers or pointers. Generally, equality of floating point numbers cannot be safely tested with *is* (==).

Many simple but important arithmetic operations are best performed with macros. Here are some examples:

```
#if compiler is MicroSoftCompiler
        #define mag(x)      ((double)(x) > 0. ? (x) : -(x))
    #else
        #define mag(x)      ((x) > 0 ? (x) : -(x))
    #endif
#define max(a, b)           ((a) > (b) ? (a) : (b))
#define min(a, b)           ((a) < (b) ? (a) : (b))
#define up(a, b)            if (b) > (a) then (a) to (b); else
#define down(a, b)          if (b) < (a) then (a) to (b); else
#define power(pwr, base, n) \
 {short MCRi; pwr to base; for (MCRi to 2; MCRi <= n; MCRi++) pwr *= base;}
```

The important considerations to keep in mind are:

- Macros are faster than function calls, but complex ones will increase the size of a program.
- Beware of unwanted side effects. For example, mag(x++) will increment x twice.

There are some useful tricks for manipulating complex numbers and matrices in C. I learned most of mine from *Numerical Recipes in C* [87aWHP, Appendices D, E], to which I defer this discussion on those subjects.

Stream operations

Reading and writing to and from files can often be simplified using macros. The following examples use the macro *put* defined above under "Conditional debugging."

```
#define PutItem(stream, item)              put(stream, &(item), SizeOf(item), 1)
#define PutItems(stream, item, count)      put(stream, &(item), SizeOf(item),count)
#define PutList(stream, item, count)       put(stream, &(item), SizeOf(item)*count, 1)
#define PutString(stream, string)          put(stream, string, StrLen(string), 1)
#define PutAt(stream, position, source, size, count) \
        {seek(stream, position); put(stream, source, size, count);}
```

The quintessential header file: prototyp.h

This file contains what make up the main contents of most of the standard header files, that is, the function prototypes. Included are prototypes for all of the functions that are ever used in any of my programs, so it serves universally, although personally. If at some point I write my own function or macro to replace a standard library function, then I remove the prototype from this file. That way, if I inadvertently call the standard function, the compiler will warn me that there is no prototype for it.

Beyond headers

That completes the description of the header library. But it is often useful to define macros in regular source files as well.

Collapsing code

Any body of code that repeats the same sequence of steps can be collapsed into a series of macro calls. If the sequence of steps is fairly long and complicated, then it is better to define it as a function rather than a macro. But for fairly simple but repetitive operations, macros are very handy.

The following example is used in a program that allows the operator to change the values of data items on the screen. Any one item can be changed before moving on to the next, but the operator can move around the screen at will before changing anything. The program looks for a flag that indicates that *something* has changed. Then it looks through all the fields on the screen to see which one is current, and changes the data for that item. The search through the fields is coded as:

```
if        window->field is item1 then data->item1 to *(double *)item1->value;
  else if window->field is item2 then data->item2 to *(double *)item2->value;
  else if window->field is item3 then data->item3 to *(double *)item3->value;
  else ...
```

where the *item*n's are the names of fields on the screen as well as elements of the structure *data*, and *window->field* is the current field. This long list of repetitive code can be replaced by:

```
#define update(item)    \
        if window->field is item then data->item to *(double *)item->value

update(item1); else update(item2); else update(item3); else . . .

#undef update
```

Collapsing code in this way can go a long way to making programs easier to understand. But be careful about indiscriminate use of macros. Remember that every macro call expands into the full text of the macro before it is compiled. So if your macros are very long and complicated, or if you often have several layers of nested macro calls, then a segment of code that appears on the screen as very short may compile into a lot of object code.

E.3 Using Word for Windows to format large, technical documents

To call MicroSoft Word for Windows a word processor is like calling the *Mona Lisa* a picture. The features of this program handle all the details of compiling a technical book, such as:

- Mathematical symbols, including the whole Greek alphabet, with a powerful equation editor for generating integrals, matrices, tensors, etc.
- Importing graphics, rescaling it, and positioning it anywhere on the page. If desired, only the horizontal position can be specified, so that the figure will move from page to page as the preceding text is modified.
- Generating text by performing arithmetic and logical calculations on other text. You can build an active spreadsheet into a document!
- Making tables, with automatic resizing of rows to fit the text.
- Automatic cross-referencing by page number, section number, figure number or selected text.
- Definition of paragraph styles with any combination of formatting commands, and with the freedom to adjust any of those commands in an individual paragraph without needing to define a new style.
- Viewing the document in outline form.
- Generation of various tables of contents, with customizable formats.
- An impressive collection of tools for selecting, cutting, pasting and archiving segments of text and graphics.
- A dictionary that not only checks spelling, but also gives definitions and synonyms.
- Annotation by footnotes, endnotes, marginal notes, hidden text and initialled reviewer's comments.
- Customizing the whole system by defining macros and changing the menus.

What follows is a collection of tricks and pointers that I have collected through over a year of using Word for Windows to prepare my Ph.D. dissertation and other technical documents, along with some complaints about problems encountered.

This is not a tutorial on how to use Word for Windows. A knowledge of its commands and basic operating procedures is assumed. Anyone who has ever used a word processor will have little trouble getting started in Word[2]. As for the advanced features, there is no question that learning them will take time and effort. Word is an amazingly complex program, and after a year of intense use there are still many features that I have never tried. Word comes with a tutorial, as well as a comprehensive documentation set, including separate instructions written for current users of various other major word processors. The *User's Reference* will become your main tool for exploring advanced capabilities. Perhaps these results of my own experience will also be of some help to you.

[2] *Word* is used here to refer to *Word for Windows*. Some of what is said here may apply to the similar *Word for Macintosh*, but this has not been verified. None of what is said here applies to the very different, text-based *Word for DOS*.

Mathematical symbols

The Word documentation is, on the whole, excellent. But amazingly, it leaves out the most important information you need to have in order to begin using it for technical documents: the mathematical symbols, including the Greek alphabet. It's not that they are not supplied. They are. The problem is that you have to do some detective work to find them. Here are the results of that search.

When you choose a font in Word, the characters in that font depend not only on the typeface that the font was made in, but also on the character set represented. There are two different character sets represented in the fonts supplied with Word, and those made for Windows by the BitStream font making software. All of the fonts except symbols represent what is known as the *ANSI Windows* character set. Here is a table of this character set in the BitStream Dutch typeface:

ANSI Windows character set in Dutch typeface, 10 point										
code	0	1	2	3	4	5	6	7	8	9
30	-			!	"	#	$	%	&	'
40	(	)	*	+	,	-	.	/	0	1
50	2	3	4	5	6	7	8	9	:	;
60	<	=	>	?	@	A	B	C	D	E
70	F	G	H	I	J	K	L	M	N	O
80	P	Q	R	S	T	U	V	W	X	Y
90	Z	[	\	]	^	_	`	a	b	c
100	d	e	f	g	h	i	j	k	l	m
110	n	o	p	q	r	s	t	u	v	w
120	x	y	z	{	|	}	~			
140						‘	’	“	”	o
150	—	-								
160		¡	¢	£	¤	¥	¦	§	¨	©
170	ª	«	¬	-	®	¯	°	±	2	3
180	´	µ	¶	·	¸	1	º	»	¼	½
190	¾	¿	À	Á	Â	Ã	Ä	Å	Æ	Ç
200	È	É	Ê	Ë	Ì	Í	Î	Ï	Ð	Ñ
210	Ò	Ó	Ô	Õ	Ö	–	Ø	Ù	Ú	Û
220	Ü	Ý	Þ	ß	à	á	â	ã	ä	å
230	æ	ç	è	é	ê	ë	ì	í	î	ï
240	ð	ñ	ò	ó	ô	õ	ö	•	ø	ù
250	ú	û	ü	ý	þ	ÿ				

This table is also given, although in a less handy format, in Appendix C of the Word *User's Reference*. The codes for the characters are obtained by adding the numbers in the far left column to the numbers in the top row. For example, "½" is character number 189.

As you can see, this set has all of the ordinary English letters and the Arabic numerals as well as all the standard punctuation symbols in the top half. These are the ordinary ASCII characters, and are inserted into a document just by pressing a single key or a shifted key on the keyboard. The second half of the set contains special symbols such as the curly apostrophe, ', the curly quotes, "", the section symbol, §, the plus-or-minus, ±, and others. These

characters are entered by toggling the NumLock key to on and then holding down the Alt key while entering on the numeric keypad the *four-digit* (i.e., the first digit is "0") integer for the character code.

The other character set is the one that turns your laser printer into a technical typesetter. This is the *PS Math* character set, and is represented in the Windows *symbol* font.

PS Math character set in Windows "symbol" typeface, 10 point										
code	0	1	2	3	4	5	6	7	8	9
30	−			!	∀	#	∃	%	&	∋
40	(	)	*	+	,	−	.	/	0	1
50	2	3	4	5	6	7	8	9	:	;
60	<	=	>	?	≅	Α	Β	Χ	Δ	Ε
70	Φ	Γ	Η	Ι	ϑ	Κ	Λ	Μ	Ν	Ο
80	Π	Θ	Ρ	Σ	Τ	Υ	ς	Ω	Ξ	Ψ
90	Ζ	[	∴	]	⊥	_		α	β	χ
100	δ	ε	φ	γ	η	ι	φ	κ	λ	μ
110	ν	ο	π	θ	ρ	σ	τ	υ	ϖ	ω
120	ξ	ψ	ζ	{	|	}	~			
140										ο
150	–	–								
160		ϒ	′	≤	/	∞	ƒ	♣	♦	♥
170	♠	↔	←	↑	→	↓	°	±	″	≥
180	×	∝	∂	•	÷	≠	≡	≈	…	|
190	—	↵	ℵ	ℑ	ℜ	℘	⊗	⊕	∅	∩
200	∪	⊃	⊇	⊄	⊂	⊆	∈	∉	∠	∇
210	®	©	™	∏	√	·	¬	∧	∨	⇔
220	⇐	⇑	⇒	⇓	◇	〈	®	©	™	∑
230	⎛	⎜	⎝	⎡	⎢	⎣	⎧	⎨	⎩	⎪
240		〉	⌡	⌠	⎮	⌡	⎫	⎬	⎭	⎪
250	⎢	⎦	⎞	⎤	⎥	⎦		.	.	.

You access these symbols in exactly the same way that you do those from the other set, except that you choose the *symbol* font. So, for example, in the ANSI set, the letter "p" has code 122. Code 122 in the Math set is "π". So all you have to do to get a "π" is to select the symbol font and type "p". Similarly, you access the symbols in the second half of the set using the same method as for the second half of the ANSI set. For example, to insert the infinity symbol, "∞", into your text, you toggle the NumLock key to on, hold down the Alt key, and enter "0165" on the numeric keypad.

Compound symbols not found above can be constructed using the overstrike and other features of the equation editor. Here are some useful examples:

Making compound symbols		
Symbol		Code
h bar	$\hbar$	{eq \o(*h*,/)}
minus-or-plus	$\mp$	{eq \o(\s\do1(+),\s\up1(-))}
much greater than	$\gg$, >>	{eq >\d\ba5()>}, {eq >\d\ba2()>}
vector	$\vec{x}, \vec{X}$	{eq \o(*x*,\s\up4(→))}, {eq \o(*X*,\s\up7(→))}
dagger	$A^{\dagger}$	{eq *A*\s\up5(\o(!,\s\up1(-)))}

Notice that in the minus-or-plus and dagger symbols, the components are reduced to 6 point size. It would be helpful if MicroSoft would implement these two symbols directly in their symbol fonts. Also notice a problem with the vector symbol. This is made by raising the right arrow symbol to a superscript position and the line spacing algorithm makes extra room for the superscript by moving down the line that the vector appears on, as it does to this line for example: $\vec{x}$. But as you can see, the line is moved down far more than is necessary. This is because Word fails to notice that the arrow is not a full-height character.

A note on the minus sign: The character obtained from the keyboard, "-", is really designed to serve as a hyphen. It is too short for a minus sign. I find that character number 173, "−", looks much better in equations.

For symbols which you use very often, it is handy to define macros that enter them for you and to assign these macros to single keystrokes.

Enlargement of special symbols like brackets and integrals are handled very well by the equation editor, as in:

$$I = \frac{4\sqrt{mF}}{\pi} \int_0^{\pi/2} \left(\sqrt{1 - \frac{E}{2F}\sin^2\left[\frac{y}{2}\right]} - \frac{1 - \frac{E}{2F}}{\sqrt{1 - \frac{E}{2F}\sin^2\left[\frac{y}{2}\right]}} \right) d\left[\frac{y}{2}\right],$$

although, as you can see, the square root symbols don't come out very pretty.

Sometimes the equation editor messes up and does not expand a set of brackets properly:

$$A_M\left(e^{i\omega t}|n+M\rangle + e^{-i\omega t}|n-M\rangle\right).$$

A fix for this situation is to push up and down on some space-characters somewhere inside the brackets. In the above example, if a space is added before and after the central plus sign, and if the one of those spaces is subscripted by four points, and the other is superscripted by ten, then the brackets expand nicely:

$$A_M\left(e^{i\omega t}|n+M\rangle + e^{-i\omega t}|n-M\rangle\right).$$

Headings and sequential numbers

It was not easy to figure out how to use the sequence fields to obtain systematic numbering and referencing of chapters, sections and figures. The description of the *seq* field in the *User's Reference* is not very helpful. (In fact, I think it's wrong.) A method that was found to work very well is given here.

Chapter headings are entered in the following format:

{set *nickname* "{seq chapter}"}{ref *nickname*}{ eq section \r 0 * CharFormat}{ eq figure \r 0 * CharFormat}→*FullName*

The fields here work as follows:

- The first *seq* field, {seq chapter}, sets a sequential chapter number, which changes if the chapter is moved or another chapter is inserted in order before it.
- Next, the *set* field, {set ...}, assigns the text of that chapter number to the bookmark *nickname* for use in cross references. *Nickname* should not be more than 20 characters long.
- The *ref* field, {ref *nickname*}, becomes the first such reference, inserting the chapter number at this location.
- The next field is *not* an *eq* field. It is a *seq* field in which the formatting of the first character, the "s", has been changed so that its color is white! This field, because of the "\r 0", specifies that section numbering should be restarted at zero. It then inserts that section number, "0", in the text. But the CharFormat switch tells Word to format the section number the same as the first letter of "seq", so the section number is invisible. The net effect of this field then is that the next section number will be a "1."
- The next field, in just the same way, restarts figure numbering also at "1."
- The arrow signifies a tab.
- *FullName* is the name of the chapter, typed in normally.

Appendix headings have exactly the same syntax, except that a switch is added to the first *seq* field to obtain numbering in capital letters instead of Arabic numerals:

{set *nickname* "{seq chapter * Alphabetic}"} . . .

In addition, the first appendix uses the reset switch to start the numbering of appendices at "A" instead of continuing in the sequence where the chapter numbers left off:

{set *nickname* "{seq chapter \r 1 * Alphabetic}"} . . .

Section headings use the field structure:

{set *nickname* "{seq chapter \c}.{seq section}"{ref *nickname*}→*FullName*

Here, the sequential number is set for the section by {seq section}, while the field {seq chapter \c} inserts the most recent chapter number. A period is inserted between these values, and the resulting composite section number is set to the bookmark *nickname*. The *ref* field then inserts this composite number at this location.

Figure numbers use a similar structure:

Figure {set *nickname* "{seq chapter \c}.{seq figure}"}{ref *nickname* * CharFormat}

The character format switch, "* CharFormat," specifies that the result should appear in the character format of the first character of the field instruction "ref," which in the actual figure numbers is Swiss Bold 10 point. If the CharFormat switch were not used, then the number would appear in the default format of the paragraph, which in the case of the captions where figure numbers are set is Dutch 8 point.

A chapter, section or figure number is referenced with a *ref* field. So, for example, the field {ref Stn_CmptrWinWord} inserts the number of this section: E.3. But since figure numbers are created in bold face, they are reproduced by default in that same style. For example, the field {ref Fig_IntroLabData} inserts the figure number of the laboratory data in the introduction: 1.1. To make this appear in ordinary type, use the CharFormat switch, as in {ref Fig_IntroLabData * CharFormat} to get 1.1. Another way this switch is used here is to produce section references in 6 point type, as in [§{ref Stn_CmptrWinWord * CharFormat}] to get [§E.3].

Section numbers and titles are reproduced in the page headers using a *styleref* field. This field copies the text of any preceding paragraph of a particular style. So the text of the headers is:

§{styleref 4} →[tab] {page}

The "4" is shorthand for "heading 4". But here is a sticky problem: What if a chapter begins with a long introduction that is not given a section number, as is the case for Chapter 1? Or what about a chapter that does not have any section divisions at all, like Appendix F? The second page of such a chapter will be headed with the number and title of the last section of the previous chapter, which is definitely not desirable. There is a way to get around this problem which is similar to the use of the *seq* fields with the "\r 0" switches in the chapter headings, mentioned above. The trick is to follow every chapter heading with a paragraph with the following properties:

- It contains only the field {styleref 1}, which reproduces the chapter number and title, including any changes made later.
- It has paragraph style "heading 4" (but with Border Above turned off), so that its contents are reproduced in the page headers. And (here's the trick:)
- It is made invisible by changing its character color to white (Alt-T-C, Alt-L, W, ↵). When *styleref* copies the text to the header, it does not copy the text characteristics, so the text is visible. It does not work to *hide* the text (Alt-T-C, H, ↵) because then *styleref* wouldn't find it.

There has been one problem arise in the use of the *styleref* field. For some strange reason, *styleref* translates curly quotes into straight ones. This happens in Appendix F, as you can verify by looking at the second page thereof. But, on the other hand, if I hadn't pointed it out, I'll bet you would never have noticed.

Bookmarks

In general, the bookmark facility in Word is tremendous. I use it for moving around in the text, cross referencing section and page numbers, and even reproducing entire equations and tables when I wish to repeat them exactly.

There are two ways to set a bookmark, and each is best used only for a separate set of circumstances:

- Use the *Insert Bookmark* command at a particular cursor location, or on selected text. This method is best used only for setting a *temporary* bookmark with a name that you set aside only for such use, such as "temp".
- Insert a *set* field, and if the bookmark contains text, also a *ref* field. This method is demonstrated above in setting and showing all of the chapter, section and figure numbers. This is the method of choice for setting permanent bookmarks because it allows you to see where you have put your bookmarks, what you have called them, and exactly what text is included in them, all by turning *View Codes* on.

It can actually be dangerous to use the *Insert Bookmark* command for permanent bookmarks. If you insert text immediately in front of (i.e., to the left of) a bookmark set in this way, then the bookmark will expand to include this text. This can cause several deleterious effects which are best not experienced.

There is a problem common to both types of bookmarks. If you copy a selection of material (text and/or graphics) to the clipboard and then paste it somewhere else, any bookmarks in the material are moved to the new location. Usually this is not what is wanted in a copy and paste procedure. Be careful to remove any unwanted bookmarks from the pasted material, and then to update any *set* fields in the original material. If would be nice if MicroSoft would arrange it so that bookmark settings remain where they were originally set unless the *set* field is actually cut from the text.

Here is an undocumented trick for setting an equation as a bookmark. This is useful if you want to repeat the equation in several places without retyping it. The following code:

{set Einstein "{eq *E*=*mc*\s\up5(2)}"}{ref Einstein}

does not work. I don't know why, but the *ref* field inserts nothing. Here is what you use instead:

{set Einstein "*E*=*mc*\\s\\up5(2)"}{eq {ref Einstein}}

This works, and yields $E=mc^2$. Note that the formula codes must now be preceded with two backslashes instead of one.

The *sic* field

This is a field that MicroSoft forgot to implement, but you can invent it on your own. The idea of the *sic* field is to specify a particular occurrence of a word that the spelling checker should skip over, as in:

Don't tell me I've made a spelling misteak *[sic]*.

You can get the spelling checker to ignore this intentional mistake by using an *eq* field:

Don't tell me I've made a spelling {eq misteak} *[sic]*.

This works because the spelling checker does not look inside of equations. It does not work to use the *quote* field, inside of which the checker does look.

Dealing with long documents

The *Sampler* that comes with Word warns against creating very large document files. The *User's Reference* has an entry that explains that you should break long documents into smaller pieces, and manage these parts with *include* and *RD* fields. I have some different advice for you: Type away to your heart's content.

I have one file that is over 1½ megabytes in size. It is an electronic dictionary under development by Ennex Technology Marketing, Inc. and, printed out, it would be 443 pages long. That's long. I find it most convenient to be able to keep all of that data in one unit, and I see nothing in Word that prevents me from doing so. In fact some features make it especially practical to work with long documents:

- *FastSave* is most important. It only saves changes so it only takes a few seconds to complete, no matter how big the document is.
- *Go*ing to a bookmark usually only takes a second or two.
- Even searching is quite fast, taking only a few minutes to go through a very long document.

This ability to work with long documents does not come from having a large memory machine. For the last six months I have been working on a notebook 386SX with three megabytes of RAM and a 20 megabyte hard disk, most of which is full.

There are, of course, some drawbacks to working with long documents:

- Every five or ten saves or so will be a full save and these can take several minutes. To make Word more efficient with long documents, MicroSoft should consider extending the amount of changes that can be saved with *FastSave*.
- There is a great deal of time wasted on repeated pagination whenever anything is printed. Even if you paginate the document first, and then go directly to print it out, Word will repaginate it again before printing. If you ask Word to print a single page, even just the first page, Word will repaginate the document before giving you that page. Even if you print out a single line of selected text, repagination will always take place first. In a long document, repagination can take a long time, so this is a terrible nuisance.
- Hyphenation is a problem if you have graphics, tables, or other items given specific positioning on the page, with other text flowing around them. That text cannot be hyphenated correctly in the normal editing mode; you must be in *Page View*. Unfortunately, trying to hyphenate a long document in *Page View* will exhaust the memory. So you can either hyphenate the document in segments, all in *Page View*, or you can hyphenate the whole document in normal editing mode, and then go into *Page View* to hyphenate the text flowing around the positioned items. However, hyphenation in *Page View* suffers from the same sickness as printing: it repaginates too much. (Actually it is worse than printing, because it repaginates more slowly and more often, once when you enter *Page View*, once every time you start hyphenating a selection, then again after the selection has been hyphenated). The results of hyphenation may

not be worth the wait. Unfortunately, it is in flowing text that hyphenation is most important, because it comes in narrower-than-usual columns. I would say that fixing the repagination routine should be the Number One priority for improvements to Word, at least with respect to making it easy to work with long documents.

- Printing a long document can crash the system if the computer runs out of disk space for the temporary files generated in printing. There is no warning. Processing simply stops and the computer is hung. When you reboot, you find that your hard disk is full, and the culprit is a mess of files in the \temp directory. The solution is, after first clearing the \temp directory, to either free up some more disk space or print the document in segments.

I find that, despite these problems, I enjoy the convenience of dealing with a large document as a single unit. I should point out, however, that a colleague of mine disagrees, preferring to work with smaller, more manageable files. It is a matter of personal preference.

Problems

The errant spelling checker

The worst part of Word for Windows is the spelling checker. It has many fairly severe deficiencies:

- There needs to be an option for *Ignore Once*. For example, if I allow one occurrence of *dir*, that should not automatically mean that I accept every occurrence.
- There needs to be an option for *Change Once*. For example, one occurrence of *essentiall* may need to be corrected to *essential*, but the next may need to be *essentially.*
- Some words continue to be flagged even after being added to the dictionary. This has been the case with *adjoint*, *conjugacy*, *counterexample*, *Davydov*, *eigenbasis*, *eigenstates*, *Hamiltonian* and *Hermitian*. However these errors are not consistent.
- *Orthogonal* is not in the main dictionary!
- Capitalization of a word in a custom dictionary needs to indicate required capitalization. For example, *Hamilton* should not be equivalent to *hamilton*. The current situation seems to be that capitalization in the custom dictionary is ignored. Another symptom of the problem: I have *GHz* in my dictionary, with that form of capitalization. The spelling checker highlights *GHz* in a document and complains of "Uncommon Capitalization".
- There is no documentation on the checker messages *Uncommon Capitalization*, *Repeated Word*, *All Letters Not Capitalized* and *First Letter Not Capitalized*. These last two are strange. I get *All Letters Not Capitalized* when Word finds "gm" (for "gram") in a document, and Word suggests (even with *Always Suggest* off) changing it to "GM." Is that supposed to be for General Motors? I get *First Letter Not Capitalized* when Word finds the C keyword "goto," and it suggests changing this to "Goto."
- The usual default action for the checker is *Ignore*. But in that last example, when Word suggests changing "gm" to "GM" and "goto" to "Goto," the default is *Change*. This is a dangerous inconsistency that at least once led me to make a change inadvertently.
- During the spelling check, the status line should show the current page and position.

- The suggestion algorithm needs some work. For example, the first suggestion for *permissable* is *perishable*. For *coumpound*, Word suggests *southbound* and *soupcon* (which, by the way should be *soupçon*) and does not suggest *compound*.
- When a questionable word is displayed, it should be positioned in the middle of the visible part of the screen, not at the top, to allow examination of the context. The visible part of the screen is that part not taken up by the dialog window.
- The checker has an undocumented message: *Out of global memory*. This should be documented in the *Messages* appendix of the *User's Reference*. When the message comes up, the status line invites me to press F1 for help, but doing so only brings a beep from the computer.

In conclusion, it looks like the quality control team went to sleep during this part of the project.

While they are at work fixing those problems, here are some desirable features that MicroSoft should consider implementing as improvements:

- Common abbreviations, including punctuation, should be accepted as words. For example, *Prof.* should be accepted if capitalized and with the period, but *prof* should not. Other examples: Mr., Mrs., Ms., Dr., Inc., Corp., Ltd., etc., e.g., i.e., 1st, 2nd, 3rd, 4th, ...
- Common contractions, including the apostrophe, should be supported for addition to the custom dictionary. For example: it's, don't, won't, wouldn't. Currently, adding these items to the dictionary does not seem to have any effect.
- A possessive formed with an apostrophe should be recognized as a word if the root is recognized. At the very least, it must be possible to add special possessives to the dictionary, such as *Hamilton's* and *Schrodinger's*.
- Certain words should be allowed only in specified combinations. For example, I would like to add *Runge-Kutta* to my dictionary, but not *Runge* and *Kutta* individually. *de Broglie* should be recognized, but *Broglie* alone should not.
- Words added to the dictionary should automatically imply their cognates. For example, adding any one of *vectorize*, *vectorized*, *vectorizes* or *vectorizing* should imply the others.
- A nice option would be *background spell checking* that would check spelling as text is entered.

Problems with tables

- There is no documented way to keep a table from being split by a soft page break. I have found that it usually works to format all the rows of the table except the last as *Keep with next*, but that seems to fail sometimes. This is an important feature that should be provided and documented.
- It would be nice to be able to merge cells vertically.
- It would be nice to be able to automatically center the contents of a cell vertically, instead of having to do it manually with *Space Before* in *Format Paragraph*.

Other complaints

- It would be helpful if hyphenation were done in real time, instead of requiring a special operation. As the program is now, the view of the document is not really WYSIWYG until hyphenation is run.
- Some printer setup options, especially orientation and resolution, should be in the document format with a section or page override available. For example, it would be nice to be able to include the occasional chart in landscape mode.
- As is suggested for the spelling checker above, the search facility (and likewise the search and replace facility) should display the found text in the middle of the (visible part of the) screen, not at the top.

F "Energy" and "Hamiltonian"

This work makes a semantic break with convention by using the word *energy* in place of *Hamiltonian* for that function (in classical mechanics) or operator (in quantum mechanics) which governs the evolution of a system. This appendix expresses the reasons for this use of language.

Energy is one of the most important concepts in physics. The energy of a system, in both classical and quantum mechanics, governs the evolution of that system. In classical mechanics, energy is a function of the system's dynamical variables, and the evolution follows Hamilton's equations. In nonrelativistic quantum mechanics, energy is an operator in Hilbert space, and the evolution follows Schrodinger's equation. If the system is *conservative*, then the energy value is constant in time. This means, in classical mechanics, that the energy function is time-independent, and in quantum mechanics, that the system stays in a particular eigenstate of the energy operator. If the system is not conservative, then the energy value is not constant in time. In quantum mechanics, this means that the system is not required to have a definite value of energy at all times.

There are various ways that the energy can be expressed.

In the Lagrangian formulation of classical mechanics, the energy of a system is the difference between the Lagrangian and the scalar product of the velocity with the velocity gradient of the Lagrangian [801HGo, (2-53); 760LDL, (6.1)]:

$$E(\vec{q}, \frac{d\vec{q}}{dt}, t) = \sum_i \frac{dq_i}{dt} \frac{\partial L}{\partial \frac{dq_i}{dt}} - L(\vec{q}, \frac{d\vec{q}}{dt}, t),$$

Goldstein calls this the *energy function* or *Jacobi's integral*, while Landau and Lifshitz call it simply the *energy*. Both show that it is time-constant if the Lagrangian is not explicitly time-dependent [801HGo, (2-54); 760LDL, (6.1)].

In classical Hamiltonian dynamics, the velocity gradient of the Lagrangian is identified as the conjugate momentum, so the energy becomes [801HGo, (8-8); 760LDL, (40.2)]:

$$E(\vec{q}, \vec{p}, t) = \sum_i \frac{dq_i}{dt} p_i - L(\vec{q}, \frac{d\vec{q}}{dt}, t)),$$

where the velocity, $d\vec{q}/dt$, is considered as a function of $(\vec{q}, \vec{p}, t)$. Goldstein calls this the *Hamiltonian*, while Landau and Lifshitz call it that or *Hamilton's function*.

Goldstein justifies giving the energy this different name when expressed in this coordinate system, claiming that the "Hamiltonian" has (except for time) twice as many independent variables as the "energy function" [801HGo, 61•]. However, Weinberg has pointed out [Quantum field theory lectures, 1985] that while the velocities are not functionally independent of the configura-

tion, the initial conditions and therefore the time developments of the velocities are just as independent of the configuration coordinates as the momenta are. So, in this limited sense, there are the same number of independent variables in both expressions.

In developing the above two expressions, Landau and Lifshitz define the *Hamilton's function* or *Hamiltonian* as the "energy ... expressed in terms of [canonical] coordinates" [760LDL, (40.2)]. In their text on quantum mechanics, however, they define *energy* as a "Hamilton's function which is conserved" [770LDL, 27 ¶2]. Not only is this pair of definitions circular, it is also inconsistent.

Dirac, in the context of classical mechanics, defines the *Hamiltonian* as the "energy expressed as a function of ... canonical coordinates and momenta ... and possibly also of [time]" [675PAD, (28-14)]. He does not define *energy*.

Davydov calls the operator that appears in Schrodinger's equation the *Hamilton operator* or *Hamiltonian*. He uses the term *energy operator* to refer to a time-independent special case of a Hamiltonian [730ASD, (15.1), (16.5)].

Goldstein also uses another term, the *total energy* to refer to the sum of the kinetic and potential energies [801HGo, >(1-18), (2-58), (8-15)]. Sometimes he calls this just the *energy* [801HGo >(10-26)]. He preserves this terminology even in cases where this quantity is *not* constant and the "Hamiltonian" is [801HGo, 349 ¶1].

Another common form of usage is for *Hamiltonian* to refer to the function (in classical mechanics) or the operator (in quantum mechanics) which governs the evolution of a system, and use *energy* for a particular value of this function or eigenvalue of this operator [801HGo, (10-14); 770LDL, (10.2); 730ASD, (15.3)]. Sometimes this practice is restricted to conservative systems, thereby bringing it into conformity with the aforementioned definitions of *energy* as a time-constant *Hamiltonian* [801HGo, (10-14), (10-64); 770LDL, (10.2)]. But this usage stands in stark contrast to that applied to all other physical quantities, where the function, operator and value all bear the same name, as in *position*, *velocity*, *momentum*, *electric field*, etc. When it is important, the type of quantity can be specified, as in *position variable*, *position operator* and *position eigenvalue*.

The above examples show that the usage of the term *Hamiltonian* in the literature is inconsistent and that the term is therefore ill-defined. The reason for this is that the attempts to define it are attempts to formalize a distinction which does not exist. In the early days of quantum mechanics it was not clear just what stood on either side of the equal sign in the so-called time-independent Schrodinger equation:

$$H\psi = E\psi,$$

In fact, this equation is nothing but the eigenvalue equation for the energy operator, and should be written:

$$\hat{E}\psi = E\psi.$$

Historically, the concepts of *Hamiltonian* and *energy* arose in the separate contexts of particle dynamics and thermodynamics. It is one of the triumphs of modern physics that we now understand that these two concepts are one. Use of the term *Hamiltonian* is at best superfluous, and is not made in this work.

References

References appear in the text in 6-point type, enclosed in square brackets, thus: [reference]. A reference that consists of just a section number, [§99], or just a page number, [page 99], is a cross reference, referring to that section or page of this work. Other references begin with a 6-character reference code, and refer to one of the following works, listed alphanumerically.

26cPAD *The Physical Interpretation of the Quantum Dynamics*, P.A.M. Dirac, *Proc. Roy. Soc.* London, A113-765, 621..41

272PAD *The quantum theory of the emission and absorption of radiation*, P.A.M. Dirac, *Proc. Roy. Soc.* London, A114, 243..65

276ETW *A course of modern analysis*, E.T. Whittaker and G.N. Watson, Cambridge University Press, 1902, 4th edition: 1927

408WPa *The connection between spin and statistics*, W. Pauli, *Phys. Rev.* 58, 716..22

413GNW *A treatise on the theory of Bessel functions*, G.N. Watson, Cambridge Univeristy Press, 1922, 2nd edition: 1944

46aWHF *Two notes on phase-integral methods*, W.H. Furry, *Phys. Rev.* 71-6, 360..71

538WHe *The quantum theory of radiation*, W. Heitler, 1936; 3rd edition: 1954, Dover, New York, 1984

636DJu *On the uncertainty relation for* L_z *and* ϕ and *On the commutator* $[L_z,\phi]_-$, D. Judge and J.T. Lewis, *Phys. Let.* 5-3, 189 and *Phys. Let.* 5-3, 190

638MHe *The applicability of the third integral of motion: Some numerical experiments*, Michel Henon and Carl Heiles, *Astron. Jour.*, 69-1, 73..9

639WHL *Amplitude and phase uncertainty relations*, W.H. Louisell, *Phys. Let.* 7-1, 60..1

645LSu *Quantum Mechanical Phase and Time Operator*, Leonard Susskind and Jonathan Glowgower, *Physics*, 1-1, 49..61

645LVK *Ionization in the field of a strong electromagnetic wave*, L.V. Keldysh, (*Sov. Phys.*) *JETP*, 20-5, 1307..14

64aERD *On derivations of the uncertainty principle*, Ernest R. Davidson, *J. Chem. Phys.* 42, 1461..2

675PAD *The Principles of Quantum Mechanics*, P.A.M. Dirac, Oxford University Press, Oxford, 1930, revised 4th edition: 1967

677HMK *Comments on separability operators, invariance ladder operators, and quantization of the Kepler problem in prolate-spheroidal coordinates*, H.M. Kiefer and D.M. Fradkin, *J. Mod. Phys.* 9-4, 627..32

677REP *The Villars formalism for nuclear rotation*, R.E. Peierls and J.N. Urbano, *Proc. Phys. Soc.* 2-1-1, 1..10

684ECL *Harmonic-oscillator phase operators*, E.C. Lerner, *Nuovo Cimento* B56, 183..6 and *Nuovo Cimento* B57-1

684PCa *Phase and angle variables in quantum mechanics*, P. Carruthers and Michael Martin Nieto, *Rev. Mod. Phys.* 40-2, 411..40

689MRS *Mathematical Handbook*, Murray R. Spiegel, McGraw-Hill (Schaum's Outline Series), New York, 1968

693BLe *Canonical transformations and spectra of quantum operators*, Boris Leaf, *J. Mod. Phys.* 10-11, 1971..9

693GHW *Amplitude instability and ergodic behavior for conservative nonlinear oscillator systems*, Grayson H. Walker and Joseph Ford, *Phys. Rev.* 188-1, 416..32

694BLe *Canonical operators for the simple harmonic oscillator*, Boris Leaf, *J. Mod. Phys.* 10-11, 1980..7

696ECL *Some mathematical properties of oscillator phase operators*, E.C. Lerner, H.W. Huang and G.E. Walters, *J. Mod. Phys.* 11-5, 1679..84

69bJJL *Pade approximants and the anharmonic oscillator*, J.J. Loeffel, A. Martin, B. Simon and A.S. Wightman, *Phys. Let.* B30-9, 656..8

69cJCG *Canonically conjugate pairs, uncertainty relations, and phase operators*, John C. Garrison and Jack Wong, *J. Mod. Phys.* 11-8, 2242..9

700EMe *Quantum Mechanics*, Eugen Merzbacher, John Wiley & Sons, New York, 1961, 2nd edition: 1970

709EKI *Abstract formulation of the quantum mechanical oscillator phase problem*, Evangelos K. Ifantis, *J. Mod. Phys.* 12-6, 1021..6

719GMZ *Stochastic instability of non-linear oscillations*, G.M. Zaslavskii and B.V. Chirikov, *Usp. Fiz. Nauk.* 14-5, 549..68

725DJS *Bohr-Sommerfeld orbits and quantizable symplectic manifolds*, D.J. Simms, *Proc. Camb. Phil. Soc.* 73, 489..91

72cMAb *Handbook of Mathematical Functions*, edited by Milton Abramowitz and Irene A. Stegun, Dover Publications, New York, 1964, 9th Dover printing: 1972

730ASD *Quantum Mechanics*, A.S. Davydov, translated by D. ter Haar, Pergamon Press, Oxford, 2nd edition, 1976

736YAh *Oscillator phase states, thermal equilibrium and group representations*, Y. Aharonov, E.C. Lerner, H.W. Huang and J.M. Knight, *J. Mod. Phys.* 14-6, 746..56

740JDJ *Classical Electrodynamics*, John David Jackson, John Wiley & Sons, New York, 2nd edition, 1975

744JEB *Multiphoton ionization of highly excited hydrogen atoms*, J.E. Bayfield and P.M. Koch, *Phys. Rev. Let.* 33-5, 258..61

745JDo *Spectral properties of phase operators*, J. Dombrowski, *J. Mod. Phys.* 15-5, 576..7

750LDL *The Classical Theory of Fields*, L.D. Landau and E.M. Lifshitz, translated by Morton Hamermesh, Pergamon Press, Oxford, 1951, 4th edition: 1975

760LDL *Mechanics*, L.D. Landau and E.M. Lifshitz, translated by J.B. Sykes and J.S. Bell, Pergamon Press, Oxford, 1960; 3rd edition, 1976

763JML *Who is afraid of nonhermitian operators? A quantum description of angle and phase*, Jean-Marc Levy-Leblond, *Ann. Phys.* 101, 319..41

770CCT *Quantum Mechanics*, Claude Cohen-Tannoudji, Bernard Diu and Franck Laloe, translated by Susan Reid Hemley, Nicole Ostrowsky and Dan Ostrowsky, John Wiley & Sons, New York, 1977

770LDL *Quantum Mechanics / Non-Relativistic Theory*, L.D. Landau and E.M. Lifshitz, translated by J.B. Sykes and J.S. Bell, Pergamon Press, Oxford, 3rd edition, revised, 1977

773JEB *Observation of resonances in the microwave-stimulated multiphoton excitation and ionization of highly excited hydrogen atoms*, James E. Bayfield, Larry D. Gardner and Peter M. Koch, *Phys. Rev. Let.* 39-2, 76..9

778GCa(a) *Stochastic behavior of a quantum pendulum under a periodic perturbation*, G. Casati, B.V. Chirikov, F.M. Izraelev and Joseph Ford, pages 334..52 in *Stochastic behavior in classical and quantum Hamiltonian systems*, proceedings of Volta Memorial Conference, Como, Italy, Summer, 1977, edited by Giulio Casati and Joseph Ford, Springer-Verlag, 1979

780MVB *Regular and irregular motion*, M.V. Berry in *Topics in nonlinear dynamics*, American Institutue of Physics Conference Proceedings, Volume 46, 1978

782NBD *Diffusion mechanism of ionization of highly excited atoms in an alternating electromagnetic field*, N.B. Delone, B.A. Zon and V.P. Krainov, (*Sov. Phys.*) *JETP*, 48-2, 223..7

782REP *Surprises in Theoretical Physics*, Rudolf Peierls, Princeton University Press, Princeton, New Jersey, 1979

783CIt *Quantum Field Theory*, Claude Itzykson and Jean-Bernard Zuber, McGraw-Hill, New York, 1980

787JGL *Microwave ionization and excitation of Rydberg atoms*, J.G. Leopold and I.C. Percival, *Phys. Rev. Let.* 41-14, 944..7

789JGL *Ionisation* [sic] *of highly excited atoms by electric fields III. Microwave ionisation* [sic] *and excitation*, J.G. Leopold and I.C. Percival, *J. Phys.* B12-5, 709..21

78aABR *Stochastic instability of a nonlinear oscillator*, Alexander B. Rechester and Thomas H. Stix, *Phys. Rev.* A19-4, 1656..65

791BVC *A universal instability of many-dimensional oscillator systems*, Boris V. Chirikov, *Phys. Rep.* 52-5, 263..379

795RGN *Quantum action-angle variables for harmonic oscillators*, Roger G. Newton, *Ann. Phys.* 124, 327..46

798DAJ *Ionisation* [sic] *of highly excited atoms by electric fields IV. Frequency and amplitude dependence for linearly polarised* [sic] *fields*, D.A. Jones, J.G. Leopold and I.C. Percival, *J. Phys.* B13, 31..40

79bJMo *Hidden Symmetries in Dynamical Systems*, Jurgen Moser, *American Scientist*, 67-5, 689..95

800ISG *Table of Integrals, Series, and Products*, I.S. Gradshteyn and I.M. Ryzhik, corrected and enlarged by Alan Jeffrey, Academic Press, 1980

800RSP *A Modern Course in Statistical Physics*, L.E. Reichl, University of Texas Press, 1980

801HGo *Classical Mechanics*, Herbert Goldstein, Addison-Wesley, Reading, Massachusetts, 2nd edition, 1980

80bPMK *Precise measurement of the static electric-field ionization rate for resolved hydrogen Stark substates*, Peter M. Koch and David R. Mariani, *Phys. Rev. Let.* 46-19, 1275..8

811DFE *Renormalization method for computing the threshold of the large-scale stochastic instability in two degrees of freedom Hamiltonian systems*, D.F. Escande and F. Doveil, *J. Stat. Phys.* 26-2, 257..84

813DFE *Renormalization method for the onset of stochasticity in a hamiltonian system*, D.F. Escande and F. Doveil, *Phys. Let.* A83-7, 307..10

815GMZ *Stochasticity in quantum systems*, George M. Zaslavsky, *Phys. Rep.* 80-3, 157..250

81cSPG *Probabilities of radiative transitions between highly excited atomic states*, S.P. Goreslavskii, N.B. Delone and V.P. Krainov, (*Sov. Phys.*) *JETP* 55-6, 1032..6

820VBB *Quantum Electrodynamics*, V.B. Berestetskii, E.M. Lifshitz, and L.P. Pitaevskii, translated by J.B. Sykes and J.S. Bell, Pergamon Press, Oxford, 1971, second edition: 1982

822RAL *Hamilton-Jacobi/action-angle quantum mechanics*, Robert A. Leacock and Michael J. Padgett, *Phys. Rev.* D28-10, 2491..502 (also *Phys. Rev. Let.* 50-1, 3..6)

826NBD *Dynamic polarizability of highly excited atomic states*, N.B. Delone and V.P. Krainov, (*Sov. Phys.*) *JETP* 56-6, 1170..3

827RVJ *Stochastic ionization of surface-state electrons*, Roderick V. Jensen, *Phys. Rev. Let.* 49-19, 1365..8

830AJL *Regular and Stochastic Motion*, A.J. Lichtenberg and M.A. Lieberman, Springer Verlag, New York, 1983

832DRM *Observation and quasistatic analysis of structure in microwave ionization of highly excited helium atoms*, D.R. Mariani, W. van de Water, P.M. Koch and T. Bergeman *Phys. Rev. Let.* 50-17, 1261..4

836DLS *Quantum diffusion limitation at excitation of Rydberg atom in variable field*, D.L. Shepelyansky, pages 187..204 in *Chaotic behavior in quantum systems*, proceedings edited by Giulio Casati, Plenum, New York, 1985

836MVB *Quantal phase factors accompanying adiabatic changes*, M.V. Berry, *Proc. Roy. Soc.*, London, A392, 45..57

836RVJ *Stochastic ionization of bound electrons*, Roderick V. Jensen, pages 171..86 in *Chaotic behavior in quantum systems*, proceedings edited by

Giulio Casati, Plenum, New York, 1985

837NBD *Highly-excited atoms in the electromagnetic field*, N.B. Delone, B.P. Krainov and D.L. Shepelyanskii, *Usp. Fiz. Nauk.* 26-7, 551..72

837RBl *Quantum mechanical suppression of classical stochasticity in the dynamics of periodically perturbed surface-state electrons*, R. Blumel and U. Smilansky *Phys. Rev. Let.* 52-2, 137..40

83bRVJ *Stochastic ionization of surface-state electrons: Classical theory*, Roderick V. Jensen, *Phys. Rev.* A30-1, 386..97

841RBl *Suppression of classical stochasticity by quantum-mechanical effects in the dynamics of periodically perturbed surface-state electrons*, R. Blumel and U. Smilansky, *Phys. Rev.* A30-2, 1040..51

845MVB *Classical adiabatic angles and quantal adiabatic phase*, M.V. Berry, *J. Phys.* A18, 15..27

847AGa *Phase and number*, A. Galindo, *Let. Math. Phys.* 8, 495..500

847JEB *Diffusionlike aspects of multiphoton absorption in electrically polarized highly excited hydrogen atoms*, J.E. Bayfield and L.A. Pinnaduwage, *Phys. Rev. Let.* 54-4, 313..6

848JHH *Angle variable holonomy in adiabatic excursion of an integrable Hamiltonian*, J.H. Hannay, *J. Phys.* A18, 221..30

84aJEB *Microwave multiphoton n-decreasing transitions in electrically polarised* [sic], *highly excited hydrogen atoms*, J.E. Bayfield and L.A. Pinnaduwage, *J. Phys.* B18, L49..53

852RBl *Ionization of surface-state electrons by microwave fields: Quantum treatment*, R. Blumel and U. Smilansky *Phys. Rev.* A32-3, 1900..2

853JGL *The effect of a resonant electric field on a one-dimensional classical hydrogen atom*, J.G. Leopold and D. Richards, *J. Phys.* B18, 3369..94

853JNB *Microwave absorption by hydrogen atoms in high Rydberg states*, J.N. Bardsley and B. Sundaram *Phys. Rev.* A32-1, 689..91

855JGL *The effect of a resonant electric field on a classical hydrogen atom*, J.G. Leopold and D. Richards, *J. Phys.* B19, 1125..42

858KvL *Microwave ionization of hydrogen atoms: Experiment versus classical dynamics*, K.A.H. van Leeuwen, G.v. Oppen, S. Renwick, J.B. Bowlin, P.M. Koch, R.V. Jensen, O. Rath, D. Richards and J.G. Leopold, *Phys. Rev. Let.* 55-21, 2231..4

859WAL *External field induced chaos in an infinite square well potential*, W.A. Lin and L.E. Reichl, *Physica* D19, 145..52

85aJNB *Quantum dynamics for driven weakly bound electrons near the threshold for classical chaos*, J.N. Bardsley, B. Sundaram, L.A. Pinnaduwage, and J.E. Bayfield, *Phys. Rev. Let.* 56-10, 1007..10

860RVJ *Stochastic ionization of highly excited hydrogen atoms*, Roderick V. Jensen, pages 149..65 in *Oji international seminar on highly excited states of atoms and molecules*, Invited papers edited by S.S. Kano and M. Matsuzawa, Fuji-Yoshida, Japan, 1986

861LER *Resonance overlap in quantum systems*, L.E. Reichl and W.A. Lin, pages 251..5 in *Quantum chaos and statistical nuclear physics*, proceedings of the 2nd International Conference on Quantum Chaos and the 4th International Colloquium on Statistical Nuclear Physics, Cuernavaca, Mexico, 86 01 06..10, edited by T.H. Seligman and H. Nishioka, Springer-Verlag, Berlin, 1986

862LER *Exact quantum model of field-induced resonance overlap*, L.E. Reichl and W.A. Lin, *Phys. Rev.* A33-5, 3598..601

865PMK *Microwave ionization of highly excited hydrogen atoms: experiment and theory*, P.M. Koch, K.A.H. van Leeuwen, O. Rath, D. Richards and R.V. Jensen, pages 106..13 in *The physics of phase space*, proceedings edited by H. Araki, J. Ehlers, K. Hepp, R. Kippenhahn, H.A. Weidenmuller, J. Wess and J. Zittartz, Springer-Verlag, 1987

866WMZ *Level mixing in the stretched hydrogen atom*, W.M. Zheng and L.E. Reichl, *Phys. Rev.* A35-1, 474..6

869JGL *The effect of a combined static and microwave field on an excited hydrogen atom*, J.G. Leopold and D. Richards, *J. Phys.* B20, 2369..82

869JLi *The recently recognized failure of predictability in Newtonian dynamics*, James Lighthill, *Proc. Roy. Soc.*, London, A407-1832, 35..50

86bRVJ *Effects of classical resonances on the chaotic microwave ionization of highly excited hydrogen atoms*, R.V. Jensen, *Physica Scripta* 35, 668..73

871MMS *Chaotic ionization of highly excited hydrogen atoms*, M.M. Sanders, R.V. Jensen, P.M. Koch and K.A.H. van Leeuwen, *Nuc. Phys.* B (*Proc. Sup.*) 2, 578..81

872LER *The search for a quantum KAM theorem*, L.E. Reichl and W.A. Lin, *Found. Phys.* 17-7, 689..97

872RBl *Microwave ionization of highly excited hydrogen atoms*, R. Blumel and U. Smilansky, *Z. Phys.* D6, 83..105

873RVJ *Classical chaos*, Roderick V. Jensen, *American Scientist*, 168..81

874LER *Breakdown of invariants in nonlinear systems*, L.E. Reichl and W.A. Lin, pages 54..60 in *Energy Transfer Dynamics*, edited by T.W. Barrett and H.A. Pohl, Springer-Verlag, Berlin, 1987

877PMK *Microwave ionization of highly-excited hydrogen atoms: A driven quantal system in the classically chaotic regime*, Peter M. Koch, in *Electronic and atomic collisions, invited papers of the 15th International Conference on the Physics of*, Brighton, U.K., 87 07 22..8, edited by H.B. Gilbody, W.R. Newell, F.H. Read and A.C.H. Smith, North-Holland, Amsterdam, 1988, 501..15

878WAL *Transition of spectral statistics due to overlap of quantum resonance zones*, W.A. Lin and L.E. Reichl *Phys. Rev.* A36-10, 5099..102

87aWHP *Numerical recipes in C, The art of scientific computing*, William H. Press, Brian P. Flannery, Saul A. Teukolsky and William T. Vetterling, Cambridge University Press, 1988

87bBEc *Quantum mechanics of classically non-integrable systems*, Bruno Eckhardt, *Phys. Rep.* 163-4, 205..297

87cWAL *Spectral analysis of quantum-resonance zones, quantum Kolmogorov-Arnold-Moser theorem, and quantum-resonance overlap*, W.A. Lin and L.E. Reichl *Phys. Rev.* A37-10, 3972..85

882GCa *Hydrogen atom in monochromatic field: Chaos and dynamic photon localization*, Giulio Casati, Italo Guarneri and Dimitri L. Shepelyansky, *IEEE J. Quantum Electronics* 24-7, 1420..44

887JEB *Excited atoms in strong microwaves: Classical resonances and localization in experimental final-state distributions*, James E. Bayfield and David W. Sokol, *Phys. Rev. Let.* 61-18, 2007..10

888EJG *Microwave ionization of H atoms: Breakdown of classical dynamics for high frequencies*, E.J. Galvez, B.E. Sauer, L. Moorman, P.M. Koch and D. Richards, *Phys. Rev. Let.* 61-18, 2011..4

88bJEB *Localization of classically chaotic diffusion for hydrogen atoms in microwave fields*, J.E. Bayfield, G. Casati, I. Guarneri and D.W. Sokol *Phys. Rev. Let.* 63-4, 364..7

88cLER *Mechanism for extension of the wave function in quantum dynamics*, L.E. Reichl, *Phys. Rev.* A39-9, 4817..27

894VIB *Laser optics of neutral atomic beams*, Victor I. Balykin and Vladilen S. Letokhov, *Phys. Today* 23..8

902LER *Self-similarity in quantum dynamics: A quantum KAM theory*, L.E. Reichl and Li Haoming, *Phys. Rev.* A42-8, p 4543..61

904RVJ *Chaotic ionization of highly excited hydrogen atoms: comparison of classical and quantum theory with experiment*, R.V. Jensen, S.M. Susskind and M.M. Sanders *Phys. Rep.* (To appear.)

Acknowledgments

Of the teachers listed in the dedication on page iii, the one who stands out most obviously in relation to this dissertation is Prof. Linda E. Reichl, who has motivated and led this research through five years. Her patient guidance and stalwart confidence are as much the cause of any value that may be found in this work as all of my effort and time.

In addition to the influence of Prof. Reichl, I have also gained valuable insight from conversations with Prof. Luis J. Boya, Mr. Steve Cocke, Dr. Ben Schumacher and many other colleagues in the Center for Statistical Mechanics and the Physics Department of the University of Texas at Austin.

When I think about the accomplishment that this thesis represents, I am immediately reminded of the many wise and caring teachers who have advanced and enriched my life to bring me to this stage. I have acknowledged in the dedication those who have had the most pivotal influence on my development. In addition, I am grateful for guidance received from Prof. Robin L. Armstrong, Prof. Anthony P. French, Ms. Shamaan Ochaum and Mr. E. James Rohn.

The quote on the dedication page suits well my intention to thank the teachers in my life. But actually, Emerson was talking about *friends* when he wrote it. Here is a longer passage from the essay:

> Our chief want in life, is, somebody who shall make us do what we can. This is the service of a friend. With him we are easily great. There is a sublime attraction in him to whatever virtue is in us. How he flings wide the doors of existence!

I have made many friends during the time of researching and writing this dissertation. Their friendship has carried me through the dark times when I didn't know what I was doing, or where I was going. Many of these friends are my brothers and sisters in $A\Phi\Omega$, including my adopted brother, David Hulme, my Little Brothers, Steve DeZeeuw and Jason Reifsnider, my Big Sister, Nancy Nierth, and Scott Collins, Thomas Hawkins, Elaine Kessler, Kevin Koym, and Stephanie Lane. Others, who have appeared in various other walks of my life, are Carlos Castro, Mackey Devlin, Jon Graf, Alan Sager, Jeanne Slobod, Mary Teeple and Monty Wood. Without these people, the pursuit of this goal would have been empty and somber.

Finally, I would like to thank the shareholders of Ennex Corp. (Toronto, Canada) and Ennex Technology Marketing, Inc. (Austin, Texas) for giving me the freedom to pursue this project, and remaining confident that this esoteric track of my business will be turned to profitable advantage.